

## Chapter 5 Advanced Topics in Overhead Line Design

Overhead Lines were often constructed over years. Current projects of overhead lines are often replacement of tower member, replacement of overhead lines from HVAC to HVDC, or **uprating** the overhead lines to a larger thermal capacities, or a higher voltage. O&M activities are application of **insulation coating** on insulator or replacement of broken insulator after flashover. It is time to study again the **design of insulator** and **theory of corona and flashover**, discuss the challenges faced in **HVDC overhead lines application**, embrace the idea on dynamic line rating with **electrothermal model**, **ground potential rise (GPR)** under fault and EM Field application as the end of this course.

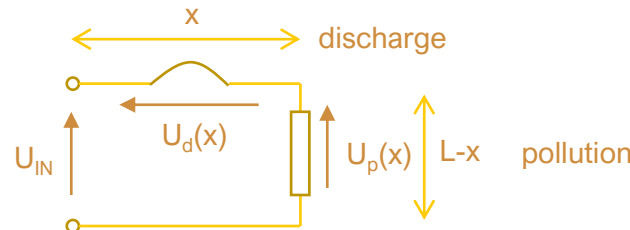
### 5.1 Theory of Insulator and its Design

Insulator flashover is a problem for overhead line applications in the world. It is due to the recovery of the insulator surface by a **conductive layer of pollution** associated with humidity producing local arcs that propagate until shunting the insulators string with an arc earth-fault. In this part, **discharge characteristics** and **arc reignition condition** is studied, before the introduction of **deposition modelling**. Then, **finite element method (FEM)** is introduced for the pollution flashover modeling under different contamination profile. Flashover voltage for different insulator design and hence the **optimal profile** for insulator are introduced based on optimization with genetic algorithm (GA), support vector machines (SVM) and neural network. At last, field across insulator is observed.

To model dry band arc with pollutant as a cylindrical discharge with length  $x$ , **Obenau's equation** is employed.

$$V = NxI^{-n} + R_p(x)I = NxI^{-n} + \frac{\rho_p(L - x)}{S_p} \quad (5.1)$$

where  $I$  is leakage current,  $x$  is arc discharge length,  $n$  and  $N$  are discharge characteristics constants and  $R_p(x)$  represents the unabridged part of the pollution layer with  $\rho_p(x)$ ,  $S_p$  and  $r_p$  the resistivity, cross section and linear resistance of pollution layer.  $L$  is the total leakage length of insulator.



Constant  $n$  and  $N$  depend on experimental conditions in which discharge is burning. Slama proved that discharge constant ( $n, N$ ) are dynamic and depend upon the element of electrical equivalent circuit and **thermal characteristics** of discharge.

$$n = \frac{m(m-1)}{m-1 + (\omega \varepsilon_p \rho_p)^2}, \quad N = r_p \frac{m}{\alpha} \left( \frac{\pi \lambda(T_d) T_d \alpha}{r_p^m} \right)^{\frac{m+1}{2}} \quad (5.2)$$

where  $m$  is the **discharge instability condition** defined by

$$m = \alpha \frac{r_d}{r_p} \quad (5.3)$$

Consider the electrical equivalent circuit representing the electrical discharge in series with the pollutant deposit, whereas the resistance in parallel with the capacitor represents the pollution layer of unabridged portion. For the flat plate model, the pollution capacitance and arc resistance are expressed as:

$$C_p(x) = \frac{\epsilon_p S_p}{L - x}, R_{arc} = \frac{\rho_a x}{S} \quad (5.3)$$

where  $\epsilon_p$  is the permittivity of polluted layer, arc with section  $S$ , length  $x$  and resistivity  $\rho_a$ .

Discharge will be **unstable** when

$$\frac{dV}{dI} = Z_{eq} = R_{arc} + \frac{R_p}{1 + j\omega R_p C} = \frac{\rho_a S}{x} + \frac{\rho_p(L - x)}{S_p(1 + j\omega \rho_p \epsilon)} > 0 \quad (5.4)$$

The square modulus of  $Z_{eq}$  is

$$|Z_{eq}|^2 = \frac{1}{(S_p S k)^2} \left( \rho_a S_p k x + S \rho_p (L - x)^2 + \rho_p^2 (\omega \epsilon \rho_p)^2 (L - x)^2 \right) \quad (5.5)$$

where  $k = S_p + j\omega \rho_p \epsilon$ . Taking  $\alpha = (\rho_a S_p k - S \rho_p)^2 + s^2 \rho_p^2 (\omega \epsilon \rho_p)^2$

$$|Z_{eq}|^2 > \frac{1}{(S_p S k)^2} \left( \alpha x^2 - 2Lx(\alpha + \rho_a S_p k(S \rho_p - \rho_a S_p k)) + k(S \rho_p L)^2 \right) > 0 \quad (5.6)$$

It is an inequality of variable  $x$ . In order to solve the inequality (5.6), we calculate the discriminant  $\Delta$  of inequality (5.6) as the value

$$\Delta = 4L^2 \left( \alpha + S_p k \rho_a (S \rho_p - S_p k \rho_a)^2 \right) - \alpha k (L S \rho_p)^2 \quad (5.7)$$

In further simplification,

$$\Delta = 4L^2 (S_p S \rho_a \rho_p k)^2 (1 - k) \quad (5.8)$$

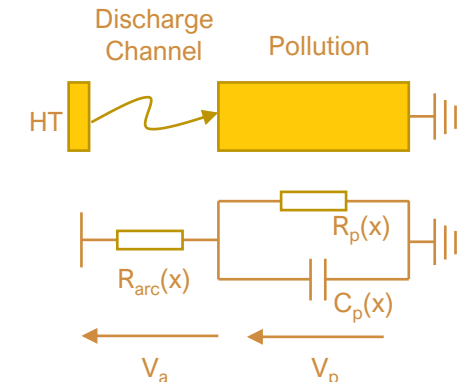
It is noted that  $k^2(1 - k)$  is always negative.

Then the solution of  $x$  in (5.6) is

$$\frac{x}{L} = 1 + \frac{S_p k \rho_a}{\alpha} (S \rho_p - S_p k \rho_a) \pm j \frac{S S_p \rho_p \rho_a k (\rho_p \omega \epsilon)}{\alpha} \quad (5.9)$$

with squared modulus

$$\left( \frac{x}{L} \right)^2 = \left[ 1 + \frac{S_p k \rho_a}{\alpha} (S \rho_p - S_p k \rho_a) \right]^2 + \left[ \frac{S S_p \rho_p \rho_a k (\rho_p \omega \epsilon)}{\alpha} \right]^2 \quad (5.10)$$



The arc can propagate if the ratio between its length and the overall length is less than 1. Hence,

$$\frac{x}{L} < 1 \quad \text{or} \quad \left(\frac{x}{L}\right)^2 - 1 < 0 \quad (5.11)$$

From (5.10) and (5.11),

$$\left(\frac{x}{L}\right)^2 - 1 < \left[1 + \frac{S_p k \rho_a}{\alpha} (S \rho_p - S_p k \rho_a)\right]^2 + \left[\frac{SS_p \rho_p \rho_a k (\rho_p \omega \varepsilon)}{\alpha}\right]^2 - 1 \quad (5.12)$$

Putting

$$\Omega = \left[1 + \frac{S_p k \rho_a}{\alpha} (S \rho_p - S_p k \rho_a)\right]^2 + \left[\frac{SS_p \rho_p \rho_a k (\rho_p \omega \varepsilon)}{\alpha}\right]^2 - 1 \quad (5.13)$$

We distinguish three cases for parameter  $\Omega$ .

$\Omega > 0$ :

$$\left[1 + \frac{S_p k \rho_a}{\alpha} (S \rho_p - S_p k \rho_a)\right]^2 > 1 - \left[\frac{SS_p \rho_p \rho_a k (\rho_p \omega \varepsilon)}{\alpha}\right]^2 \quad (5.14)$$

**Case 1.1 (DC case):**

$$\left[\frac{SS_p \rho_p \rho_a k (\rho_p \omega \varepsilon)}{\alpha}\right]^2 = 0 \rightarrow \frac{S_p k \rho_a}{\alpha} (S \rho_p - S_p k \rho_a) > 0 \quad (5.15)$$

It means discharge may elongate and leads to an arc propagation criterion:

$$\boxed{\frac{d|Z_{eq}|}{dx} < 0 \rightarrow S \rho_p - S_p k \rho_a > 0} \quad (5.16)$$

With

$$\begin{cases} E_{arc} = \frac{\rho_a}{S} I_{arc} \\ E_p = \frac{\rho_p}{S \sqrt{k}} I_f \end{cases} \rightarrow E_{arc} < \frac{E_p}{\sqrt{k}} \rightarrow E_{arc} < E_p \quad (5.17)$$

### Question 1

(a) Derive the arc propagation criterion (5.16) starting from  $\frac{d|Z_{eq}|}{dx} < 0$ .

(b) Consider the case where (i)  $\frac{S_p k \rho_a}{\alpha} (S \rho_p - S_p k \rho_a) < -1$ , (ii)  $-1 < \frac{S_p k \rho_a}{\alpha} (S \rho_p - S_p k \rho_a) < 0$

Explain when the arc will not elongate and arc will glow until it exceeds the length  $x_0$ , whereupon it extinguishes.

(c) Given the circuit voltage with thermal model can be written as

$$U = \frac{kx}{I_{arc}^n} + r_p(L - x)I_{arc}$$

Determine the critical current and hence the critical flashover voltage by differentiating U w.r.t. x and  $I_{arc}$ .

It is given that the length  $x_1$ , whereupon the arc will extinguish will be

$$-1 < \frac{S_p k \rho_a}{\alpha} (S \rho_p - S_p k \rho_a) < 0 \rightarrow \frac{x_1}{L} = 1 + \frac{S_p k \rho_a}{\alpha} (S \rho_p - S_p k \rho_a) \quad (5.18)$$

The critical current and hence the flashover voltage are

$$\frac{dU}{dx} = 0 \rightarrow I_C = \left( \frac{k}{r_p} \right)^{\frac{1}{n+1}} \quad (5.19)$$

$$\frac{dU}{dI_{arc}} = 0 \rightarrow I_C = n^{\frac{1}{n+1}} \left( 1 + \frac{1}{n} \right) \left( \frac{k}{r_p} \right)^{\frac{1}{n+1}} \rightarrow U_c = n^{\frac{1}{n+1}} \left( \frac{1}{(n+1)^{n+1}} + n^{n-1} \right) k^{\frac{1}{n+1}} r_p^{\frac{n}{n+1}} L \quad (5.20)$$

**Case 1.2 (AC):**

$$\left[ \frac{SS_p \rho_p \rho_a k (\rho_p \omega \varepsilon)}{\alpha} \right]^2 \neq 0 \rightarrow \left[ 1 + \frac{S_p k \rho_a}{\alpha} (S \rho_p - S_p k \rho_a) \right]^2 > 1 - \left[ \frac{SS_p \rho_p \rho_a k (\rho_p \omega \varepsilon)}{\alpha} \right]^2 \quad (5.21)$$

The propagation is conditioned by the second part of (5.21), hence

$$\left[ 1 + \frac{S_p k \rho_a}{\alpha} (S \rho_p - S_p k \rho_a) \right]^2 > 0 \rightarrow \frac{S_p k \rho_a}{\alpha} (S \rho_p - S_p k \rho_a) > -1 \text{ or } -1 < \frac{S_p k \rho_a}{\alpha} (S \rho_p - S_p k \rho_a) \quad (5.22)$$

For the arc propagates more, the second part of (5.21) must be zero, i.e.

$$\frac{x_1}{L} = \frac{SS_p \rho_p \rho_a k (\rho_p \omega \varepsilon)}{\alpha} = \frac{SS_p \rho_p \rho_a k (\rho_p \omega \varepsilon)}{(\rho_a S_p k - S \rho_p)^2 + s^2 \rho_p^2 (\omega \varepsilon \rho_p)^2} = 1 \quad (5.23)$$

Recall the discharge instability condition, or propagation condition m,

$$\frac{x_1}{L} = \frac{1}{\frac{1}{m} \left( \frac{(m-1)^2}{(\rho_p \omega \varepsilon)} + (\rho_p \omega \varepsilon) \right)} \quad (5.24)$$

On the other hand, the total power per unit length supplied by the source is given by

$$P_t = \left( r_a + \frac{r_p}{\sqrt{k}} \right) I^2, \quad I^2 = \frac{\pi \lambda T_d}{r_a} \rightarrow P_t = \frac{(m + \sqrt{k}) \pi \lambda T_d}{m} \quad (5.25)$$

where  $T_d$  is the axial temperature provided the necessary amount of thermal ionization and  $\lambda$  is thermal conductivity.

Consider also the total power per unit length supplied by the source according to Ohm's Law as  $P_t = E_t I$ , and combining (5.24) with (5.25),

$$x_1 = \frac{VI}{\frac{\pi \lambda T_d}{m^2 (\rho_p \epsilon \omega)} (m(m-2) + k)(m + \sqrt{k})} \quad (5.26)$$

Consider the empirical formula by Claverie and Porcheron on the re-ignition condition of discharge.

$$V_{in} = M x_1 I^{-m} \quad (5.27)$$

with

$$m = 1, \quad M = \frac{\pi \lambda T_d}{m^2 (\rho_p \epsilon \omega)} (m(m-2) + k)(m + \sqrt{k}) \quad (5.28)$$

or

$$\frac{V_{in}}{x_1} = MI^{-1} \quad (5.29)$$

It is the **re-ignition voltage** required for the discharge to re-ignites after the supply voltage passes through the natural current zeros, moreover the discharge extinguishes due to the natural current zeros with

$$\frac{x_1}{L} = 1 + \frac{S_p k \rho_a}{\alpha} (S \rho_p - S_p k \rho_a) \quad (5.30)$$

from (5.21).

In AC voltage after turning off the current at the end of the half period, it does not recover immediately in the next alternation, a minimum voltage is then necessary to re-ignites the discharge. Furthermore, the AC flashover voltage is now possible, if and only if the **re-ignition condition** (5.26) and the flashover condition deducted in the case of the DC voltage (5.21) are checked simultaneously.

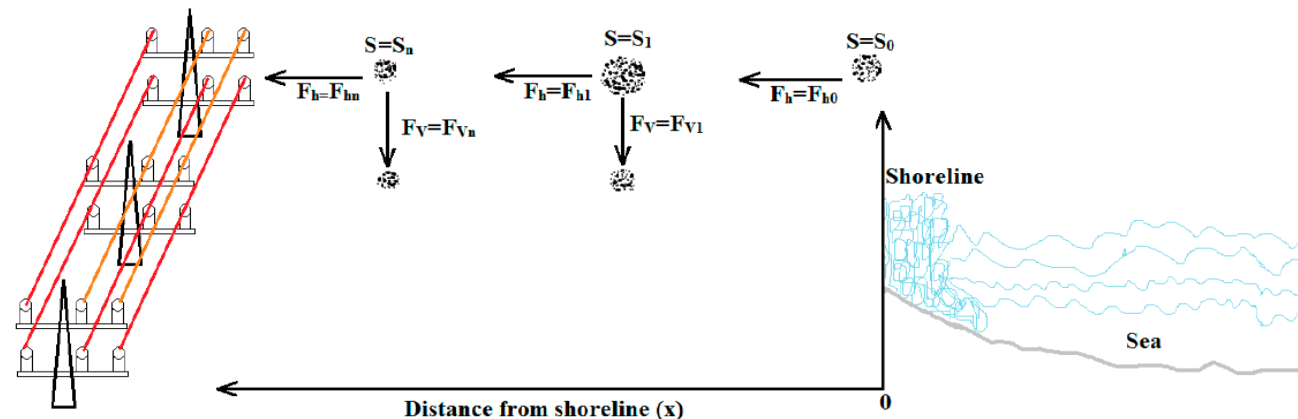
It is noted that:

1. When peak value of the leakage current is increased, the **critical re-ignition voltage** decreases due to the thermal-ionization process.
2. Mathematical parameter governing the **re-inception condition** are dynamic and depend on the electrical equivalent circuit elements and the thermal proprieties of the arc discharge.

The process of **saline deposition** on an insulator surface, associated with flashover and consequent power outages has been a major problem for power network systems since the early 1900s. The time to surface flashover initiation depends on (i) **deposition of saline contamination**, and (ii) **penetration and diffusion of salt particles on insulator surface** through various wetting agents such as rain, fog, snow, dew or drizzle.

It is recognized that saline deposition and diffusion are affected by various natural processes such as **temperature exposure**, **relatively humidity** or **moisture level**, **counter-diffusion of hydroxide ions** and environmental load of salts and other adverse weather conditions. Types of **contamination deposition** on the insulator surface influence surface flashover.

Initially, non-ceramic insulators prevent **water filming** on the surface due to their **hydrophobic properties**. Yet, this resistance gradually decreases due to physical and chemical changes in the silicone materials which can lead to **dry-band arcing** and **surface discharges**.



Consider the mechanism of sea salt transportation and deposition, with saline concentration ( $S$ ) and its variation ( $S_0, S_1, \dots, S_n$ ). In this model, oceanic winds, distance from sea, diffusion and penetration of saline and **gravitational settlement** of saline on outdoor insulators are taken into account. The vertical resultant deposition flux ( $F_v$ ) is represented with deposition rate ( $V_{dep}$ ) with

$$F_v = V_{dep}S \quad (5.31)$$

From (5.31), it is possible to determine the saline concentration ( $S$ ) with variation ( $S_0, S_1, \dots, S_n$ ) from the shoreline to the surface of insulator, and deposition rate. It follows that the mass of saline deposited per unit of time is a negative function of the resultant vertical deposition flux, with  $dt$  as time variation,  $h$  as the thickness of saline contamination layer. It is noted that the negative sign represents the reduction of saline concentration ( $S$ ) due to deposition.

$$\frac{dS}{dt} = -\frac{SV_{dep}}{h} \quad (5.32)$$

The deposition rate is constant with time and for any distance from the shoreline and its decay function may be estimated as

$$S = S_0 e^{-\alpha x}, \quad \alpha = \frac{V_{dep}}{vh} \quad (5.33)$$

As deposition velocity decreases with time, the saline concentration at a distance  $x$  from seashore, given wind speed ( $v$ ), saline concentration ( $S_0$ ), initial deposition rate of saline at shoreline ( $V_{dep0}$ ) and  $\alpha$  the coefficient of deposition rate reduction that characterizes saline contamination distribution and its influence on deposition rate.

$$S = S_0 e^{-\alpha x}, V_{dep} = V_{dep0} e^{-\alpha t} \rightarrow S = S_0 e^{\frac{V_{dep0}}{\alpha h} (e^{-\alpha \frac{x}{v}} - 1)} \quad (5.34)$$

where  $\beta$  is a coefficient characterizing particles distribution and has its influence on deposition velocity decrease. It is called the coefficient of deposition velocity reduction.

Similarly, **saline deposition** ( $D$ ) on the surface can be represented by  $D = \eta(vS)$ , where  $\eta$  is capture efficiency constant for the saline depending on climate conditions and outdoor insulators,  $v$  is the wind speed and  $S$  is the saline concentration.

$$D = D_0 e^{\left(\frac{V_{dep0}}{\alpha h}\right) \left(e^{-\alpha \frac{x}{v}} - 1\right)} \quad (5.35)$$

Contamination deposition mechanisms rather than gravitational settlement, like high-speed wind and the scavenging effects due to heavy rainfall or dense fog precipitation were also considered at this stage in the model and related experimental investigations are presented.

Attachment and penetration of saline ions and moisture onto silicone rubber (SiR) can be described by Fick's Law of Diffusion, assuming constant diffusivity and direct saline binding.

$$\frac{\partial S}{\partial t} = D \frac{\partial^2 S}{\partial^2 x} \quad (5.36)$$

where  $S$  is the saline penetration ( $\text{mg/cm}^2$ ) as a function of time ( $t$ ) at a distance  $x$  from the shoreline and  $D$  is the diffusion coefficient of moisture. The solution for saline penetration and moisture diffusion on an insulator surface is given by

$$S(x, t) = S_C \left( 1 - \operatorname{erf} \frac{x}{2\sqrt{Dt}} \right) \quad (5.37)$$

The error function ( $\operatorname{erf}$ ) may be determined from the standard table of Fick's Law.

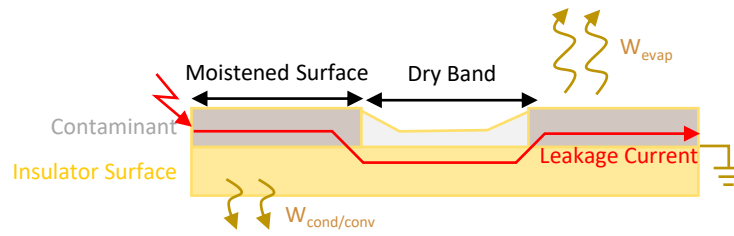
The development of dry band formation on the surface of a silicone rubber model in normal cold fog can be mathematically formulated by considering the energy balance equation, which can be expressed as:

Energy in = Energy out + Energy related to change in and on insulator surface

i.e.

$$W_{LC} = W_{\Delta T} + W_{evap} + W_{cond/conv} \quad (5.38)$$

$W_{LC}$  = Energy generated by leakage current,  $W_{\Delta T}$  = Energy generated by change in temperature,  $W_{evap}$  = energy loss by evaporation due to ambient temperature,  $W_{cond/conv}$  = Energy loss by convection and conduction



The power dissipated per unit area of the insulator surface is:

$$p = \rho_s J_s^2 \quad J_s = \frac{I}{\Delta L} \quad (5.34)$$

Due to the dissipated power, the temperature of the pollution layer is rising because of heat transfer to the surroundings. Due to heat transfer, the temperature and dry band area increased by  $\Delta T$  and  $\Delta s d(\Delta s)$  respectively, in a differential time  $dt$ . Cold fog is made of condensed water droplets which are the result of humid air mass being cooled to the dew point where it can no longer hold all the water vapor.

Therefore, the corresponding volume  $d(\Delta L)l$  and mass of cold fog is  $\rho_s d(\Delta L)l$ . Heat consumed by the evaporation process is given by:

$$W_{evap} = -L_e \rho_s d(\Delta L)l \quad (5.35)$$

where  $L_e$  is the latent heat of fog.

The resistance of dry band region is  $l/\sigma\Delta s$  due to small volume of length  $L$ . Hence the heat generated by current in AC system is:

$$W_{LC} = I^2 R dt = (J_s \Delta L)^2 \frac{l}{\sigma \Delta L} dt \quad (5.36)$$

The change in temperature of cold fog is in relationship with specific heat with  $mC_h \Delta T$  and the latent heat of cold fog to moisture due to evaporation is  $L_m \Delta m$ . Surface resistivity changes with the change of temperature along insulator surface length  $l$  in a short period of time  $dt$  so that

$$W_{\Delta T} = C_h \rho_s \Delta L l dT, dT = \frac{\partial T}{\partial t} dt \quad (5.37)$$

where  $\rho_s$  is the medium density.

If the volume of moisture is very small and does not interact with air or insulator surface, then there is no convection or conduction. If it interacts with the insulator surface, then the area of interaction is  $k_e \rho_e l$ . In a short period of time  $dt$ , the dissipated heat is given by

$$W_{cond/conv} = H_e (T_m - T_p) k \rho_e l dt \quad (5.38)$$

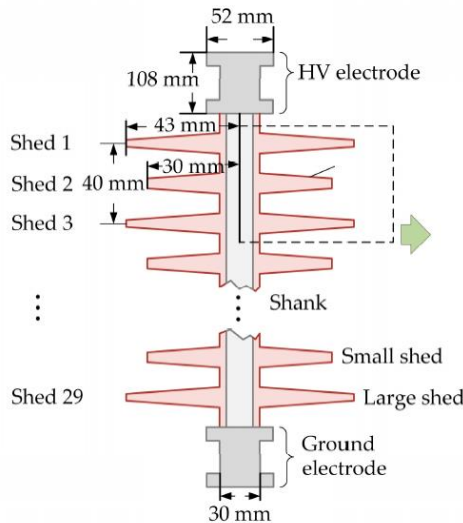
Combining,

$$(J_s \Delta L)^2 \frac{l}{\sigma \Delta L} dt = -L_e \rho_s d(\Delta L)l + C_h \rho_s \Delta L l dt + H_e (T_m - T_p) k \rho_e l dt \quad (5.39)$$

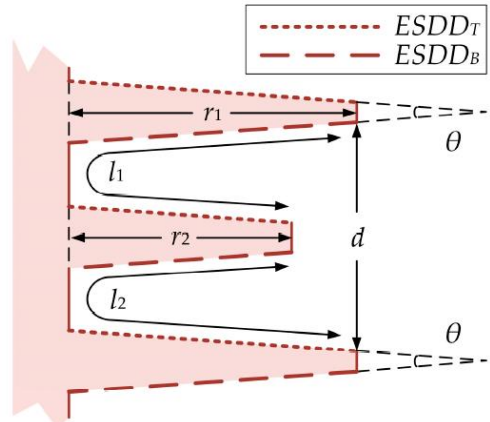
which results in

$$\frac{J_s^2}{\sigma} = -L_e \rho_s \frac{d \ln L}{dt} + \rho_s C_h \frac{dT}{dt} + k \rho \frac{H_e}{L} (T_m - T_p) \quad (5.40)$$

It shows that the development of dry band, i.e. dL, is a function of  $\sigma, L, T, \rho_s, t$ .



(a) Composite insulator schematic



(b) Geometry parameters

The pollution distribution on the top and bottom surface of the insulator was defined as  $ESDD_T$  and  $ESDD_B$ . The flashover voltage reduces with the increase of the ratio of  $ESDD_T / ESDD_B$ . The range of the ratio was 0.1 to 1. It is often to set the ratio as 1 to simulate the **dry band formation** and arcing phenomena under a severe polluted scenario with relatively low **flashover voltage**.  $ESDD$  value was  $0.1 \text{ mg/cm}^2$  and surface resistivity is  $8.3 \times 10^5 \Omega\text{m}$  under the influence of environment temperature and humidity.

Given the shed angle  $\theta$  and CF is defined as the ratio of insulation creepage distance to arcing distance.  $K_{shed}$  is defined as the ratio of  $r_2$  to  $r_1$ .

$$CF = \frac{l_1 + l_2}{d}, \quad k_{shed} = \frac{r_2}{r_1} \quad (5.41)$$

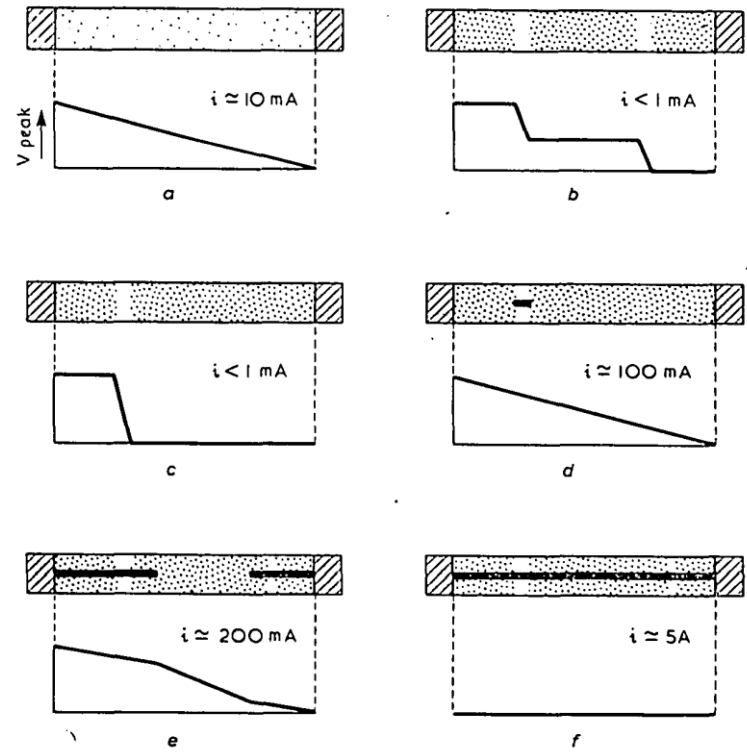


**Fig. 1**

*Typical voltage distributions on a polluted strip*

- a Wetting begins
- b Dry bands form
- c One dry band predominates
- d Dry band flashes over
- e Arcs extend
- f Flashover complete

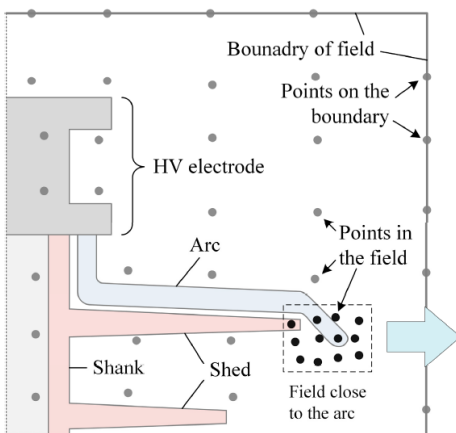
In order to reduce the probability of dry band arcing and arc propagation, the geometry structure of insulator can be optimized under the premise that creepage distance remains the same. The optimization variable of insulator geometry are CF,  $k_{\text{shed}}$  and  $\theta$ .

The problem formulation is as follows.

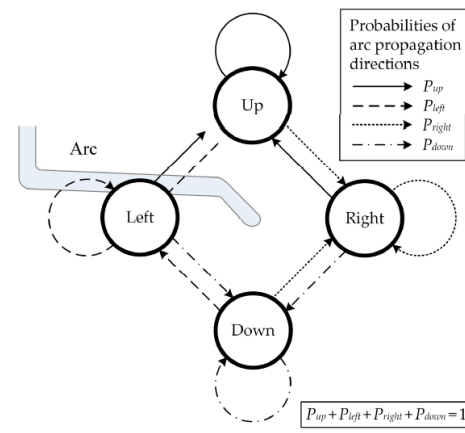
### Electric Field and Arc Propagation Model:

$$\begin{cases} \nabla^2 \varphi = \frac{\partial^2 \varphi}{\partial x^2} + \frac{\partial^2 \varphi}{\partial y^2} = -\frac{\rho_c}{\varepsilon} & \text{Poisson Equation} \\ \varphi(x, y) \Big|_{\Gamma} = f_1(\Gamma) & \text{Dirichlet Boundary Condition} \\ \frac{\partial \varphi}{\partial n} \Big|_{\Gamma} = f_2(\Gamma) & \text{Neumann Boundary Condition} \end{cases} \quad (5.42)$$

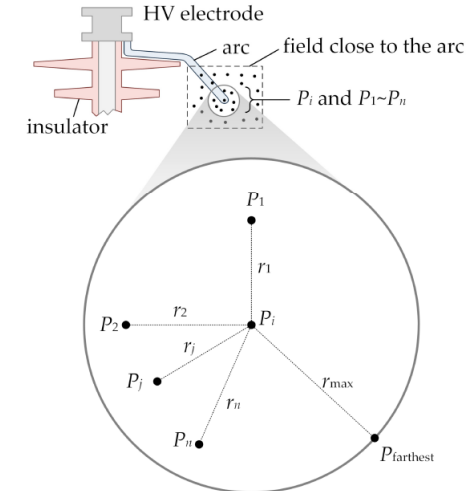
where  $\varphi$  is electric potential,  $\rho_c$  is bulk charge density and  $\varepsilon$  is permittivity.



(a) Discrete points in the field domain



(b) Random walk theory



Consider the electric and thermal field distribution with generalized finite difference time domain method (GFDTD).

$$\frac{\partial u}{\partial t} = \frac{\partial^2 u}{\partial x^2} + \frac{\partial^2 u}{\partial y^2} + C \rightarrow u_j = u_i + h_{ij} \frac{\partial u_i}{\partial x} + k_{ij} \frac{\partial u_i}{\partial y} + \frac{1}{2} \left( h_{ij}^2 \frac{\partial^2 u_i}{\partial x^2} + k_{ij}^2 \frac{\partial^2 u_i}{\partial y^2} + 2h_{ij}k_{ij} \frac{\partial^2 u_i}{\partial x \partial y} \right) + \dots \quad i = 1, 2, \dots, m \quad (5.43)$$

$P_i$  is the point among  $P_1, P_2, \dots, P_n$ . The value of each point  $P_i$  and  $P_1 \sim P_n$  is  $u_i$  and  $u_1 \sim u_n$ . The distance from each point  $P_1 \sim P_n$  to  $P_i$  is  $r_1 \sim r_n$  and the farthest distance is  $r_{\max}$ . The residual function of two points  $B(u)$  is defined as

$$B(u) = \sum_{j=1}^n \left[ \left( u_i - u_j + h_{ij} \frac{\partial u_i}{\partial x} + k_{ij} \frac{\partial u_i}{\partial y} + \frac{1}{2} \left( h_{ij}^2 \frac{\partial^2 u_i}{\partial x^2} + k_{ij}^2 \frac{\partial^2 u_i}{\partial y^2} \right) \right) w_j \right]^2 \quad (5.44)$$

The weight function of the j-th point  $w_j$  is calculated as:

$$w_j = 1 - 6\left(\frac{r_j}{r_{MAX}}\right)^2 + 8\left(\frac{r_j}{r_{MAX}}\right)^3 - 3\left(\frac{r_j}{r_{MAX}}\right)^4 \quad (5.45)$$

Derive  $B(u)$  for  $\partial^2 u / \partial^2 x$  and  $\partial^2 u / \partial^2 y$ .

$$[A][D_u] = [b] \quad (5.46)$$

$$[A] = \begin{bmatrix} \sum_{j=1}^n \frac{h_{ij}^4 w_j^2}{4} & \sum_{j=1}^n \frac{h_{ij}^2 k_{ij}^2 w_j^2}{4} \\ \sum_{j=1}^n \frac{h_{ij}^2 k_{ij}^2 w_j^2}{4} & \sum_{j=1}^n \frac{k_{ij}^4 w_j^2}{4} \end{bmatrix}, \quad [D_u] = \begin{bmatrix} \frac{\partial^2 u}{\partial x^2} & \frac{\partial^2 u}{\partial y^2} \end{bmatrix}^T, \quad [b] = \begin{bmatrix} \sum_{j=1}^n (u_j - u_i) \frac{h_{ij}^2 w_j^2}{2} & \sum_{j=1}^n (u_j - u_i) \frac{h_{ij}^2 w_j^2}{2} \end{bmatrix}^T \quad (5.47)$$

Decompose the matrix  $[b]$  as  $[b] = [B][u]$ , where

$$[B] = \begin{bmatrix} \sum_{j=1}^n \frac{-h_{ij}^2 w_j^2}{2} & \frac{-h_{i1}^2 w_1^2}{2} & \frac{-h_{i2}^2 w_2^2}{2} & \dots & \frac{-h_{in}^2 w_n^2}{2} \\ \sum_{j=1}^n \frac{-k_{ij}^2 w_j^2}{2} & \frac{-k_{i1}^2 w_1^2}{2} & \frac{-k_{i2}^2 w_2^2}{2} & \dots & \frac{-k_{in}^2 w_n^2}{2} \end{bmatrix} \quad [u] = [u_i \ u_1 \ u_2 \ \dots \ u_j \ \dots \ u_n]^T \quad (5.48)$$

The matrix  $[D_u]$  is written in another form, i.e.

$$[D_u] = [A]^{-1}[b] = [A]^{-1}[B][u] = [D][u], \text{ where } [D] = [A]^{-1}[B] \quad (5.49)$$

Then  $\partial^2 u / \partial^2 x$  and  $\partial^2 u / \partial^2 y$  can be written as

$$\begin{cases} \frac{\partial^2 u}{\partial x^2} = d_{1,1} u_i + \sum_{j=1}^n d_{1,(j+1)} u_j \\ \frac{\partial^2 u}{\partial y^2} = d_{2,1} u_i + \sum_{j=1}^n d_{2,(j+1)} u_j \end{cases} \rightarrow \boxed{\frac{u_i^{t_{n+1}} - u_i^{t_n}}{\Delta t} = d_{1,1} u_i^{t_n} + \sum_{j=1}^n d_{1,(j+1)} u_j^{t_n} + d_{2,1} u_i^{t_n} + \sum_{j=1}^n d_{2,(j+1)} u_j^{t_n} + C_i^{t_n}} \quad (5.50)$$

where superscript " $t_n$ " and " $t_{n+1}$ " are the present and next stages of the point  $u$ , respectively.

Before the arc ignition, the electric field calculation model computed the electric field distribution to determine the **arc ignition** and obtain the **leakage current density** on the insulator surface. After arc ignition, the electric field and arc propagation model computed the instantaneous electric field strength around the arc leader during propagation. **Random theory** was utilized to determine the arc propagation directions based on the instantaneous electric field.

**Random walk theory** calculated the probability of arc propagation in all directions. The random number was generated at each step of arc propagation to determine the exact direction of next step. Therefore, **arc growth direction** could be different even when the electric field distribution remains the same, which describe the stochastic characteristics of arc propagation.

$$P = \frac{E^2}{\Sigma E^2} a(E - E_c) \quad (5.51)$$

where  $E$  is the electric field strength summation of all possible directions with  $E > E_c$  (2.1kV/mm), the RMS value of threshold field.  $a$  is the step function. The arc propagation velocity is in proportion to the magnitude of the electric field strength.

For the heat transfer model, which simulates the energy balance of the evaporation process, including the **leakage current injection energy**, heat conduction and convection energies on the insulator surface, heat radiation energy of the arc, and **water evaporation energy of phase changing**.

Before arc ignition, the source of thermal field was the accumulated energy on the insulator surface generated by leakage current density. After the arc ignition, the heat transfer model including heat radiation of the arc as the dominant energy source to affect the **dry band formation** during arc propagation. The leakage current injection energy is calculated as

$$W_{leakage} = \sum_{t=0}^{t_0} \sum_{i=1}^l \frac{E_i^{t_n}}{\rho_r}^2 \quad (5.52)$$

Heat conduction and convection are the main form of heat dissipation on the composite insulator surface before arc initiates. Heat conduction partial differential equation (PDE) and the boundary conditions are listed as follows.

$$\begin{cases} \rho c \frac{\partial T}{\partial t} = \lambda \left( \frac{\partial^2 T}{\partial x^2} + \frac{\partial^2 T}{\partial y^2} \right) + \Phi & \text{Heat Conduction PDE} \\ T(x, y) \Big|_{\Gamma} = f_1(\Gamma) & \text{Dirichlet Boundary Condition} \\ \frac{\partial T}{\partial n} \Big|_{\Gamma} = f_2(\Gamma) & \text{Neumann Boundary Condition} \end{cases} \quad (5.53)$$

where  $T$  is the thermal temperature w.r.t time  $t$ ,  $\rho, c$  and  $\lambda$  are the density, specific heat capacity and thermal conductivity of different insulating materials, respectively.  $\Phi$  is the internal heat source caused by dry band arcing and leakage current density of insulator surface. Similarly, the discrete heat transfer is as follows

$$\rho_i c_i \frac{(T_i^{t_{n+1}} - T_i^{t_n})}{\Delta t} = \lambda_i d_{1,1} T_i^{t_{n+1}} + \sum_{j=1}^n \lambda_j d_{1,(j+1)} T_j^{t_{n+1}} + \lambda_i d_{2,1} T_i^{t_{n+1}} + \sum_{j=1}^n \lambda_j d_{2,(j+1)} T_j^{t_{n+1}} \quad (5.54)$$

where the internal energy source, i.e. leakage current, can be represented by

$$\Phi_i = E_i^{t_n} J_i^{t_n} = \frac{(E_i^{t_n})^2}{\rho_r} \quad (5.55)$$

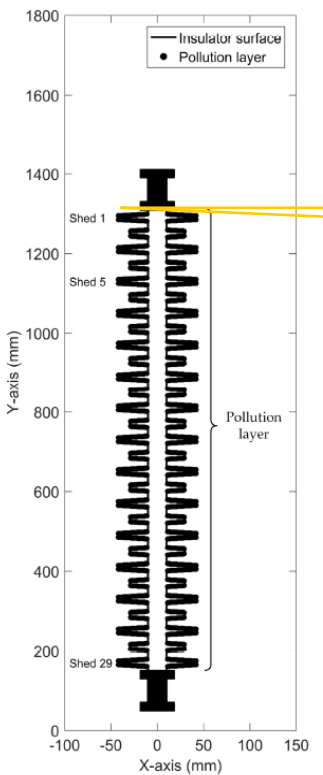
Thermal conduction, convection and arc radiation on insulator surface are calculated below.

$$W_{cond} = \sum_{t=0}^{t_0} \sum_{i=0}^l \lambda \Delta T_i^{t_n}, \quad W_{conv} = \sum_{t=0}^{t_0} \sum_{i=0}^l h(T_i^{t_n} - T_0), \quad W_{arc} = \sum_{t=0}^{t_0} \sum_{i=0}^l \varepsilon \sigma (T_i^{t_n})^4 \quad (5.56)$$

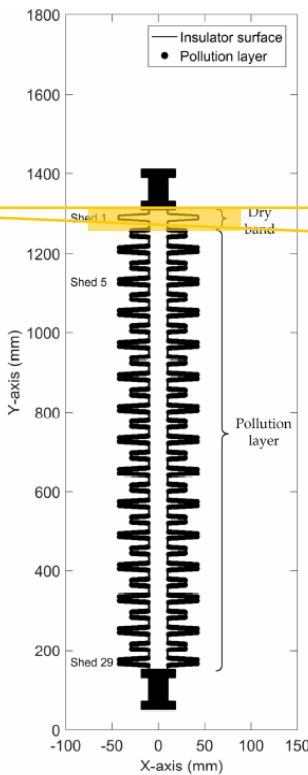
Water in the pollutant layer evaporates during the heat transfer process. The [Clausius-Clapeyron Equation](#) describes enthalpy variation based on air pressure and thermal temperature.

$$\ln\left(\frac{P_2}{P_1}\right) = \frac{\Delta H_{water}^{steam}}{R} \left(\frac{1}{T_1} - \frac{1}{T_2}\right) \rightarrow \Delta H_{water}^{steam} = \frac{RT_1}{T_2}, \quad W_{water_{steam}} = \Delta H_{water}^{steam} V_{water} \quad (5.56)$$

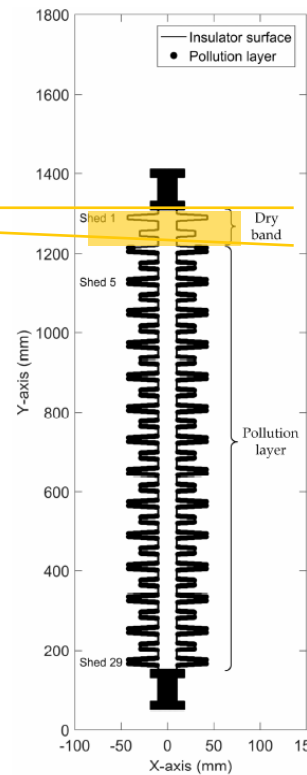
where  $\Delta H_{water}^{steam}$  is the phase-change enthalpy of water,  $R = 8.314$  and  $P_1$  and  $P_2$  remain the same as standard atm pressure (101.325 kPa), and  $T_1$  and  $T_2$  are the thermal temperature change before and after arc initialization. Therefore  $\Delta H$  is a function of thermal temperature during dry band formation and arc propagation process.



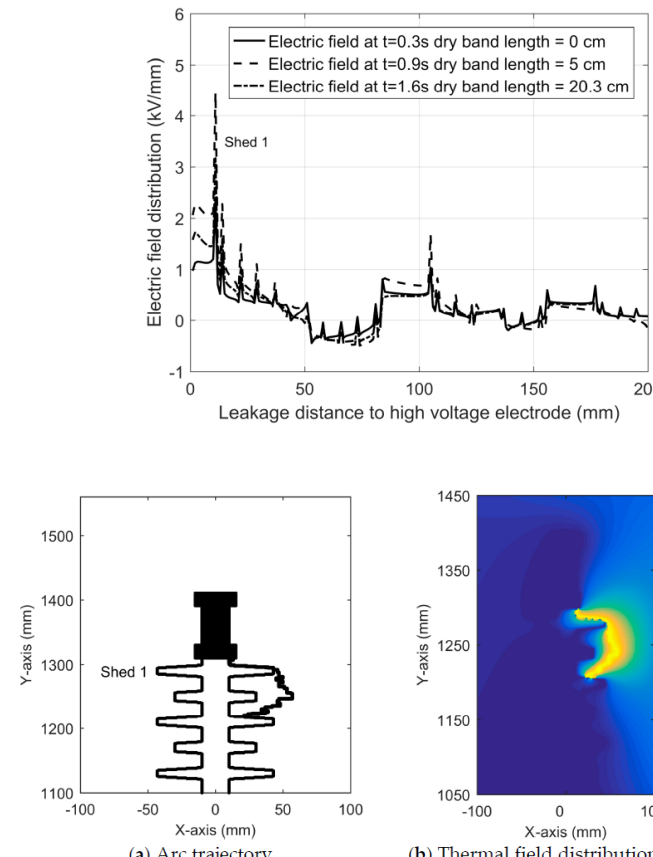
(a)  $t = 0$  s



(b)  $t = 0.9$  s

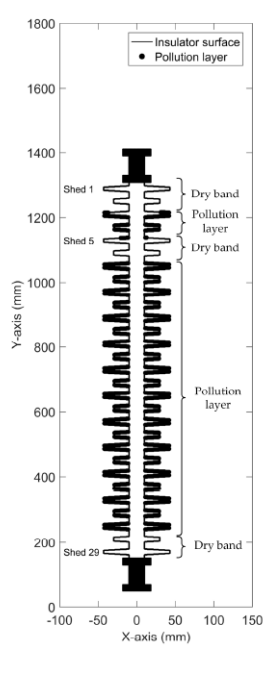


(c)  $t = 1.6$  s

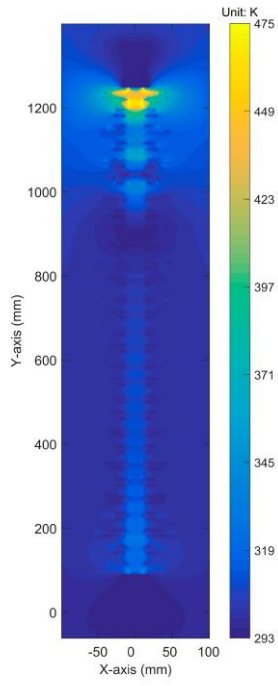


(a) Arc trajectory

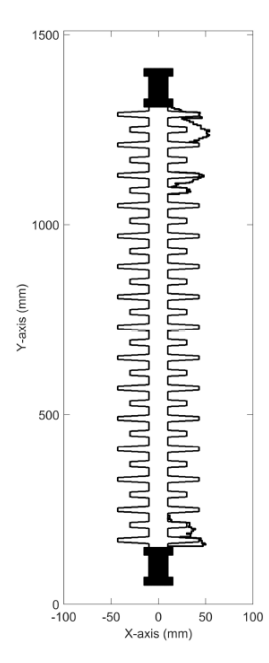
(b) Thermal field distribution close to the arc



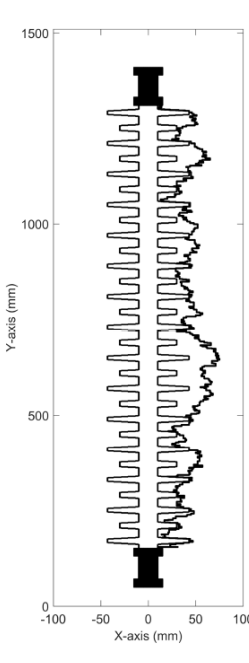
(a) Dry bands distribution



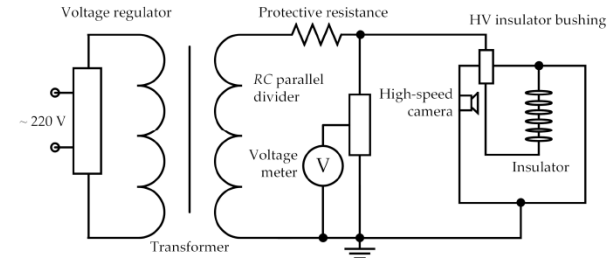
(b) Thermal field distribution



(a)  $t = 9.89$  s



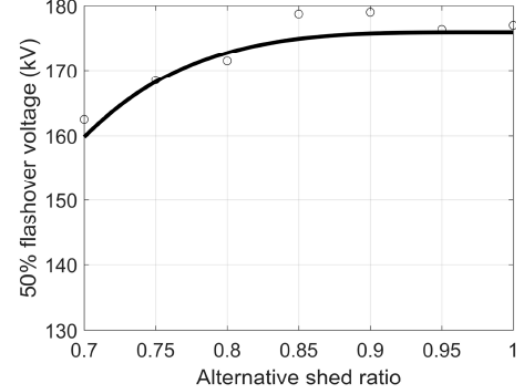
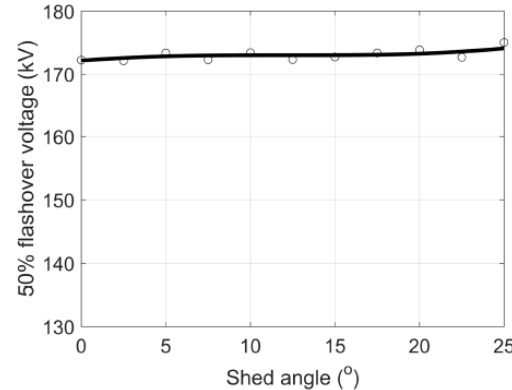
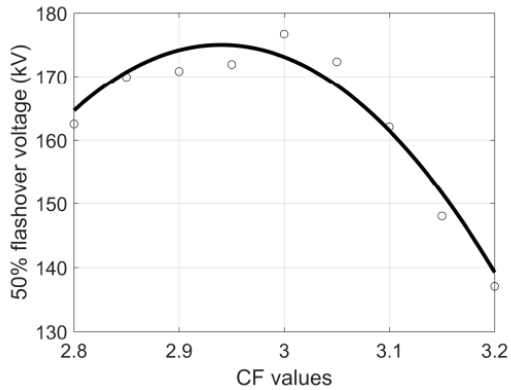
(b)  $t = 14.64$  s



(c)  $t = 10.1$  s



(d)  $t = 15.4$  s



## Conclusion:

1. Maximum electric field decreases with the expansion of dry band.
2. **Leakage current density** and **arc radiation** are the dominant factor in heat transfer model **before and after arc initialization** to form the dry band.
3. The 50% flashover voltage increases with the decrease of CF value and increase of alternative shed ratio.

Finite element method (FEM) was one approach to simulate the numerical models of the dry band effect. These models were used to describe the dry band effect on the distribution of electric field and voltage on the insulators. Effect of simultaneous presence of uneven wet contamination, multi-dry band, and pollution location on the flashover voltage of glass insulators is studied.

Again, E-field is solved to study the effect of contaminant profile and humidity on flashover characteristics on polluted insulator.

$$E = -\nabla V \rightarrow \nabla \cdot (\sigma \nabla V) + \frac{\partial}{\partial t} \nabla \cdot (\epsilon \nabla V) = 0 \quad (5.57)$$

The change of E-field can be calculated using Maxwell's expression.

$$\nabla E = \frac{\rho}{\epsilon} \rightarrow -\nabla \cdot (\epsilon \nabla V) = \rho \rightarrow \nabla^2 V = -\frac{\rho}{\epsilon} \quad (5.58)$$

When  $\rho = 0$ ,

$$\nabla^2 V = 0 \quad (5.59)$$

Putting (5.59) in cylindrical coordinate,

$$\frac{\partial^2 V}{\partial r^2} + \frac{1}{r} \frac{\partial V}{\partial r} + \frac{\partial^2 V}{\partial z^2} = 0 \quad (5.60)$$

Energy Function  $F(v)$  of 2D in cylindrical coordinate is defined as:

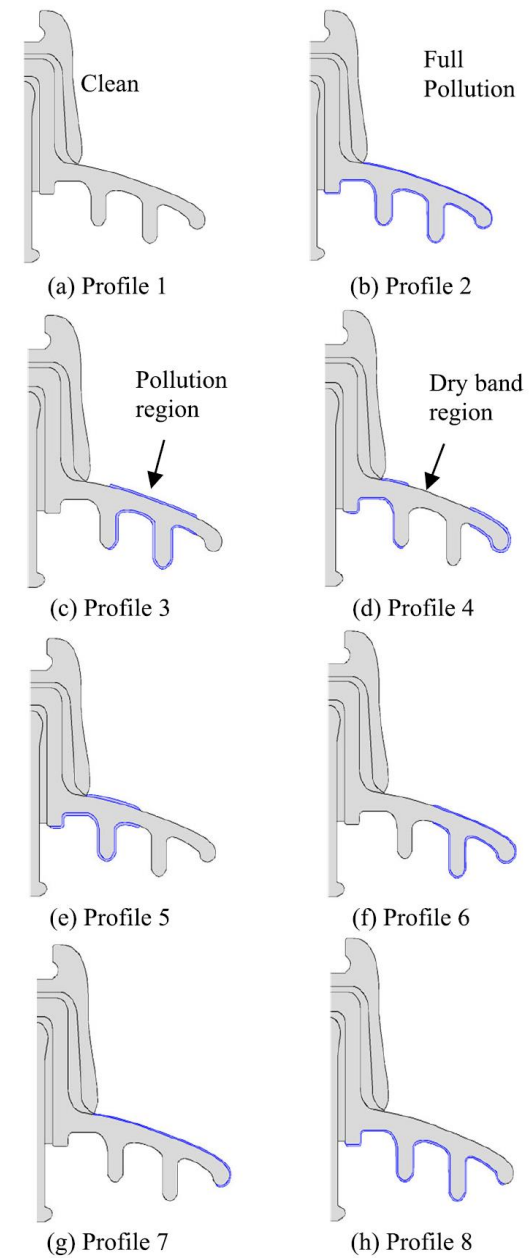
$$F(v) = \frac{1}{2} \iint \epsilon_r \left( \frac{dv}{dr} \right)^2 + \epsilon_z \left( \frac{dv}{dz} \right)^2 dr dz \quad (5.62)$$

As distribution of permittivity is isotropic,  $\epsilon_r = \epsilon_z = \epsilon$ , (5.62) can be written as:

$$F(v) = \frac{1}{2} \iint \epsilon |\nabla^* v|^2 ds \quad (5.63)$$

The contribution to the rate of change of  $F$  with  $V$  from the variance of the potential of node  $i$  in element  $e$  only,  $x_e$ , can be determined as:

$$\begin{aligned} x_e &= \frac{dF(v)}{dv} = \frac{1}{2} \iint \frac{\epsilon}{dv} \left( \left( \frac{dv}{dr} \right)^2 + \left( \frac{dv}{dz} \right)^2 \right) dr dz \\ &= \frac{\epsilon}{2} \iint \left( 2 \frac{dv}{dr} \frac{d}{dv_i} \left( \frac{dv}{dr} \right) + 2 \frac{dv}{dz} \frac{d}{dz_i} \left( \frac{dv}{dz} \right) \right) dr dz \end{aligned} \quad (5.64)$$



Considering the effect of pollutant conductivity on distribution of electric field,

$$F^*(v) = \frac{1}{2} \iint (\sigma + j\omega\varepsilon) |\nabla^* v|^2 ds \quad (5.65)$$

where  $\sigma$  is conductivity,  $\omega$  is angular frequency,  $\varepsilon$  is permittivity and  $v$  is the electric potential. The electric potential of any arbitrary point inside each sub-domain is expressed as

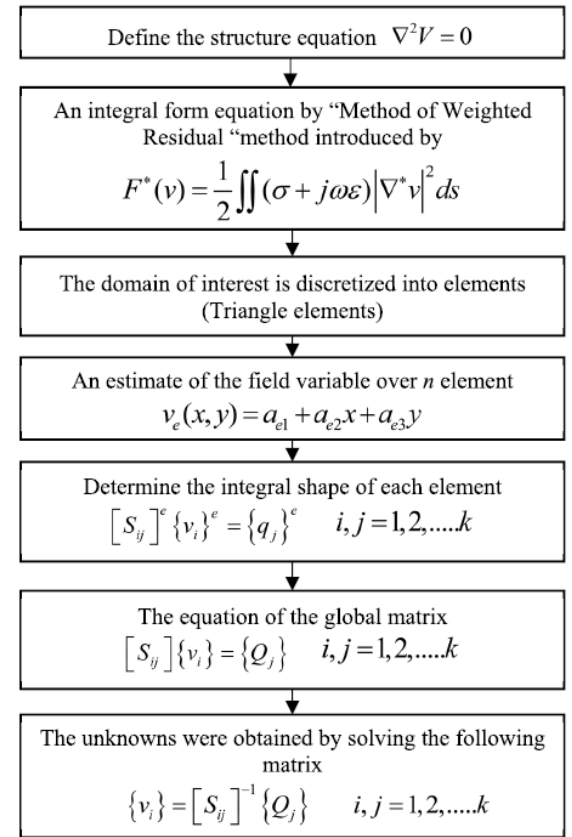
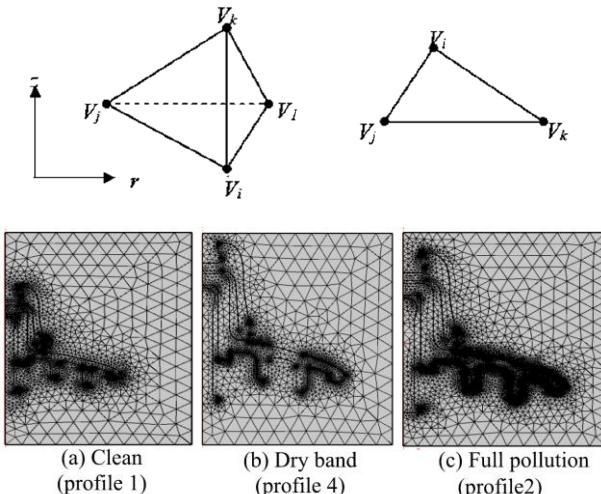
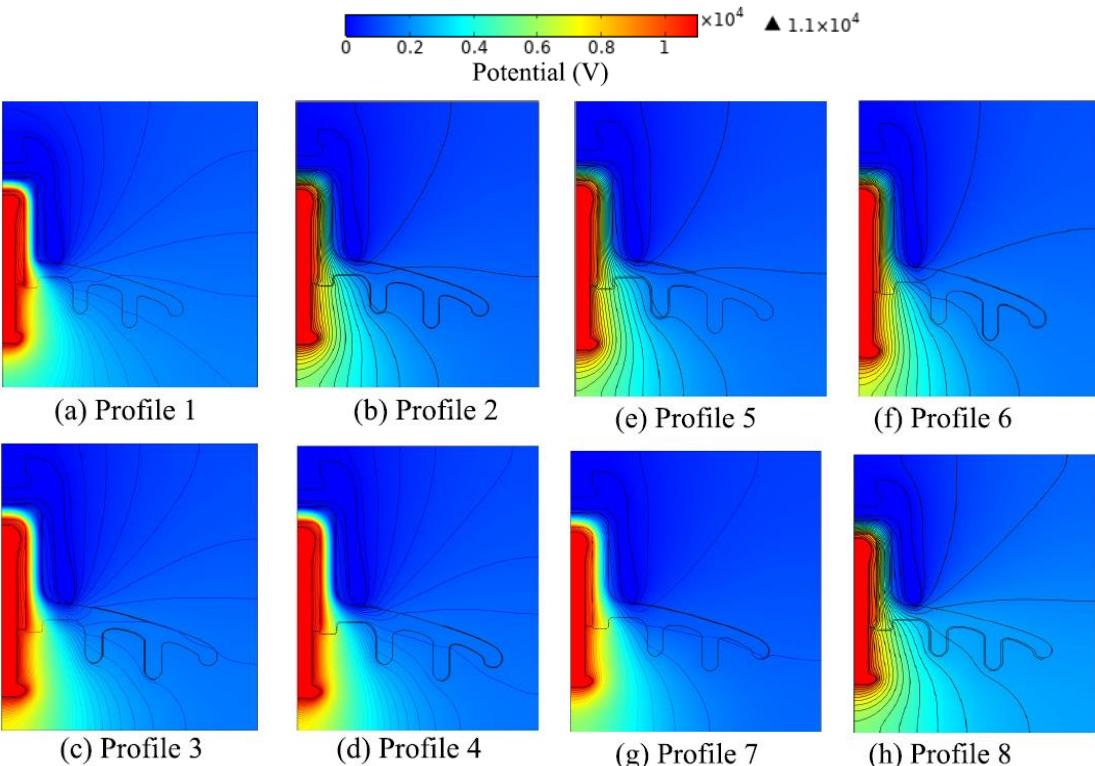
$$v_e(x, y) = a_{e1} + a_{e2}x + a_{e3}y \quad (5.66)$$

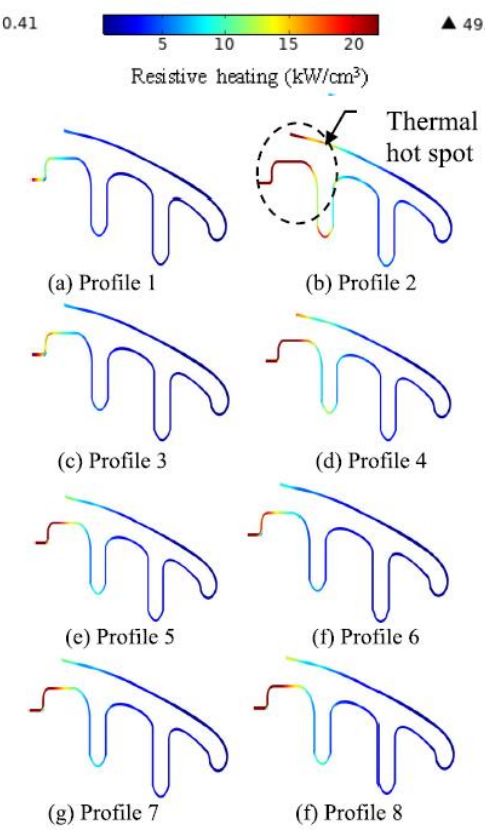
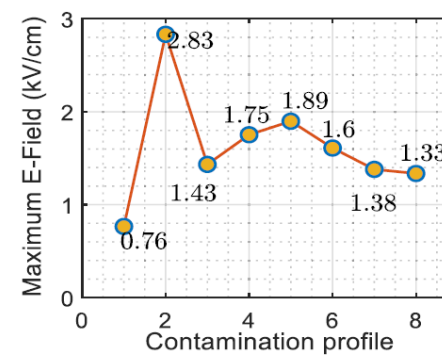
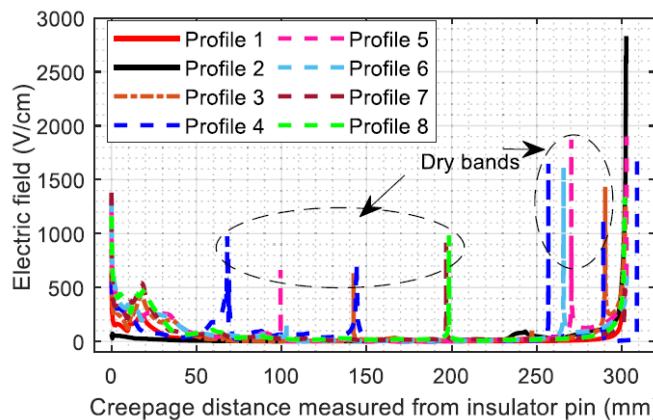
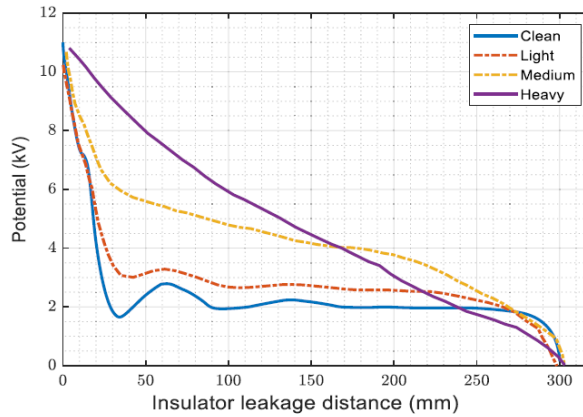
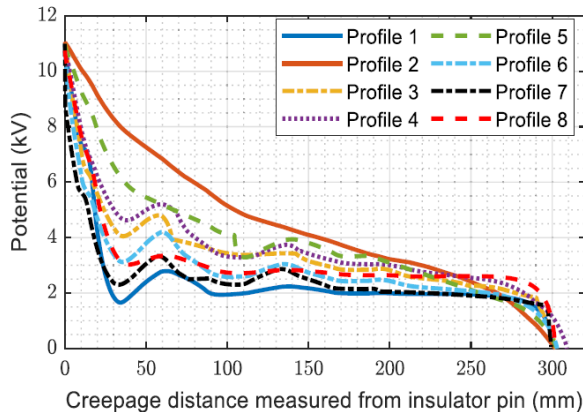
The electric potential at each node in the total network composed of many triangular elements is calculated by minimizing  $F(v)$ , potential energy, as

$$\frac{\partial F(v_i)}{\partial v_i} = 0, i = 1, 2, 3, \dots, k \quad (5.67)$$

The final matrix is written as

$$[S_{ij}]^e \{v_i\}^e = \{q_j\}^e, \quad j = 1, 2, \dots, k \quad (5.68)$$





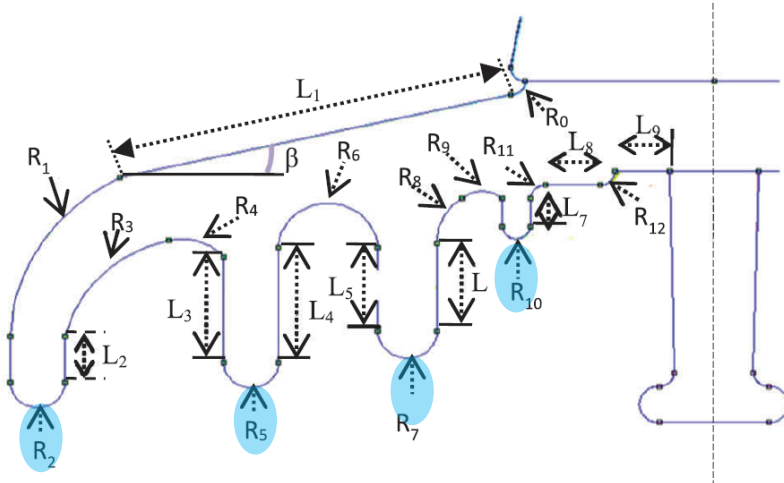
## Conclusion:

- Under the proposed contamination profiles, the increase in range of maximum electric field was found to be between 3% and 29%.
- The region of thermal hot spots appeared to be growing with a rise in the amount of contamination level in the region that is *close to the electrodes of the insulator*.
- It can be concluded that **flashover voltage gradient** decreases with an increase in salinity on the insulator surface. An increase in salinity (from 20 g/L to 80 g/L) decreases the flashover voltage gradient (within 0.731.1 kV/cm)
- Insulator with full pollution had a *lower value of flashover voltage gradient* compared to other contamination profiles.
- The use of glass insulators under pollution either *all-covered* or *in the presence of a dry band* has adverse effect on the performance of the insulators and hence instability of the insulation system used on the transmission lines.

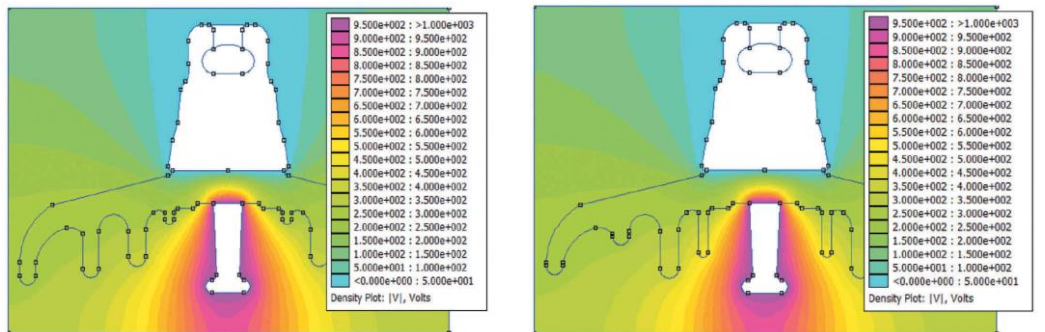
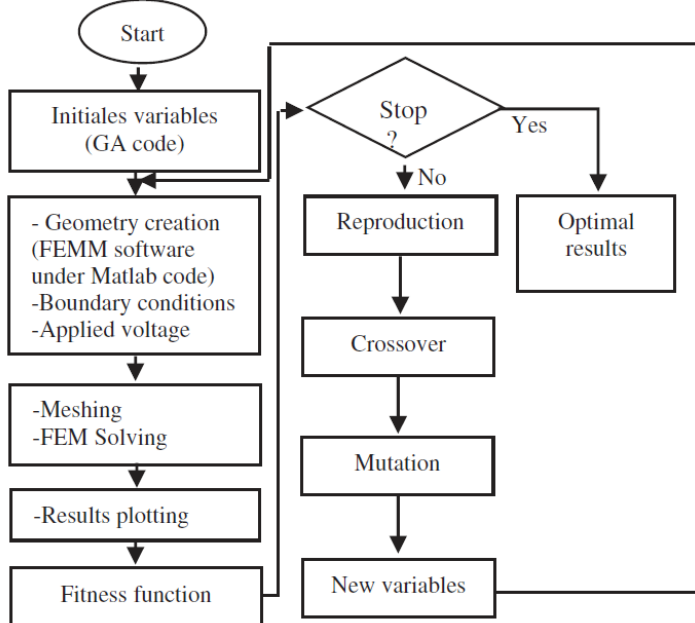
The next question is if the “optimal” shape of insulator can be determined.

## Assumption:

- The insulator shape is circular and symmetrical, and the model is examined on a bi-dimensional space using axis-symmetry.
- Any discharge event that may appear due to high electric field magnitudes is ignored.
- The effect of water droplet deformation due to the electric field stresses is neglected



Radius (mm)	Angles (°)	Lengths (mm)
$R_0 = 3$	$\varphi_0 = 90$	$L_1 = 81$
$R_1 = 42$	$\varphi_1 = 60$	$L_2 = 8.5$
$R_2 = 5.5$	$\varphi_2 = 180$	$L_3 = 21.5$
$R_3 = 21$	$\varphi_3 = 63$	$L_4 = 23.5$
$R_4 = 11$	$\varphi_4 = 61$	$L_5 = 16$
$R_5 = 5.5$	$\varphi_5 = 180$	$L_6 = 17$
$R_6 = 10$	$\varphi_6 = 180$	$L_7 = 4.1$
$R_7 = 6$	$\varphi_7 = 180$	$L_8 = 10$
$R_8 = 10$	$\varphi_8 = 62$	$L_9 = 11$
$R_9 = 4$	$\varphi_9 = 90$	-
$R_{10} = 3$	$\varphi_{10} = 180$	-
$R_{11} = 3$	$\varphi_{11} = 90$	-
$R_{12} = 3$	$\varphi_{12} = 90$	-



- In the GA model, **electric field minimization** at the insulator pin is used as the fitness function (objective function)
- For each calculation step, the electric field is computed at the pin, and the Genetic Algorithm compares it to the last value until it reaches a minimum.
- Further benefit of this optimization is realized through the reduction of the lateral surface of the insulator, and hence, reducing the weight of the insulator
- Maximum E-field on the pin was reduced from 1.84 kV/cm for the standard reference model to 1.55 kV/cm for the optimized Model 1 shape, corresponding to a 16% reduction. As expected, the voltage distribution on the insulator surface is **highly non-linear**, which leads to extremely high **localized electrical stresses** around the pin region. These stresses, in turn, lead to dry band formation and initiation of surface discharges

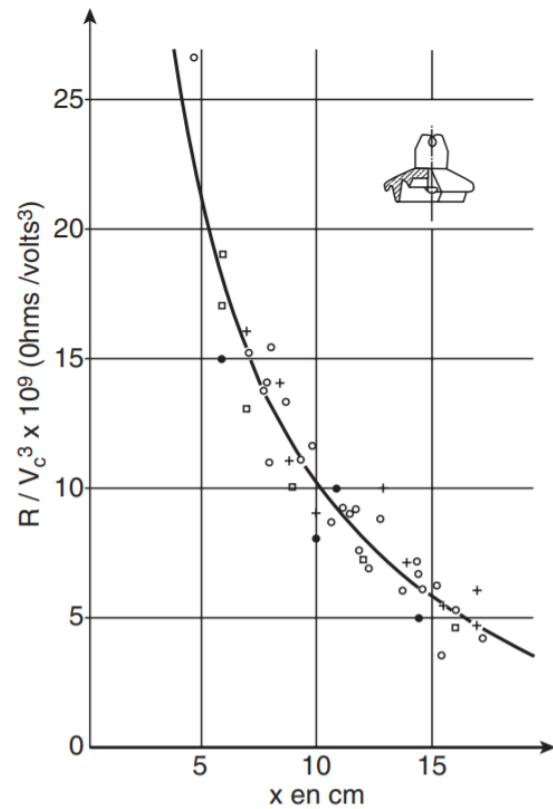
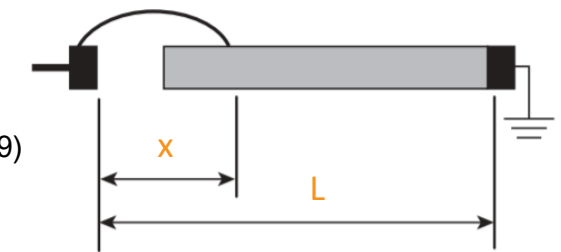
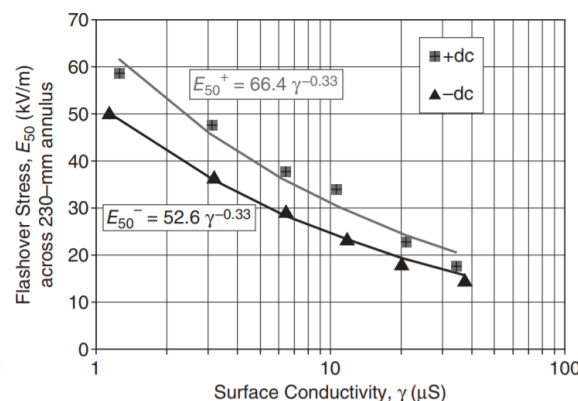
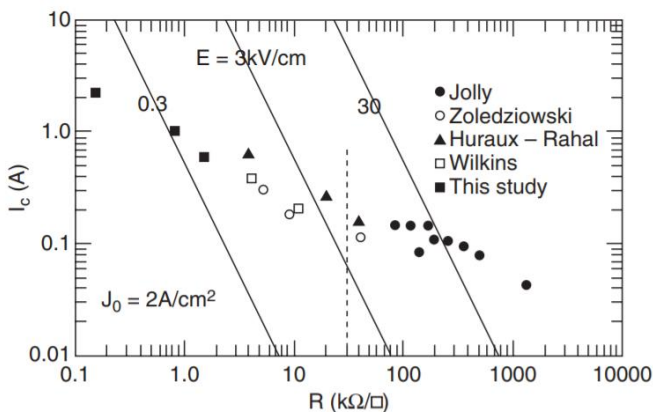
Recall the AC flashover on a polluted surface is considered as an arc in series with a residual resistance consisting of an ice layer that is not bridged by the arc. The circuit equation for this model is as follows:

$$\text{Obenaus Model: } V_m = AxI_m^{-n} + I_m R_p(x), \quad \text{AC Min Reignition Gradient: } V_m + \frac{kx}{I_m^b} = \frac{716x}{I_m^{0.526}} \quad (5.69)$$

where  $V_m$  is peak value of applied voltage (V), A and n are arc constants, x is local arc length (cm),  $I_m$  is the peak value of leakage current (A), and  $R_p(x)$  is the residual resistance ( $\Omega$ ) of pollutant layer from the arc root at x to the ground electrode.

For DC condition, an electrode voltage drop  $V_e$  is added.

The following is the flashover data with breakdown induced arc propagation model for arc root current density  $2\text{A}/\text{cm}^2$  versus surface resistivity.

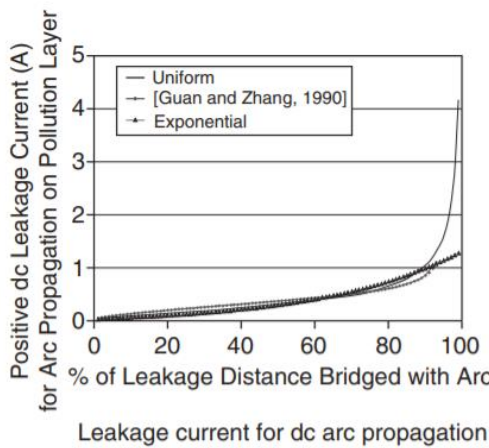


Anti-fog disk insulator

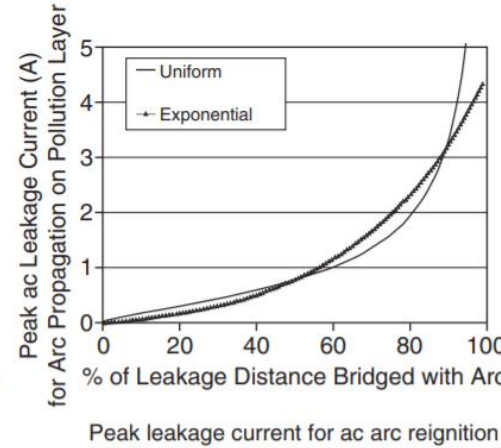
To evaluate the flashover voltage, engineering solution often for each value of x

1. Select a trial current I.
2. Calculate the corresponding arc root radius  $r_0$
3. Calculate the pollutant layer resistance  $R_p(x)$  from the arc root location to the insulator terminals
4. Calculate total voltage with (5.69), or reignition voltage for AC case as well.
5. Find the trial current I that minimize V, the sum (square of the difference for AC case) of arc voltage and voltage drop along the pollution layer, for each position x.
6. Read out the maximum value of V for all value of x.

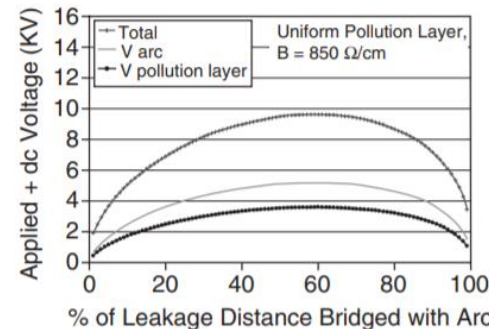
A LS-SVM regression method was proposed to construct a **dynamic flashover model** of the polluted insulators. The LS-SVM model are developed by getting the relationship between **critical flashover voltage** (FOV) and input variables, such as **insulator height**, **insulator diameter**, **leakage length of the insulator for an element**, **surface conductivity**, **number of element on a chain** and **number of shed**.



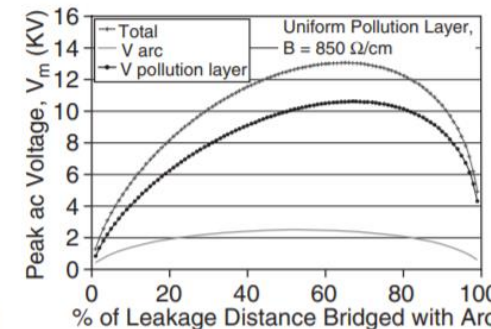
Leakage current for dc arc propagation



Peak leakage current for ac arc reignition



Uniform pollution layer  $R_p(x) = 850\Omega/\text{cm}.(L - x)$



Given a training set  $\{x_i, y_i\}$ ,  $i = 1, 2, \dots, N$  with input data  $x_i$  and output data  $y_i$ . The following regression model is constructed by a non-linear mapping function  $\varphi(\cdot)$ , where  $w$  is the weighting vector and  $b$  is the bias term.

$$y = w^T \varphi(x) + b \quad (5.70)$$

In SVM, it is necessary to minimize a cost function  $C$  containing a penalized regression error, i.e.

$$\min C(w, e) = \frac{1}{2} w^T w + \frac{1}{2} \gamma \sum_{i=0}^N e_i^2 \quad \text{subj to. } y = w^T \varphi(x) + b + e_i, \quad i = 1, 2, \dots, N \quad (5.71)$$

To solve the optimization problem, the following Lagrange Function can be used.

$$L(w, b, e; \alpha) = \frac{1}{2} \|w\|^2 + \gamma \sum_{i=0}^N e_i^2 - \sum_{i=1}^N \alpha_i (w^T \varphi(x_i) + b + e_i - y_i) \quad (5.72)$$

where  $\alpha_i$  is Lagrange Multiplier.

The solution of (5.71) could be found with partially differentiating w.r.t  $w, b, e_i$  and  $\alpha_i$ ,

$$\begin{aligned}\frac{\partial L}{\partial w} = 0 \rightarrow w &= \sum_{i=1}^N \alpha_i \varphi(x_i), & \frac{\partial L}{\partial b} = 0 \rightarrow \sum_{i=1}^N \alpha_i &= 0, & \frac{\partial L}{\partial e_i} = 0 \rightarrow \alpha_i &= \gamma e_i, \\ \frac{\partial L}{\partial \alpha_i} = 0 \rightarrow w^T \varphi(x_i) + b - e_i - y_i &= \gamma e_i, & i &= 1, 2, \dots, N\end{aligned}\tag{5.73}$$

then

$$w = \sum_{i=1}^N \alpha_i \varphi(x_i) = \sum_{i=1}^N \gamma e_i \varphi(x_i)\tag{5.74}$$

where a positive definite kernel is used as follows:

$$K(x_i, x_j) = \varphi(x_i)^T \varphi(x_j)\tag{5.75}$$

An important result of this approach is that the weights ( $w$ ) can be written as linear combinations of Lagrange Multipliers with the corresponding data training ( $x_i$ ). Putting the result of (5.74) into (5.70), the following result is obtained:

$$y = \sum_{i=1}^N \alpha_i \varphi(x_i)^T \varphi(x) + b = \sum_{i=0}^N \alpha_i \langle \varphi(x_i)^T, \varphi(x) \rangle + b\tag{5.76}$$

For a point  $y_i$  to be evaluated it is:

$$y_i = \sum_{i=1}^N \alpha_i \varphi(x_i)^T \varphi(x_j) + b = \sum_{i=0}^N \alpha_i \langle \varphi(x_i)^T, \varphi(x_j) \rangle + b\tag{5.77}$$

The  $\alpha$  vector follows from solving a set of linear equations:

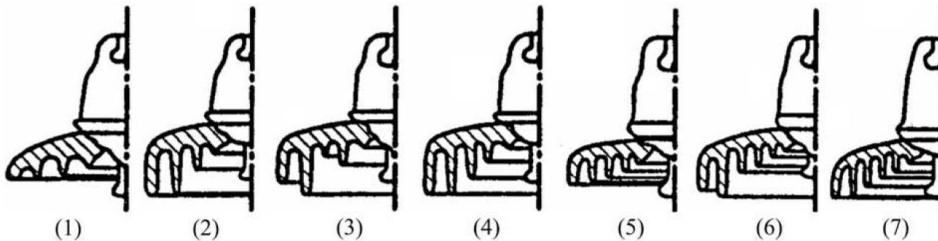
$$A \begin{bmatrix} \alpha \\ b \end{bmatrix} = \begin{bmatrix} K + 1/\gamma & 1_N \\ 1_N^T & 0 \end{bmatrix} \begin{bmatrix} \alpha \\ b \end{bmatrix} = \begin{bmatrix} y \\ 0 \end{bmatrix} \rightarrow \begin{bmatrix} \alpha \\ b \end{bmatrix} = A^{-1} \begin{bmatrix} y \\ 0 \end{bmatrix}\tag{5.78}$$

In applications involving nonlinear regression, it is enough to change the inner project  $\langle \varphi(x_i), \varphi(x_j) \rangle$  of (5.77) by a kernel function and the  $ij$ th element of matrix  $K$  equals to (5.75). If this kernel function meets **Mercer's condition** the kernel implicitly determines both a nonlinear mapping  $x \rightarrow \varphi(x)$  and the corresponding inner product  $\varphi(x_i)^T \varphi(x_j)$ . This leads to the following nonlinear regression function:

$$y = \sum_{i=1}^N \alpha_i K(x_i, x) + b, \quad y_j = \sum_{i=1}^N \alpha_i K(x_i, x_j) + b\tag{5.79}$$

For LS – SVM, there are many **kernel functions**. These kernels are linear, polynomial, radial basis function (RBF), spline, bspline, sigmoid, etc, such as

$$K(x_i, x_j) = \exp\left(-\frac{\|x_i - x_j\|^2}{\sigma^2}\right), \quad K(x_i, x_j) = (x_i^T x_j + t)^d\tag{5.80}$$



Insulator type	Hi(mm)	D(mm)	L(mm)	d
1	146	254	280	4
2	146	254	432	4
3	165	320	512	5
4	180	320	545	5
5	197	320	457	5
6	197	400	686	6
7	250	420	718	6

Each pattern of the training set contains six inputs which characterizes parameters of  $H_i, D, L, \sigma, n, d$  (height, insulator diameter, creepage distance, surface conductivity, number of element in a chain and number of shed) and one output which represents  $V_C$  the critical FOV.

To have a more accurate prediction result, the data set must be appropriately normalized before training. This prevents any parameter from domination to the output value and provides better convergence and accuracy of learning process. The transformation formula is given by:

$$u_{nor} = \frac{u}{\vec{1}_N (\sqrt{\text{diag}(u^T u)})^T} \quad (5.81)$$

where  $u$  are the input or output data sets,  $\vec{1}_N = [1 \ 1 \ 1 \ \dots \ 1]^T$  is an N-dimension vector. N represents number of patterns in the input or output set. To achieve high performance with LS – SVM model, some parameters should be tuned, such as the regularization parameter  $\gamma$  and the kernel parameter corresponding to the kernel type ( $\sigma$  or  $d$ ). An efficient search strategy is needed. A two-stage grid search process on the parameter space is employed.

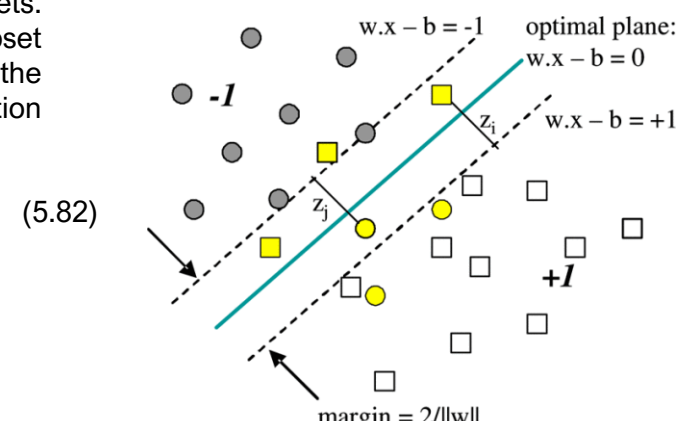
In **L-fold cross-validation**, the training data is randomly split into L roughly equal subsets. An LS-SVM prediction is trained using (L-1) of these subsets and validated on the subset left out. This procedure is repeated L times with each of the L subsets used as the validation subset in turn. Averaging the validation errors over the L trials gives a prediction of the generalization error with RMSE:

$$\text{RMSE} = \sqrt{\frac{1}{N} \sum_{k=1}^N (u_{ac,k} - y_{pre,k})^2} \quad (5.82)$$

Other statistical parameters can also be used.

$$R^2 = 1 - \sum_{k=1}^N \left[ \frac{u_{ac,k} - y_{pre,k}}{u_{ac,k}} \right]^2, \text{COV} = \frac{\text{RMSE}}{|\bar{u}_{ac,k}|},$$

$$\text{MEF} = \frac{1}{N} \sum_{k=1}^N \left( \frac{|u_{ac,k} - y_{ref,k}|}{\max(u_{ac,k}) - \min(u_{ac,k})} \right) \quad (5.83)$$



Consider again Obenous model and the associate critical voltage with arc length  $x_c$ .

$$U = xAI^{-n} + (L - x)R_p(x)I \rightarrow U_c = x_c AI_c^{-n} + (L - x_c)KR_p I_c \quad \text{where } K = 1 + \frac{L}{2\pi F(L - x_c)} \ln \frac{L}{2\pi F \sqrt{\frac{(\pi D_r \sigma_p A)^{\frac{1}{n+1}}}{1.45\pi}}} \quad (5.84)$$

At the critical condition the length of arc takes the value  $x_c$  with critical current  $I_c$  and critical voltage  $U_c$ .

$$x_c = \frac{1}{n+1}L, \quad U_c = \frac{A}{n+1}(L + \pi D_r F K n)(\pi D_r \sigma_p A)^{-\frac{n}{n+1}}, \quad I_c = (\pi D_r \sigma_p A)^{-\frac{n}{n+1}} \quad (5.85)$$

where  $D_r$  is the diameter of the insulator.

Similar to LS – SVM case, ANN can be employed to build up flashover model for insulator string. The neuron output is given by

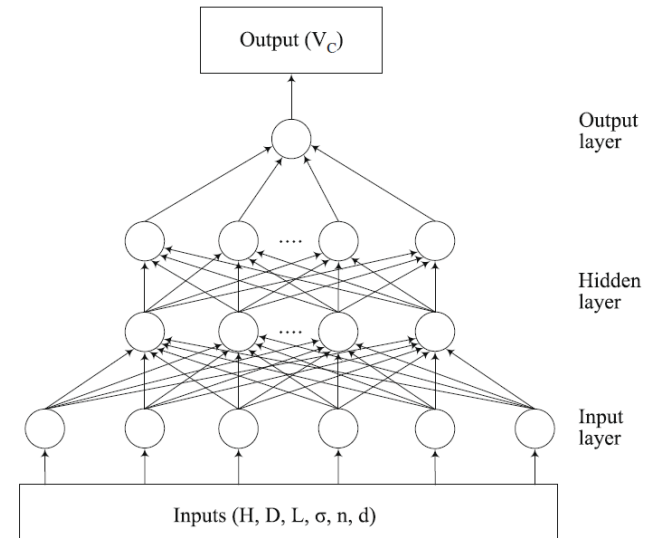
$$O_i = n_i; \quad n_k = \sum_{j=1}^{N_j} w_{kj} O_j, \quad k = 1, 2, \dots, N_k \quad (5.86)$$

where  $w_{kj}$  is the connection weight between neuron  $k$  and neuron  $j$  and  $N_k$  and  $N_j$  are the number of neurons in the output and hidden layers respectively. The neuron outputs are given by

$$O_k = \frac{1}{1 + \exp(-n_k + \theta_k)} = f_k(n_k, \theta_k) \quad (5.87)$$

where  $\theta_k$  is the threshold of neuron  $k$ , and the activation functions  $f_k$  is a sigmoid function. The error function and hence the overall error measure for all input-output pattern is given by

$$E_p = \frac{1}{2} \sum_{k=1}^{N_k} (t_{pk} - O_{pk})^2, \quad E = \sum_{p=1}^{N_p} E_p \quad (5.88)$$

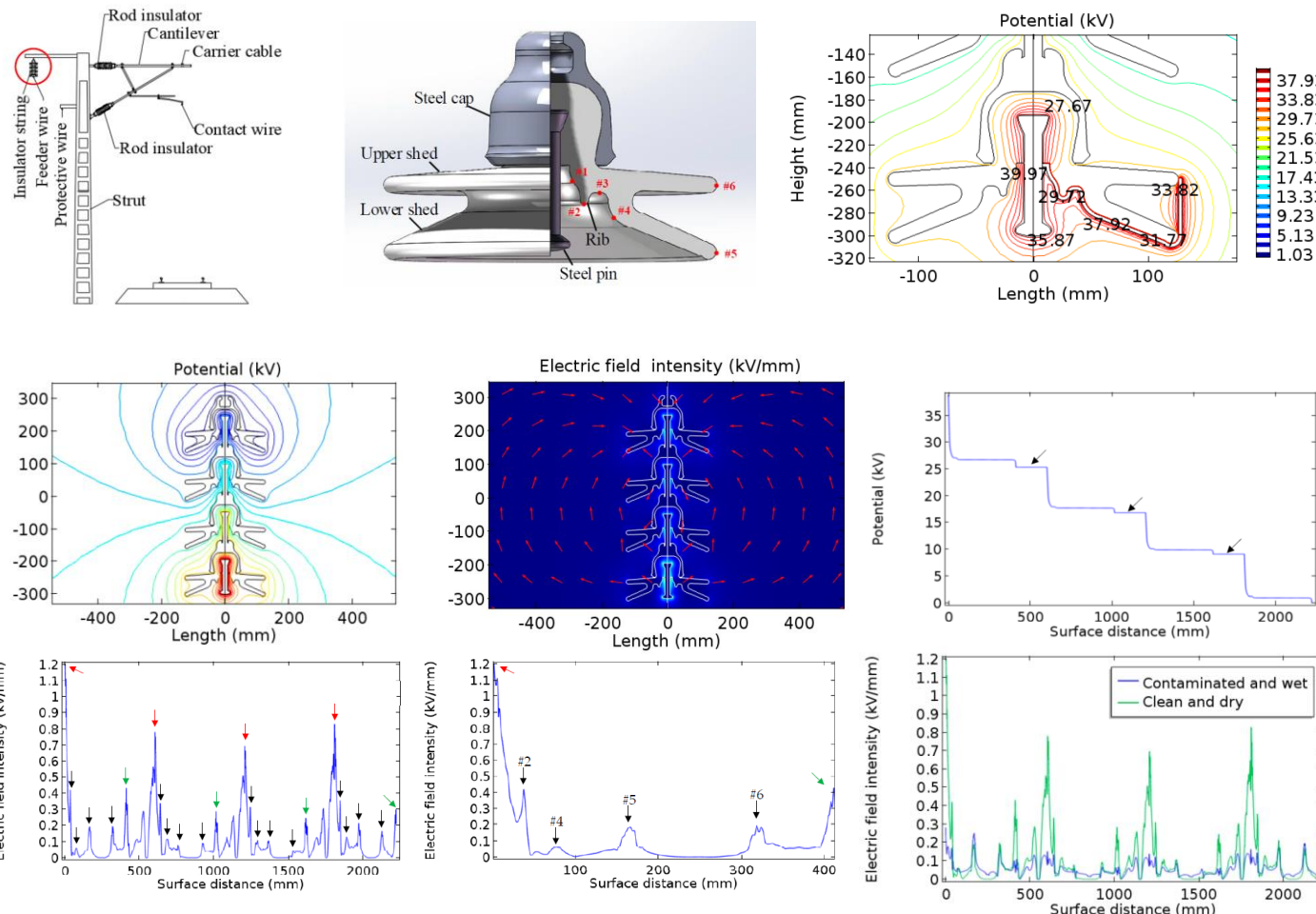


The following includes the FEM model of insulator strings under dry and clean condition and contaminated and wet condition for railway application. From the simulation results:

1. The appearance of a contaminated wet layer weakened the field intensity at high voltage and grounded ends, and the U-shaped distribution of electric field was disrupted. The overall E-field distribution was **flatter** than that under clean and dry condition. The E-field intensity and current density at high voltage end were the highest, and the partial arc was apt to occur at the high voltage end.
2. Occurrence of partial arc caused obvious distortion of E-field. In case of arc extension, the sudden rise of field intensity was mostly at the rib and shed edge. The rib and shed edge performed a certain hindrance to the extension of arc. In case of arc extension, E-field intensity of arc head and insulator surface did not exceed that of air breakdown. The reason for arc development is attributed to **thermal**

**Ionization.** Setting the rib near the insulator's high voltage end and increase number of sheds are helpful in hindering the development of arc.

3. In case of arc bridging sheds, there appeared a distinct local max field intensity at the edge of bridged shed. As arc length increased, E-field intensity of arc head also increased, which results in accelerated arc development. Main factor to promote arc development can be attributed to electric breakdown. In case arc development speed is too fast after the arc bridge shed, insulator with different diameter sheds can be used, and a **booster shed** can be attached to the top of insulator string to increase the difficulty of arc bridging shed and reducing the occurrence of flashover.
4. Influence of **different arc starting positions**, **multiple partial arcs**, **arc shapes and paths**, **different conductivities** of contaminated layer, dry zone and environment around insulator string on E-field characteristics are the topics for future research.



## 5.2 Theory of Corona and its Effect

Corona can be defined as a self-sustained, partial electrical discharge in which the field-intensified ionization is localized over only a portion of the distance between the electrodes. This partial discharge precedes total gas breakdown. The type of discharge resulting in a spark or breakdown of a gap depends on the gas pressure, the gap length and shape, and the nature of applied voltage. Corona as a partial discharge can therefore be caused by a non-uniform electric field as between electrodes in a coaxial geometry. When the applied voltage is above a certain critical voltage, free electrons will be accelerated in the highly stressed area surrounding the conductor and cause excitation and ionization of the neutral air molecules. This results in the self-sustained discharge which produce significant macroscopic events.

This section aims to discuss modelling and formation of Corona, including the drift-diffusion equations for electron flows and modelling of q-u curve for further analysis on lightning overvoltage in overhead lines. At last, optimal location and sizing of corona ring based on particle swarm optimization (PSO) are presented as a mitigation measure for Corona effects.

Given that:

$R_a$  and  $R_b$  are radii of central and outer conductor of coaxial arrangement;  $R_c$  is the radius of corona sheath with  $R_{cm}$  denoting the radius of corona sheath at peak voltage; and  $R_{cb}$  is the radius of 'back-corona' sheath.  $E_n$  is the electric field at the surface of the central conductor at the corona onset;  $E_{nb}$  is the electric field at the surface of the central conductor at the onset of back corona;  $E_c$  is the critical field at the outer edge of the corona sheath; and  $E_{cb}$  is the electric field at the outer edge of the back corona region.  $\rho_c$  is the volume charge density at unit radial length in the corona sheath;  $q_c$  is the total charge in the corona sheath;  $\rho_{cb}$  is the volume charge density at unit radial length in the back-corona sheath;  $q_{cb}$  is the total charge in the back corona region; and  $q_a$  is the charge per unit length on the central conductor;  $V(t)$  is the instantaneous voltage of the central conductor with  $V_p$  is the peak applied voltage;  $C$  is the capacitance per unit length of the coaxial arrangement; and  $T_1$ ,  $T_2$  and  $T_3$  are the time at which the applied voltage exceeding corona threshold voltage, reaching its peak value and occurring back corona from central conductor.

Assumption:

- The central conductor goes into corona whenever the electric field at the surface of the conductor exceeds a certain critical field which depends on the atmospheric conditions and the radius of the conductor. This critical field is calculated in the model simulations by appealing to Peek formula. After the inception of corona, the electric field at the surface of the central conductor decreases to the critical field necessary for the stable propagation of streamers. The time over which this downward transition in the electric field occurs is not known but will be evaluated by comparing model simulations with experimental results.
- The corona generation takes place uniformly around the central conductor and the spatial distribution of corona space charge in the corona sheath that surrounds the central conductor (i.e. the region within which corona space charge is confined) is only a function of radial distance measured from the axis of the conductor.
- At the outer boundary of the corona sheath the total electric field (i.e. the applied electric field plus the electric field created by the corona space charge) is equal to the critical field  $E''$  necessary for the continuous propagation of streamers.

- The volume charge density of the corona sheath at a given radial distance is inversely proportional to the corresponding radius. Note that such a charge distribution leads to a constant electric field inside the corona sheath.
- The instantaneous voltage applied to the coaxial cylinder (i.e. between the central conductor and the grounded outer cylinder) is equal to the voltage drop across the corona sheath plus the voltage drop in the region between the outer boundary of the corona sheath and the outer cylinder.
- The volume charge density of the advancing negative corona sheath is also assumed to decrease as the inverse of the radius.

**Stage 1:**  $t < T_1$ ,  $V(t) < V_n$

In this case, charge only resides on the central conductor and one can write

$$V(t) = \frac{q_a}{C}, \quad C = \frac{2\pi\epsilon_0}{\ln\left(\frac{R_b}{R_a}\right)} \quad (5.89)$$

The critical field necessary for corona inception  $E_n$  is given by

$$E_n = 3.15 \times 10^6 k\delta \left(1 + \frac{0.308}{\sqrt{\delta R_a}}\right) \quad (5.90)$$

where  $\delta$  is the relative density of air and  $k$  is a factor that considers the condition of conductor surface. Note that for coaxial geometry the value of  $V_n$  is related to  $E_n$  through the equation

$$V_n = E_n \log\left(\frac{R_b}{R_a}\right) R_a \quad (5.91)$$

where  $E_n$  is the electric field at which breakdown occurs in air for the atmospheric condition pertinent to the experiment.

**Stage 2:**  $T_1 < t < T_2$

After **corona inception**, E-field at the conductor surface decreases to critical field necessary for stable streamer propagation  $E_c$ .

E-field  $E(t)$  on the conductor surface at time  $t$  is given by:

$$E(t) = E_c + (E_n - E_c) \exp\left(-\frac{t}{\tau}\right) \quad (5.92)$$

The charge per unit length on the central conductor and instantaneous voltage between central conductor and outer conductor at a given time can be obtained by

$$q_a = 2\pi\epsilon_0 R_a E(t), \quad V(t) = \frac{q_a}{2\pi\epsilon_0} \log\left(\frac{R_b}{R_a}\right) + \frac{\rho_c}{\epsilon_0} \left[ (R_c - R_a) - R_a \log\left(\frac{R_c}{R_a}\right) \right] + \frac{\rho_c}{\epsilon_0} (R_c - R_a) \log\left(\frac{R_b}{R_c}\right) \quad (5.93)$$

The total charge in the corona sheath  $q_c$  is given by

$$q_c = \int_{R_a}^{R_c} 2\pi r \frac{\rho_c}{r} dr = 2\pi\rho_c (R_c - R_a) \quad (5.94)$$

Since the electric field at the outer edge of corona sheath is assumed to be  $E_c$ , the radius of the corona sheath is given by

$$R_c = \frac{q_c + q_a}{2\pi\epsilon_0 E_c} \quad (5.95)$$

The only parameter unknown in these equation is  $\rho_c$ , which can be obtained by solving these equations iteratively. Once has been done, the total charge Q in the coaxial arrangement can be obtained by

$$Q = q_a + q_c \quad (5.96)$$

It is assumed that the voltage source driving the discharge can produce instantaneously the charge demanded by the equations. Moreover, one can show that for  $t \gg \tau$ , the E-field in the corona sheath is uniform and equal to  $E_c$ . It agrees with the well-established fact that potential gradient in the streamer region is constant.

### Stage 3: $T_2 < t < T_3$

During this period, the magnitude and distribution of the charge residing on the corona sheath do not change from the values they had when the voltage was at its peak. However, the total charge in the coaxial arrangement should decrease to maintain the voltage difference between the electrodes as the applied voltage decreases. This is achieved by a reduction of charge residing on the central conductor. Recalling that  $R_{cm}$  is the maximum radius of the corona sheath and  $\rho_{cm}$  is the corresponding charge density

$$V(t) = \frac{q_a}{2\pi\epsilon_0} \log\left(\frac{R_b}{R_a}\right) + \frac{\rho_{cm}}{\epsilon_0} \left[ (R_{cm} - R_a) - R_a \log\left(\frac{R_{cm}}{R_a}\right) \right] + \frac{\rho_{cm}}{\epsilon_0} (R_{cm} - R_a) \log\left(\frac{R_b}{R_{cm}}\right) \quad (5.97)$$

Note that the situation is identical to that of a vacuum capacitor with a fixed constant charge floating between the two plates.

$$\frac{dV(t)}{dt} = \frac{1}{2\pi\epsilon_0} \log\left(\frac{R_b}{R_a}\right) \frac{dq_a}{dt} \quad (5.98)$$

The total charge at any instant is given by (5.96), where

$$q_c = \int_{R_a}^{R_{cb}} 2\pi r \frac{\rho_{cm}}{r} dr = 2\pi\rho_{cm}(R_{cm} - R_a) \quad (5.99)$$

### Stage 4: $T_3 < t$

In this stage, the voltage decreases to such an extent that the central wires goes into back-corona; and the back-corona region extends to a radius  $R_{cb}$ . During the generation of back corona the E-field at the central wire remains at the critical field necessary for the initiation of back corona. The equation which connects the instantaneous voltage to the electrical parameters of the cell is

$$V(t) = \frac{q_a}{2\pi\epsilon_0} \log\left(\frac{R_b}{R_a}\right) + \frac{\rho_{cb}}{\epsilon_0} \left[ (R_{cb} - R_a) - R_a \log\left(\frac{R_{cb}}{R_a}\right) \right] + \frac{\rho_{cb}}{\epsilon_0} (R_{cb} - R_a) \log\left(\frac{R_b}{R_{cb}}\right) + \frac{\rho_{cm}}{\epsilon_0} \left[ (R_{cm} - R_{cb}) - R_{cb} \log\left(\frac{R_{cm}}{R_{cb}}\right) \right] + \frac{\rho_{cm}}{\epsilon_0} (R_{cm} - R_{cb}) \log\left(\frac{R_b}{R_{cm}}\right) \quad (5.100)$$

Since E-field at the central conductor remains at  $E_{cb}$ ,

$$q_a = 2\pi\epsilon_0 R_a E_{cb} \quad (5.101)$$

Recall the E-field at the outer edge of the back-corona sheath is assumed to be  $E_{cb}$ , whence the radius of the back-corona region is given by

$$R_c = \frac{q_{cb} + q_a}{2\pi\varepsilon_0 E_{cb}}, \quad q_{cb} = 2\pi\rho_{cb}(R_{cb} - R_a) \quad (5.102)$$

The only unknown parameter in these equations is  $\rho_{cb}$ , and this could be found iteratively solving these equations. Note also that the sign of  $q_a$  and  $\rho_{cb}$  is opposite to that of  $\rho_{cm}$ . The total charge in the coaxial cylinder is given by

$$Q = q_a + q_{cb} + 2\pi\rho_{cm}(R_{cm} - R_{cb}) \quad (5.103)$$

### Corona Inception

The critical voltage or conductor surface gradient is often referred to as the corona inception voltage or corona onset gradient. The critical voltage is a function of conductor diameter, ambient temperature, pressure and humidity.

$$E_c = mE_0\delta \left(1 + \frac{K}{\sqrt{\delta r_c}}\right), \quad \delta = \frac{273 + t_0}{273 + t} \frac{p}{p_0} \quad (5.104)$$

where  $E_0$  and  $K$  are empirical constant depending on the nature of applied voltage,  $\delta$  is relative air density,  $r_c$  is conductor radius in cm, and  $m$  is the conductor surface roughness factor. [Given +DC:  $E_0 = 33.7$ ,  $K = 0.24$ ; - DC:  $E_0 = 31.0$ ,  $K = 0.308$ ].

A similar form for corona inception voltage gradient is given by

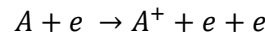
$$E_c [\text{kV/mm}] = 3m\delta \left(1 + \frac{0.301}{\sqrt{\delta r_c}}\right), \quad \delta = \frac{0.392b}{273 + t} \quad (5.104)$$

where  $b$  is the barometric air pressure in mmHg.

### Gas Discharge Process

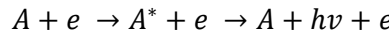
When a free electron is accelerated in the region close to a highly stressed electrode, collision with neutral air molecules cause excitation and ionization of these uncharged particles and develop successive electron avalanches. These collision between free electrons and neutral air molecules usually occur along the mean free path in direction of E-field. The effectiveness of ionization depends upon the energy that charged particles gain as they accelerate under the influence of electric stress. If energy imparted during the collision is large enough to dislodge an orbiting electron far away from the atom, the atom is said to be ionized. The mixture of ionized and neutral particles is what is then called a plasma or ionized gas.

#### Ionization:



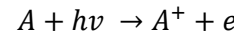
An atom (A) is said to be ionized ( $A^+$ ) if the energy imparted is large enough to dislodge an orbiting electron sufficiently far away from the atom such that it will not return to its original stage. There are several physical processes by which an atom can absorb energy, including electron collisions, ion collisions, photoionization and excitation.

#### Excitation:



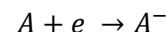
Colliding particles with energy less than ionization energy may, on collision, excite the gas atoms to higher states. An atom (A) is said to be excited ( $A^*$ ) when sufficient energy is given to the atom to allow the electrons in the outermost orbit to jump to next permissible higher energy level. The electron very quickly relaxes to its original state and excess energy is radiated as a photon having energy  $h\nu$ .

### Secondary Ionization:



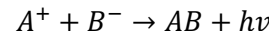
The released energy from an excitation process may ionize another atom whose ionization energy is equal to or less than the photon energy. This process is referred to as photoionization, or secondary ionization. Various other ionization methods in air including thermal ionization, nuclear emission and electric field ionization. **Ionization due to cathode collision** is also a secondary mechanism. This contributes greatly to the increase in the number of charged particles and thus higher plasma conductivity.

### Attachment and Detachment:



Atoms or molecules that lack one or two electrons in their outer orbits tends to capture free electrons, resulting in formation of negative ions ( $A^-$ ). The types of gases with atoms of this tendency are called electronegative gases. The process whereby negative ions are formed is referred to as electron attachment. The energy required for detachment is called **electron affinity** of the atom.

### Recombination:



In case where positive and negative charged particles coexist in the gas, the process of recombination can occur.

To obtain an estimate of ionization process, the electron energy distribution in a gas discharge should be considered. An **ionization coefficient**  $\alpha$  was defined by Townsend as the number of electron-ion pairs produced in the gas by a single electron moving through a unit distance in the direct of the field, the number of electrons produced by  $n(x)$  electrons advancing a distance  $dx$  in the direction of the field is given by

$$dn = n(x)\alpha dx \rightarrow \ln\left(\frac{n}{n_0}\right) = \int_0^x \alpha dx \rightarrow n = n_0 e^{\alpha x} \quad (5.105)$$

It means physically if diffusion and recombination are neglected, one electron will form  $e^{\alpha x}$  electrons when traversing a distance  $x$  from the cathode to the anode. In case of a non-uniform field where  $\alpha$  varies as a function of the electric field, then

$$n = n_0 e^{\int_0^x \alpha dx} \quad (5.106)$$

The dependence of quantity  $\alpha$  on the electric field  $E$  and pressure  $p$  can be written as

$$\frac{\alpha}{p} = f\left(\frac{E}{p}\right), \quad \frac{\alpha(p, T)}{p} = 4.778 \frac{293}{T} \exp\left(-\frac{221}{\frac{E}{p} 293}\right) \quad (5.107)$$

Electronegative gases lacking one or two electrons in their outer orbits have the tendency to accept free electrons and become negative ions. The energy that is necessary to remove an electron from a negative ion, thereby returning it to a neutral atom, is called the electron affinity of the atom. The **attachment coefficient**  $\eta$  is the number of negative ions created as a single electron moves a unit distance through the gas in direction of applied field. The number of electrons lost due to the attachment from  $n(x)$  electrons moving a distance  $dx$  is given by

$$dn - n(x)\eta dx \rightarrow n = n_0 e^{-\eta x} \quad (\text{or in general, } n = n_0 e^{\int_0^x -\eta dx}) \quad (5.108)$$

Since **ionization** and **attachment** usually takes place at the same time, the effects can be combined to obtain for a uniform field,

$$n = n_0 e^{(\alpha-\eta)x} \quad (\text{or in general, } n = n_0 e^{\int_0^x (\alpha-\eta) dx}) \quad (5.109)$$

Due to its much smaller mass, electrons behave differently to ions when subjected to an electric field. An electron will only lose a small amount of its original KE after each collision, and the applied field will cause electrons to gain energy much higher than their mean thermal energy. During inelastic collision, the cross-section due to electron impact still remains a strongly varying function of electron KE. Again, the electron drift velocity  $v_e$  is written as a function of E/p.

$$\frac{v_e}{p} = f \left( \frac{E}{p} \right) = 1.0 \times 10^6 \left( \frac{E}{p} \frac{T}{293} \right)^{0.715} \quad (5.110)$$

### Electron Diffusion:

Electrons can gain very high energies because of their small mass. The relationship between the electron drift velocity and electron diffusion is given by

$$D_e = v_e Z_m \frac{kT}{e} \frac{1}{E}, \quad Z_m = 21.0 \left( \frac{E}{p} \right)^{0.49} \quad (5.111)$$

where  $Z_m$  is known as Townsend energy factor,  $v_e$  is drift velocity,  $k$  is Boltzmann's constant,  $T$  is air temperature and  $e$  is electron charge. Townsend energy factor is the ratio of the mean agitation energy of the electrons and the mean molecular energy.

There are different modes of corona depending on the polarity, magnitude and type of voltage applied to the conductor. These various corona modes are more observable, and thus better defined, under DC voltage conditions. This is due to the inception conditions remaining constant and the space charge being moved in a constant direction away from the ionization region. In the time domain typical corona current pulses, for time  $t \geq 0$ , can be written in the form of

$$i(t) = i_p K (e^{-\alpha t} - e^{-\beta t}) \quad (5.112)$$

where  $i_p$  is current amplitude in mA and  $K$ ,  $\alpha$  and  $\beta$  are empirical constant.

Pulse Type	Amplitude	Rise Time	Duration	Repetition Rate
Positive Corona	10 – 50 mA	50 ns	250 ns	$10^3 – 5 \times 10^3$
Negative Corona	1 – 10 mA	10 ns	100 ns	$10^4 – 10^5$

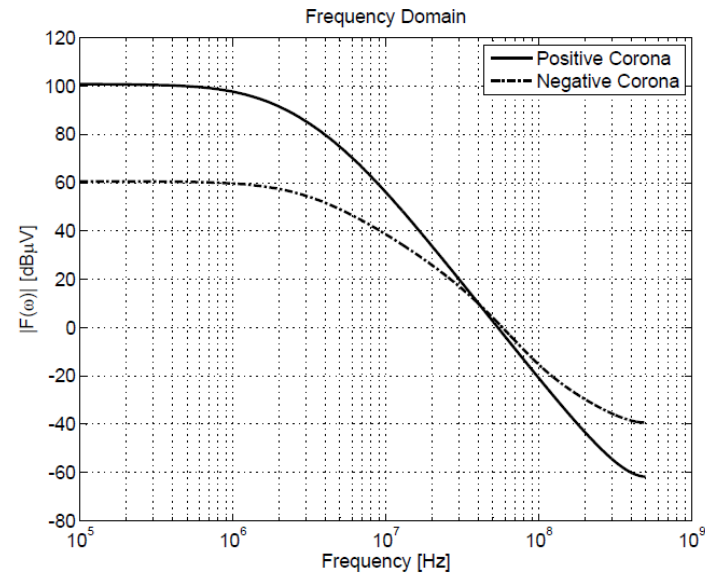
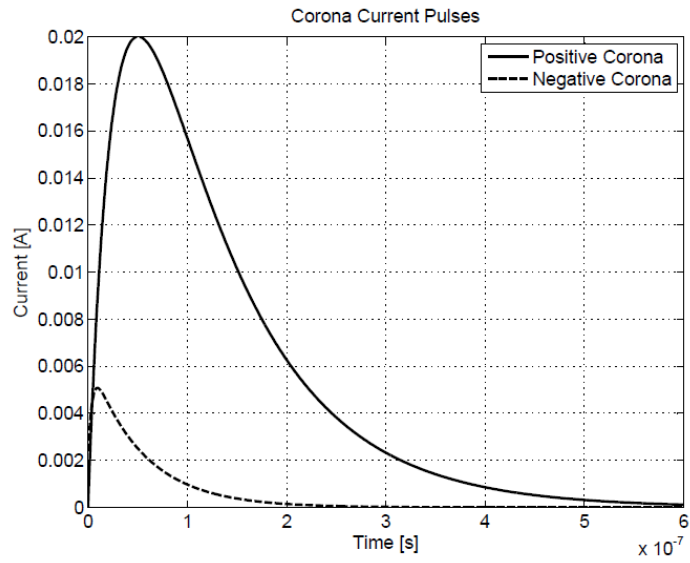
A typical corona pulse can be written as

$$\text{Positive Corona: } i_+(t) = i_p 2.335 (e^{-0.01t} - e^{-0.00345t}) \quad \text{Negative Corona: } i_-(t) = i_p 1.3 (e^{-0.019t} - e^{-0.285t}) \quad (5.113)$$

When a conductor is positive with respect to ground, electron avalanches move rapidly toward the conductor leaving behind positive ions that drift away. It is due to the rapid movement of the electrons and slower movement of the positive ions that result in the fast-rising edge of the positive corona pulse. When the conductor is negative with respect to ground, electron avalanches move away from the conductor and the heavy positive ions move toward the conductor. These ions are now moving in a very high electric field, and their movements are much faster than before. This results in the even faster rising edge of the negative corona pulse.

Consider also **Fourier Transform** version of Corona equation:

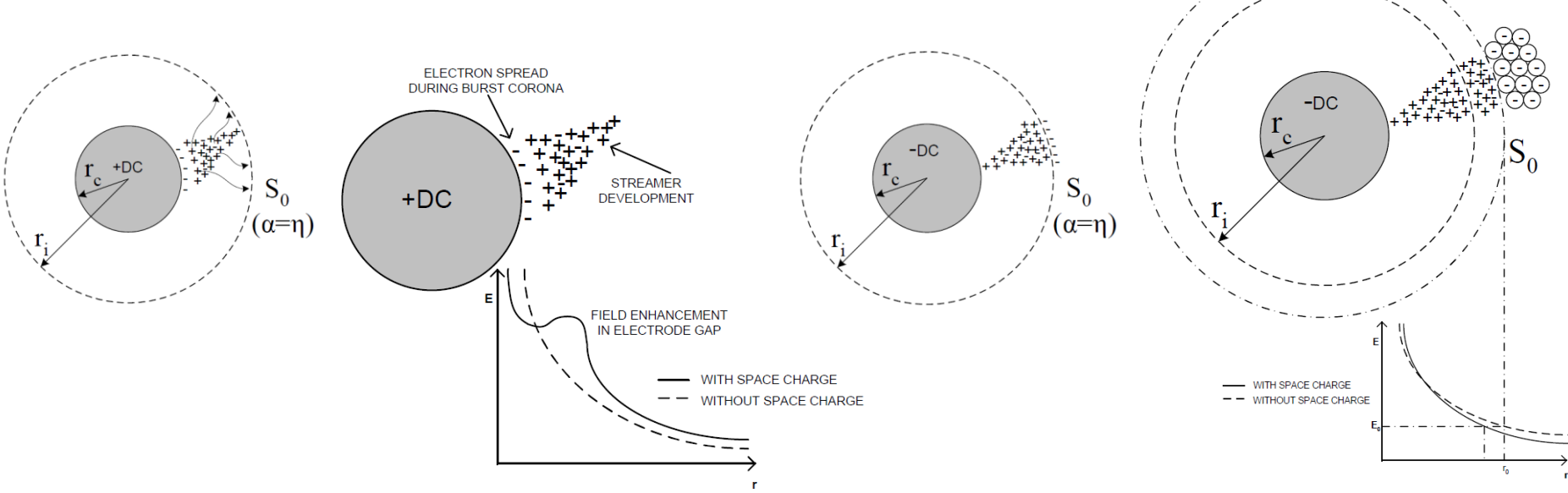
$$F(\omega) = \int_{-\infty}^{+\infty} i_p K [(e^{-\alpha t} - e^{-\beta t}) e^{-j\omega t} dt \rightarrow |F(\omega)| = i_p K \frac{\beta - \alpha}{\sqrt{(\alpha^2 + \omega^2)(\beta^2 + \omega^2)}}] \quad (5.114)$$



Critical Frequency for Different Pulse Shapes

Positive Corona     $f_\alpha = 1.59 \text{ MHz}$      $f_\beta = 5.49 \text{ MHz}$

Negative Corona     $f_\alpha = 3.02 \text{ MHz}$      $f_\beta = 45.36 \text{ MHz}$



## Positive Corona Mode

When a positive polarity is applied to an electrode and the voltage is above the inception level, there is an electron avalanche initiated at a point on the boundary surface  $S_0$  which develops towards the anode in a continuous increasing field.  $S_0$  is where  $\alpha = \eta$  and is referred to ionization region (radius  $r_i$ ). Electrons are accelerated towards high voltage conductor in this region, and will ionize the neutral air molecules. The increase in charge with the progress of electrons towards high voltage conductor in a non-uniform field is given as (5.109). During primary electron avalanche, molecules that are excited release photons that will give rise to secondary avalanche process. The highest ionization occurs in the close vicinity of anode conductor  $r_c$ .

Due to lower mobility of ions, positive space charge is left behind along the path of the avalanche development. The majority of free electrons are absorbed by the anode due to the fact that the electron attachment is less effective than in negative corona because of the high field intensity near the anode. Negative ions are therefore formed mainly in the low field region away from the anode. The positive space charge left behind in the vicinity of the anode will cause an increase of the electric field in the gap.

The highly energetic incoming electrons could not immediately be absorbed into the anode. Instead, they tend to *first spread out over the anode surface* before losing their energy through ionization of the gas particles.

**Burst Corona:** The first observable corona discharge mode results from ionization activities at the anode surface. This allows the incoming electrons to lose their energy before they are absorbed by the anode. Positive ions build up cumulatively close to the anode during this process and form positive space charge that suppresses the discharge. The spread of free electrons then move to another part of the anode. The discharge current is small positive pulses that each correspond to the spread of ionization over a small area of the anode. Its suppression is due to the positive space charge produced.

**Onset Streamer Discharge:** The next mode of corona discharge results from the radial development of the discharge. This is a discharge of large amplitude and fairly low repetition. The build up of positive ion space charge enhances the field immediately adjacent to the anode and hence attracts electron avalanches. A radially directed streamer channel develops that results in the onset streamer discharge.

**Positive Glow Discharge:** In this next mode of positive DC corona, there is a thin luminous layer that forms immediately adjacent to the anode surface where intense ionization activity takes place. The discharge current in this mode is the superposition of a DC with a small pulsating current component. The positive glow discharge is the result from a particular combination of rate of removal and creation of space charge. The field is of a nature that positive space charge forms quickly and hence promote surface ionization activities, but is low enough not to allow radial streamer or discharge development.

**Positive Streamer Discharge:** The last mode of anode DC corona is such that further increases in applied field causes streamers to form again and leads to a complete breakdown of the gap. The streamer current in this case is much more intense and may have a high repetition rate. The development of the breakdown streamer is directly related to the removal of the space charge by high field intensity.

## Negative Corona Mode

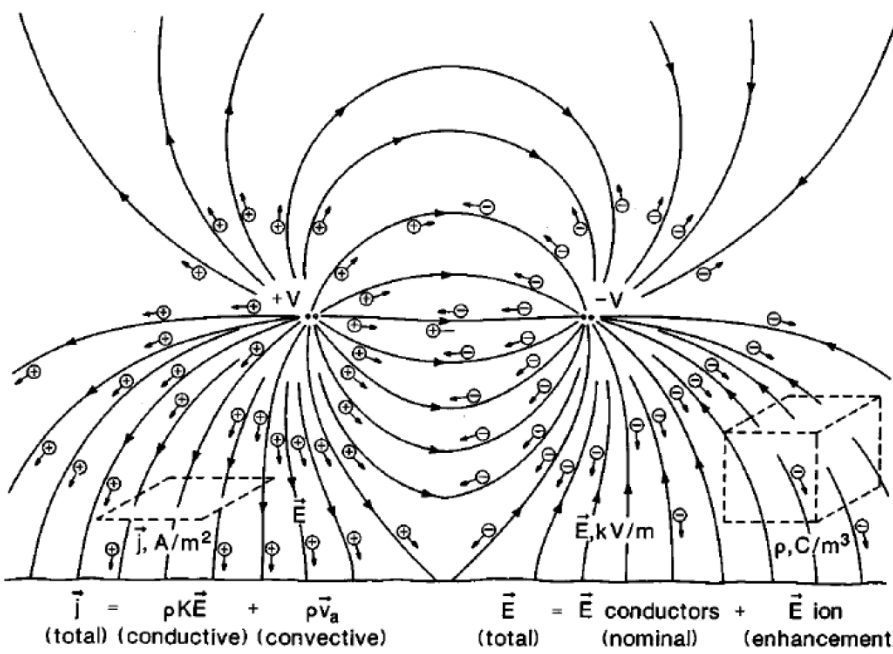
A high negative polarity direct voltage is applied to the conductor, thereby forming a nonuniform electric field in the air gap with respect to the plane at ground potential. A boundary  $S_0$  forms two regions in the air gap, where the electric field outside the boundary is not sufficient to maintain effective ionization. The electron avalanches are initiated at the cathode and develop in a continuously decreasing field toward the anode. There exists a boundary  $S_0$  where the electron avalanche will stop. The faster moving free electrons in the applied field will concentrate at the tip of the avalanche. This implies that a concentration of positive ions form in the gap between the cathode and boundary  $S_0$ , while the free electrons still move across the gap where they attach themselves to oxygen molecules to form negative ions.

These negative ions accumulate in the gap beyond the boundary  $S_0$  because of their low drift velocity, clearly leaving two space charge types in the gap.

**Trichel Streamer Discharge:** These are the first corona current pulses that can be observed. A streamer is initiated, it develops and then it is suppressed. After a short dead time the cycle is repeated. The duration of an individual streamer is a few hundred nanoseconds, while the dead time varies from a few microseconds to a few milliseconds or longer. The pulsative nature of the discharge is based on the active attachment process to suppress the ionization activity in a short period of time. The repetition rate is a function of the applied field and will increase linearly with the applied voltage. The pulse repetition rate is reduced at high electric fields, however, due to the establishment of a short duration stable discharge regime.

**Negative Pulseless Glow Discharge:** With a further increase in the applied voltage the Trichel pulses will, after reaching a critical frequency, change over into the next corona mode called the pulseless glow. In this mode of corona the wandering of the discharge on the cathode surface ceases and it becomes fixed at one point. One can distinguish between a bright spherical glow and a luminous conical positive column stretching outward from the point. The steady corona current produced increases continuously with voltage, until close to breakdown, it changes once again to negative streamers.

**Negative Streamer Discharge:** Negative streamers will appear if the applied voltage is increased further still. The glow discharge of the cathode implies that it depends on electron emission from the cathode by ionic bombardment. The streamer is characterized by intensive ionization and shows more effective space charge removal by the applied field.



The total current due to space charge created during corona processes will have displacement and conduction current components. The displacement current component is due to the induction effect and change in electric field due to the ions drifting away from the conductor, and is given by

$$\frac{dD}{dt} = \epsilon_0 \frac{dE}{dt} \quad (5.115)$$

The conduction current component is due to space charge neutralizing on the conductor, and is given by

$$J(t) = |e|n\mu E(t) \quad (5.116)$$

where  $e$  is the electron charge,  $n$  is the number density,  $\mu$  is the mobility and  $E$  is the electric field vector. The total current, integrated over some surface area  $S$ , is therefore given as:

$$i_{tot} = \int_S \left[ J(t) + \epsilon_0 \frac{dE(t)}{dt} \right] \cdot dS \quad (5.117)$$

The complex nature of problems encountered in **plasma physics** has been the **driving force** behind the development of various computer simulation techniques and numerical codes. These codes primarily focus on the **areas of kinetics and fluid description**. Particle simulation computes the motion of a collection of particles interacting with each other, with externally applied fields. It was shown that HVDC corona can be described by a fluid system which include electrons, positive and negative ions, air molecules. For simplicity, only typical fluids of positive and negative ions are considered.

**Fluid Continuity:** Total number of particles  $N$  in volume  $V$  can only change if there is a net flux of particles across the surface  $S$  bounding the volume. Considering the particles flux density as  $n\vec{v}$ , we then have by Stokes' theorem that

$$\frac{\partial N}{\partial t} = \int_V \frac{\partial n}{\partial t} dV = - \oint n\vec{v} \cdot dS = - \int_V \nabla \cdot (n\vec{v}) dV \quad (5.118)$$

Seeing that this must hold for any volume  $V$  that

$$\frac{\partial n}{\partial t} + \nabla \cdot (n\vec{v}) = 0 \quad (5.119)$$

In (5.118) and (5.119),  $\vec{v}$  is the particle velocity and  $n$  is the number density in number per  $\text{cm}^3$ . There is one such equation of continuity for each of the particle species (electrons, positive ions, negative ions). The sources and sinks of these particles are to be added to the right-hand side of these equations. The **fluid equation of motion** for any species including collisions is given by

$$mn \frac{d\vec{v}}{dt} = mn \left[ \frac{\partial \vec{v}}{\partial t} + (\vec{v} \cdot \nabla) \vec{v} \right] = \pm e n \vec{E} - \nabla p - mn v_c \vec{v} \quad (5.120)$$

with  $v_c$  being the **collision frequency**, which must be assumed a constant in order for this equation to be useful. The  $\pm e$  sign indicates the sign of the charge, while  $m$  is the particle mass and  $p$  is the pressure.

The collision frequency is given by

$$v_c = N \sigma_c \vec{v} \quad (5.121)$$

where  $N$  is the volume density of the background medium (neutral atoms per  $\text{cm}^3$ ) and  $\sigma_c$  is the effective collision cross-sectional area of the particle with velocity  $\vec{v}$  (or sufficiently large  $v_c$ ) a fluid element will not move into the regions of different  $\vec{E}$  and  $\nabla p$  in a collision time. The convective derivative is defined as

$$\frac{d\vec{v}}{dt} = \frac{\partial \vec{v}}{\partial t} + (\vec{v} \cdot \nabla) \vec{v} \quad (5.122)$$

Setting the left-hand side of (5.120) equal to zero, we have for an **isothermal plasma**

$$\vec{v} = \mu \vec{E} - D \frac{\nabla n}{n} \quad (5.123)$$

with mobility  $\mu$  and diffusion constant  $D$  connected by Einstein relation

$$\mu = \frac{|q|}{m v_c}, \quad D = \frac{K T}{m v_c} \rightarrow \mu = |q| \frac{D}{K T} \quad (5.124)$$

The electron fluid, positive ion fluid and negative ion fluid are described by the continuity equation:

$$\frac{\partial n_e}{\partial t} + \nabla \cdot (n_e \vec{v}_e) = G_e - L_e; \quad \frac{\partial n_p}{\partial t} + \nabla \cdot (n_p \vec{v}_p) = G_p - L_p; \quad \frac{\partial n_n}{\partial t} + \nabla \cdot (n_n \vec{v}_n) = G_n - L_n \quad (5.125)$$

where  $n_e$  is the number density,  $\vec{v}_e$  is the fluid velocity,  $G_e$ ,  $L_e$  are electron source and sink respectively.  $G_e$  results from process such as **electron impact ionization**, **photoionization** and also **detachment of electrons** from negative ions. Similarly,  $L_e$  is from recombination with positive ions and attachment to neutral particles.

### Momentum Conservation:

$$\vec{v}_p = \mu_p \vec{E} - D_p \frac{\nabla n_p}{n_p}; \quad \vec{v}_n = \mu_n \vec{E} - D_n \frac{\nabla n_n}{n_n} \quad (5.126)$$

It should be noted that  $\mu_n$  has a negative sign so that the negative ions drift in the  $-\vec{E}$  direction. The electric field in the momentum equations is given by Gauss's Law such that

$$\nabla \cdot \vec{E} = \frac{1}{\epsilon_0} (n_p q_p + n_e q_e + n_n q_n) \quad (5.127)$$

where  $q_e = -|e|$  is electron charge,  $q_p = +|e|$  is positive ion charge and  $q_n = -|e|$  is negative ion charge. For HVDC application, the electric field is electrostatic such that

$$\vec{E} = -\nabla \varphi \quad (5.128)$$

The rule for dynamics of particles is given by the **equation of motion**. Similar to (5.126), the velocity  $\vec{v}_i$  at the particle location is related to field quantity at the location, and the momentum conservation derived from Boltzmann equation for ions provided that

$$\frac{d\vec{x}_i}{dt} = \vec{v}_i; \quad \vec{v}_i = \mu_i \vec{E} - D_i \frac{\nabla n_i}{n_i} \quad (5.129)$$

### Field Equations:

Given the potentials on the boundaries and the space charge within this region of simulation, the potential distributions are completely specified by Poisson's equation such that

$$\nabla^2 \varphi = -\frac{|e|}{\epsilon_0} (n_p - n_e - n_n), \quad \varphi = \varphi_{sf} + \varphi_{sc} \quad (5.129)$$

where  $|e|$  is the charge magnitude,  $n_p, n_e, n_n$  are positive ion, electron and negative ions. The total potential  $\varphi$  is taken as the superposition of the **space charge free** potential ( $\varphi_{sf}$ ) and the **space charge** potential ( $\varphi_{sc}$ ).

The space charge free solution is due to the applied voltage and geometry, while the space charge solution is due to the space charge only. Due to the fast rate of change of  $\varphi$  close to the conductor, the first order FEM may result in large numerical errors. It is for this reason the **Laplacian space charge** free problem is solved using the **charge simulation method** (CSM), while the **Poissonian space charge** problem is solved using the **finite element method** (FEM).

Space Charge Free Solution	Space Charge Solution
$\nabla^2 \varphi_{sf} = 0$	$\nabla^2 \varphi_{sc} = - e  \frac{n_p - n_e - n_n}{\epsilon_0}$
$\varphi_{sf} \Big _{conductor} = \pm V$	$\varphi_{sc} \Big _{conductor} = 0$
$\varphi_{sf} \Big _{sheath} = 0$	$\varphi_{sc} \Big _{sheath} = 0$

### Conduction and Displacement Current:

Total current flowing to and experienced on the surface area (S) of the electrodes per unit length is given by

$$i(t) = \int_S \left( \vec{J} + \epsilon_0 \frac{d\vec{E}}{dt} \right) \cdot d\vec{S} \quad (5.130)$$

where  $\vec{J}$  is the conduction current density component given by

$$\vec{J} = |e|(n_p \vec{v}_p - n_e \vec{v}_e - n_n \vec{v}_n) \quad (5.131)$$

and the displacement current density component is approximated by

$$\frac{d\vec{D}}{dt} = \epsilon_0 \frac{d\vec{E}}{dt} \approx \epsilon_0 \frac{\vec{E}(t) - \vec{E}(t - \Delta t)}{\Delta t} \quad (5.132)$$

The total current flowing to the electrode per unit length can therefore be determined by

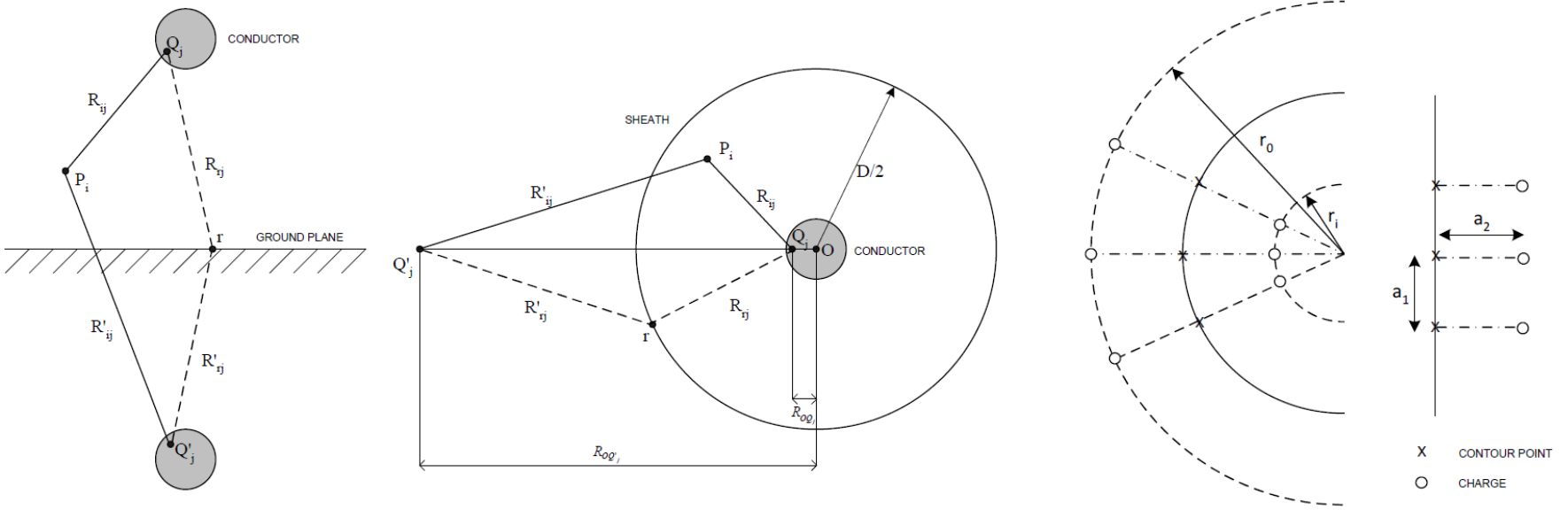
$$i_{tot}(t) = \sum_{k=1}^{N_m} \left[ \vec{J}(t) + \epsilon_0 \frac{d\vec{E}}{dt} \right]_k \cdot \hat{n}_k L_k \quad (5.133)$$

where  $m = a, c$  or  $s$  representing the anode, cathode or sheath respectively,  $N_a$ ,  $N_c$  and  $N_s$  are the number of boundary node points on the anode, cathode and sheath respectively,  $\hat{n}_k$  is the unit vector normal to the electrode surface at node point  $k$ ,  $L_k$  is the distance between the boundary node point ( $k$ ) and ( $k+1$ ).

### Charge Simulation Method (CSM)

CSM is a numerical method for the computation of electrostatic field with fictitious line charges as particular solutions of Laplace's and Poisson's Equation. The CSM has been found to be a very competitive and often superior computational method to that of FEM and FDM, particularly when accuracies within high divergent field are required. The basic principle of operation is based on replacing the distributed charge on the surface of the conductor, with  $N$  fictitious line charge  $Q_j$  inside the conductor and their image charges  $Q'_j$  w.r.t. the ground plane at set in the figure.

In order to calculate the magnitude of these charges it is required that the electrostatic potential  $\varphi_i$  at point  $P_i$  be equal to the conductor potential  $\varphi_c$  resulting from superposition of all the individual line charges



$$\varphi_c = \varphi_i = \sum_{j=1}^N P_{ij} Q_j. \quad P_{ij} = \frac{1}{2\pi\epsilon_0} \ln\left(\frac{R_{rj}}{R_{ij}} \frac{R'_{ij}}{R'_{rj}}\right) \quad (5.134)$$

where  $R_{ij}$  and  $R_{rj}$  are the distances from the charge  $Q_j$  to a point  $P_i$  and ground reference point  $r$  respectively. The application of (5.134) to the  $N$  contour points then leads to a system of  $N$  linear equations for the  $N$  charges such that

$$[P][Q] = [V] \quad (5.135)$$

The electric field at a point  $P_i$  can therefore be calculated as

$$\vec{E}_i = -\nabla\varphi_i = \left[ -\sum_{j=1}^N \frac{\partial P_{ij}}{\partial x} Q_j \right] \hat{x} + \left[ -\sum_{j=1}^N \frac{\partial P_{ij}}{\partial y} Q_j \right] \hat{y} \quad (5.136)$$

For most effective application of this method, the question of a suitable arrangement of charges and contour points is of importance. A practical criterion is obtained by defining an assignment factor such that  $f_a = a_2/a_1$  with distance  $a_1$  between two successive contour points and the distance  $a_2$  between a contour point and the corresponding charge. In the case of curved contours the formulation of a curvature criterion (radius  $r$ ) based on the geometric mean of  $a_1$  and  $a_2$  were derived such that

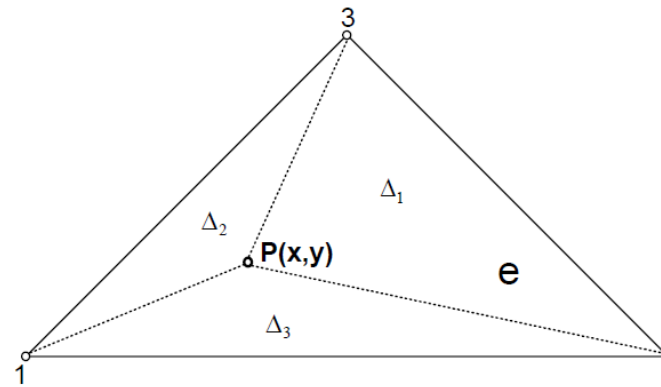
$$r_{o/i} = r \sqrt{1 + \left(f_a \frac{a_1}{r}\right)^2 \pm f_a \frac{a_1}{r}} \quad (5.137)$$

where  $r_o$  is valid for convex curvature and  $r_i$  is valid for concave curvature.

## Finite Element Method:

The principle of this method is to subdivide a continuous domain into a number of subdomains in which an unknown function is represented by interpolation functions with unknown coefficient. A system of algebraic equations is obtained by applying either the **Ritz variational** or **Galerkin weighted residual** procedure. The solution to the boundary value problem is achieved by solving the system of equations while adhering to certain boundary condition, i.e. Dirichlet boundary condition (tangential) and Neumann boundary condition (normal). The boundary problem is solved using the variational approach, where the differential equations are represented as functionals. It is shown that the variational functional for the Poisson equation is given by

$$W(\varphi_{sc}) = \frac{1}{2} \int_{\Omega} (\nabla \varphi_{sc} \cdot \nabla \varphi_{sc}) dS - \int_{\Omega} (g \varphi_{sc}) dS, \quad g(x, y) = \rho/\varepsilon = |e| (n_p - n_e - n_n)/\varepsilon_0 \quad (5.138)$$



The approximation function for these first order elements is given by

$$\varphi_e = a_e + b_e x + c_e y \rightarrow \varphi_{sc}^e = \alpha_1(x, y)\varphi_1 + \alpha_2(x, y)\varphi_2 + \alpha_3(x, y)\varphi_3 = \sum_{i=1}^3 \alpha_i(x, y)\varphi_i \quad (5.139)$$

where  $\varphi_{sc}^e$  is the potential solution due to the space charge in element  $e$ ,  $\varphi_i$  is the scalar potential at node  $i$  and  $\alpha_i$  is linear basis function. The basis function is defined such that it has a value 1 at node  $i$  and 0 everywhere else. The linear interpolation function in an element is given by

$$\alpha_i(x, y) = \frac{1}{2\Delta^e} (a_i^e + b_i^e x + c_i^e y) \quad \Delta^e = \frac{1}{2} \begin{vmatrix} 1 & x_1^e & y_1^e \\ 1 & x_2^e & y_2^e \\ 1 & x_3^e & y_3^e \end{vmatrix} = \frac{1}{2} (b_1^e c_2^e - b_2^e c_1^e) \quad (5.140)$$

where  $\Delta^e$  is the area of the triangle.

The energy functional of an element  $e$  is given with (5.139)

$$W_e = \frac{1}{2} \int_e [(\nabla \varphi_{sc} \cdot \nabla \varphi_{sc}) - g \varphi_{sc}] dS \rightarrow W_e = \frac{1}{2} \sum_{i=1}^3 \sum_{j=1}^3 \varphi_i \left[ \int_e (\nabla \alpha_i \cdot \nabla \alpha_j) dS \right] \varphi_j - \sum_{j=1}^3 \int_e g_0(\alpha_j \varphi_j) dS \quad (5.141)$$

Putting into matrix notation:

$$W_e = \frac{1}{2} \{\varphi\}_e^T [S_e] \{\varphi\}_e - \{\varphi\}_e^T \{T_e\}, \quad S_{ij}^e = \int_e (\nabla \alpha_i) \cdot (\nabla \alpha_j) dS, \quad T_j^e = \int_e g_0 \alpha_j dS \quad (5.142)$$

With continuous boundary conditions at the edge between two adjacent element and the functional for the whole domain  $\Omega$  can therefore be written as

$$W = \sum_e W_e = \frac{1}{2} \{\varphi\}^T [S] \{\varphi\} - \{\varphi\}^T \{T\} \quad (5.143)$$

The solution to the partial differential equation (PDE) is the minimization of energy functional such that

$$\boxed{\frac{\partial W\{\varphi\}}{\partial \{\varphi\}^T} = \{0\} \rightarrow [S]\{\varphi\} = \{T\}} \quad (5.144)$$

In the case of charge assignment in a linear triangular element, weighted areas are assigned to the nearby mesh points, i.e.  $\Delta_1$  to mesh 1,  $\Delta_2$  to mesh 2 and  $\Delta_3$  to mesh 3. Assigning a particle  $Q_p$ , at a point  $P(x, y)$  inside a triangular element  $e$ , to the mesh points  $i(x_i, y_i)$ ,  $j(x_j, y_j)$  and  $k(x_k, y_k)$ , it can be shown that

$$Q_i(x_i, y_i) = \lambda_i^e(x_p, y_p) Q_p; \quad Q_j(x_j, y_j) = \lambda_j^e(x_p, y_p) Q_p; \quad Q_k(x_k, y_k) = \lambda_k^e(x_p, y_p) Q_p \quad (5.145)$$

with

$$\lambda_i^e(x, y) = \frac{a_i^e + b_i^e x + c_i^e y}{2\Delta}, \quad \lambda_j^e(x, y) = \frac{a_j^e + b_j^e x + c_j^e y}{2\Delta}, \quad \lambda_k^e(x, y) = \frac{a_k^e + b_k^e x + c_k^e y}{2\Delta} \quad (5.146)$$

In case where electric field at the mesh points are known as  $\vec{E}_i$ ,  $\vec{E}_j$  and  $\vec{E}_k$ , the interpolation function to the point  $P(x, y)$  can then be defined as

$$\vec{E}_p = \vec{E}_i \lambda_i(x_p, y_p) + \vec{E}_j \lambda_j(x_p, y_p) + \vec{E}_k \lambda_k(x_p, y_p) \quad (5.147)$$

**Positive Streamer Model:** avalanches created by electrons accelerated towards the conductor at region  $\alpha \geq \eta$ , where  $\alpha, \eta$  are ionization and attachment factor. The positive ions created during the avalanche then moves into the electrode gap, while electrons neutralize on the conductor surface. If one simulates the charge of the initiatory electrons per unit length as linear line charge with density  $N_0$ , the increase in charge with the progress of the electrons towards the high voltage conductor in a non-uniform field is given as

$$N_1 = N_0 \exp \int_{r_i}^r (\alpha - \eta) dr \quad (5.148)$$

where  $r_i$  is the boundary of ionization region and  $r$  is the conductor radius. The head at the tip of the avalanche is assumed to be spherical and has a radius  $r_h$ , given by (5.149) that increases as the avalanche progresses.

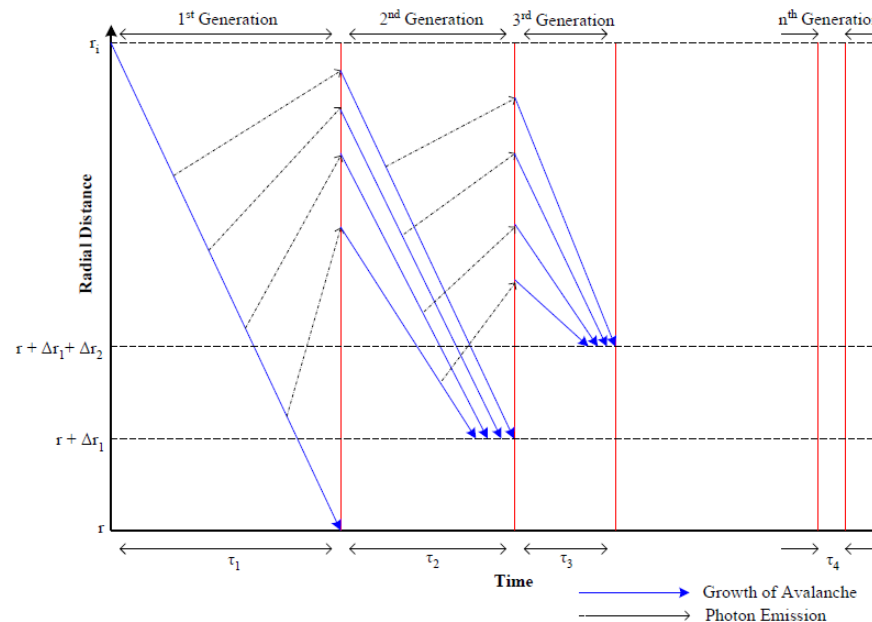
$$r_h = \sqrt{6D\tau} \quad (5.149)$$

where  $D$  is diffusion coefficient and  $\tau$  is the lifetime of avalanche.

During primary electron avalanche, molecules that are excited release photons that will give rise to **secondary avalanche processes**. For the process of avalanche ionization, the secondary electrons are significant, and the theoretical criteria for the **onset of positive burst pulse corona** was established by considering photoionization as secondary mechanism. The onset streamer consist of a number of successive generations of electron avalanches which take place in the ionization zone around the conductor. Following the onset of steady positive corona, the conductor surface voltage gradient decreases. The number of electrons photo-emitted is given by

$$N_{photo} = \int_{r_i}^r N_1 F_1 p \frac{A_2}{R_d + F_2 \frac{A_2}{\sqrt{A_1}}} dr \quad (5.150)$$

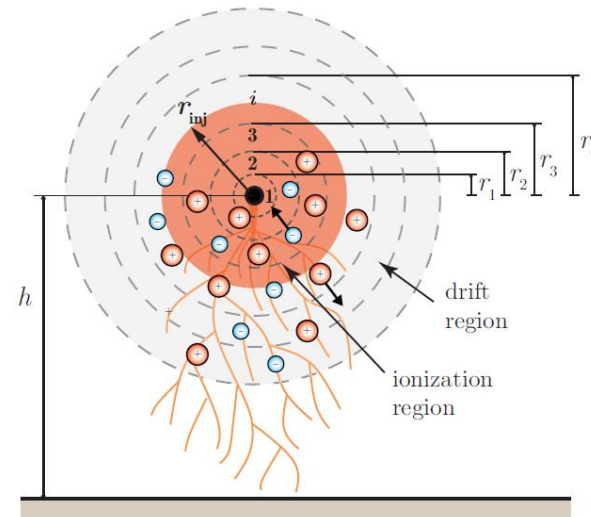
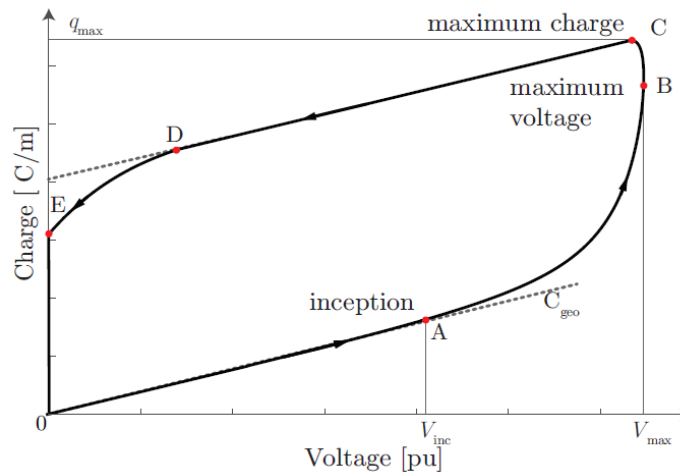
where  $N_{photo}$  is the number of photoelectrons produced after the first avalanche that will give rise to secondary processes,  $N_1$  is the number of ionizing collisions associated with the first generation,  $F_1$  is the photoionization coefficient determined from experimental data and  $F_2$  is a dimensionless constant,  $A_1$  is the area of ionizing source, and  $A_2$  is the area where photoionization is to be calculated,  $R_d$  is the distance to be travelled by the photons and  $p$  is air pressure. To depict the spatial temporal development of corona pulse due to the primary and secondary process,



In this schematic the lifetime of the second generation,  $\tau_2$  is the time required for the second generation charge to reach the positive space charge left behind the first generation with head radius  $\Delta r_1$ . The subsequent generations would then continue to develop until the ionization region is filled with space charge. The corona current is furthermore proposed to consist of both the displacement, also called convection, as well as conduction component as discussed. The instantaneous corona current component due to the electron avalanche at time  $t$  and position  $r_x$  is given by

$$i_+(t) = e N_e(r_x) \mu_e E^2(r_x)/V \quad (5.151)$$

Ionization and interactions among charges at microscopic level provoke a nonlinear and hysteretic relation between total charge and voltage at the electrode surface at macroscopic level. When a monotonically increasing voltage is applied to a reference conductor, a proportionality factor, i.e. the conductor capacitance, governs the q-v relation until corona develops, in correspondence to the inception voltage  $V_{inc}$ ; a further voltage increase results in the space charge growing at a rate faster than linear albeit delayed of time  $\tau_{sp}$  in the range between 25us and 100us in the hemisphere-plane gap configuration, depending on the gap length, and on the voltage rate of the rise and peak value necessary for its formation. Due to this delay time  $\tau_{sp}$  the peak value of the charge may be observed when the time derivatives of the applied voltage has already reversed in sign; at later times, for decreasing values of voltage, the linearity of the q-v relation is restored. The last branch of the loop (D and E) shows a larger slope w.r.t the one of branches C and D. At point E, the dynamic and the magnitude of the electric field produced by the space charge, which contributes to the mechanism of space charge subtraction, resulting in a value of derivation  $dq/dv$  larger than  $C_{geo}$ .



Experimental results indicates that the electric field inception value  $E_{inc}$  depends on the steepness of the applied voltage. As a result, different formulae for the computation of  $E_{inc}$  have been proposed in literature. For general empirical formula,

$$\text{Peek's Formula: } E_{inc} = A \delta \left( 1 + \frac{B}{(\delta r_0)^C} \right) \quad (5.152)$$

Consider not only the maximum electric field at  $r_0$  but also with the electric field trend in the area surrounding the conductor surface, still not accounting for any steepness effect by the applied voltage, Olsen and Yamazaki's formulation has considered charge formation through impact ionization, i.e. Townsend's first ionization coefficient  $\alpha$ , and space charge reduction through attachment, i.e.  $\eta$ . The inception criterion, derived from corona onset experimental data is given by

$$\text{Olsen and Yamazaki's Criterion: } \frac{K(r_0 + \delta_0)}{K(r_0)} = \exp \left( \int_{r_0}^{r_0 + \delta_0} (\alpha - \eta) ds \right) \geq 3500 \quad (5.153)$$

where  $K(r)$  represents the number of free electrons at distance  $r$  from the conductor axis. Coefficient  $\alpha = \alpha(p, E)$  and  $\eta = \eta(p, E)$  have to be intended as functions of the air pressure  $p$  and of the instantaneous electric field  $E(r)$ , assumed radial,  $\delta_0$  denotes the thickness of the corona layer, to be intended as the distance from the conductor surface at which free charges produced by impact ionization and those cancelled by attachment are equal, i.e. the distance where the following condition is verified:

$$\alpha(p, E(r_0 + \delta_0)) = \eta(p, E(r_0 + \delta_0)) \quad (5.154)$$

Expressions for  $\alpha$  and  $\eta$  can be found with empirical formula

$$\alpha(p, E) = \begin{cases} 4.7786 p e^{-0.221 \frac{p}{E}} & \text{for } 0.025 \leq \frac{E}{p} < 0.060 \\ 9.682 p e^{-0.2642 \frac{p}{E}} & \text{for } 0.060 < \frac{E}{p} < 0.24 \end{cases}, \quad \eta(p, E) = 0.01298 p - 0.541 E + 8.7 \frac{E^2}{p} \quad (5.155)$$

where  $E$  is expressed in kV/cm and  $p$  in mmHg. Both the coefficients  $\alpha$  and  $\eta$  are computed considering that the space charge influence on the electric field is negligible before inception occurs.

A modification to the general formula (5.153) for the inception electric field (in kV/cm) is proposed by Mikropoulos and Zagkanas in a coaxial arrangement.

$$\text{Mikropoulos and Zagkanas Criterion: } E_{inc} = K_s 31.53 \left( 1 + \frac{0.305}{\sqrt{r_0}} \right), \quad K_s = 0.42 \operatorname{sign} \left( \frac{dv}{dt} \Big|_{10,90} \right) \left| \frac{dv}{dt} \right|_{10,90}^{0.345} \quad (5.156)$$

where the voltage time derivative at the right hand side of (5.156) is the steepness of the applied voltage in kV/us, assuming its waveform to increase linearly between 10% and 90% of its peak value. When different impulse voltages are applied to a reference conductor, electric field onset values show a dependence on the impulse steepness, which is neglected in the expressions based on Peek's formula. Hence, steepness correction factor is introduced to take into account the increase in  $E_{inc}$  with steeper fronts of the applied voltage.

It is noted that both empirical and circuit-based models may lead to the definition or computation of voltage-dependent, also time varying, capacitance  $C'_{dyn}$ ' value. If the conductor capacitance is assumed to be non-constant, the associated per unit length capacitive current  $i'_c$  should be computed as

$$i'_c = \frac{dq'(v(t))}{dt} = \frac{dq'(v(t))}{dv} \frac{dv(t)}{dt} = C'_{dyn} \frac{dv(t)}{dt} \quad (5.157)$$

In the absence of corona,  $C'_{dyn}$ ' is a constant and equal to the conductor geometric capacitance. The dynamic capacitance approach is frequently used in calculation to account for the effect of distributed corona on propagation along HV lines. However, the general validity of this method is questionable as the adopted corona model assumes a delay between charge and voltage.

Peek's Formula Coefficient	Range
A	23 – 35
B	0.15 – 1
C	0.3 – 0.5

## Correia de Barros' Model

Assumption:

A time delay  $\tau$  exists between the time  $t_{inc}$  at which the critical inception field  $E_{inc}$  is reached and the time at which the discharge is visibly triggered in the vicinity of the conductor surface. The time delay is composed of two different time lags, i.e.  $\tau = \tau_{st} + \tau_{sp}$ , where  $\tau_{st}$  is the statistical time necessary for the formation of seed electrons by detachment (related to the electronegativity of oxygen in the air), and  $\tau_{sp}$  is the critical time required for the formation of space charge.  $\tau_{st}$  depends on gap size (conductor height), pre-existing amount of charged particles and magnitude of overvoltage w.r.t  $V_{inc}$ .

The dynamics of formation and radial spread of space charge around the conductor is modeled by considering a growing radius  $r_{inj}(t)$  of the injection layer, and an exponential growth of the generated space-charge density. The key parameter  $r_{inj}(t)$  permits here to separate two distinct phenomenological regions, i.e. the injection discharge region (glow region or ionization region) nearby the emitter conductor, where there is a source term for charge production caused by electronic impact and attachment, and drift region away from it, where charge concentration are low and charges are mainly electro-convected by the ruling electric field. The space surrounding the conductor is subdivided into  $M$  cylindrical layers with radial thickness  $s_i$  and outer boundary equal to  $r_i$  with  $i = 1, 2, \dots, M$  as depicted in the figure. The configuration is studied through an equivalent coaxial one, in which the conductor holds the same capacitance  $C'_{geo}$ , hence,

$$r_M = r_0 \exp\left(\frac{2\pi\varepsilon_0}{C'_{geo}}\right) = 2h \quad (5.158)$$

Assuming a constant streamers average velocity  $v_{st}$ , the instantaneous radius  $r_{inj}(t)$  is given at any time  $t > t_{inc} + \tau$

$$r_{inj}(t) = \min\{r_s, r_0 + v_{st}[t - (t_{inc} + \tau)]\} \quad (5.159)$$

where  $r_s$  is the outer limit for the injection area. The larger is  $r_s$ ! the wider is the resulting q-v loop; and the higher is the energy dissipated per cycle. From experimental evidences on transient events, the discharge area associated with negative polarity corona shows minor extension and typically displays a narrower loop. It can be considered through the adoption of a lower value of  $r_s$  under negative surge.

In the first step, E-field  $e_0(t)$  at  $r_0$  is evaluated by employing currently applied voltage  $v(t)$  and space charge of previous time step, Applying Green's reciprocity theorem, under the assumptions of linearity and ground permittivity much greater than that of medium surrounding the conductor, the following relation holds:

$$e_0(t) = \frac{2\pi\varepsilon_0}{r_0 \ln\left(\frac{2h}{r_0}\right)} v(t) + \frac{1}{2\pi\varepsilon_0 r_0} q'_{ind}(t) \quad (5.160)$$

where

$$q'_{ind}(t) = q_e \frac{C'_{geo}}{\varepsilon_0} \sum_{i=1}^M k_i [p_i(t) - n_i(t)] - q_{sp}'(t), \quad k_i = \int_{r_{i-1}}^{r_i} r \ln\left(\frac{r}{r_0}\right) dr \quad i = 1, 2, \dots, M \quad (5.161)$$

$Q_e = 1.602 \times 10^{-16}$  C,  $q'_{ind}(t)$  is the per unit length charge induced in the conductor by the total space-charge  $q'_{sp}(t)$ ,  $k_i$  is a geometric coefficient with the dimensions of area.  $p_i$  and  $n_i$  are the volumetric density of positive and negative charged particles in the  $i$ -th layer. The surface electric field  $e_0(t)$  is found to remain constant during discharge and close to the onset field strength  $E_{inc}$  (Kaptzov's Assumption)

Depending on the polarity of electric field  $e_0$ , when  $|e_0(t)| > E_{inc}$ , the ionization phenomenon is simulated through the injection of a new generated per unit length space charge of the same polarity, whose volumetric density  $d\rho(t)$  (charged particles injected per cubic meter) is assumed to be uniform in the injection area  $r_0 < r < r_{inj}(t)$  and is given by

$$d\rho(t) = \frac{2\pi\epsilon_0 r_0 [E_{inc} - e_0(t)]}{q_e \left[ \frac{C'_{geo}}{\epsilon_0} k_{inj}(t) - S_{inj}(t) \right]} (1 - e^{-\frac{\Delta t}{\tau_0}}) \quad (5.162)$$

where  $\tau_0$  in the exponential factor accounts for the dynamics of space charge injection. In (5.158),  $S_{inj}(t) = \pi[r_{inj}^2(t) - r_0^2]$  is the injection area and  $k_{inj}(t)$  corresponds to the integral performed from  $r_0$  to  $r_{inj}(t)$ .

The electric field  $e_i(t)$  at the separation surfaces between the M layers is found recursively from  $e_{i-1}(t)$  as the following:

$$r_i e_i(t) = r_{i-1} e_{i-1}(t) + s_i \bar{r}_i [p_i(t) - n_i(t)] \frac{q_e}{\epsilon_0} \quad (5.163)$$

where  $s_i$  and  $\bar{r}_i = (r_i + r_{i-1})/2$  are the thickness and the average radius of the i-th layer, respectively.

In the second step of the algorithm, the space-charge densities  $p_i(t)$  and  $n_i(t)$  are computed from the electric fields of the previous step through the solution of the following system of 2M non-linear differential drift equations (time dependence is dropped for clarity):

$$\frac{dp_i}{dt} + \mu_p \frac{r_i e_i p_\alpha - r_{i-1} e_{i-1} p_\beta}{s_i \bar{r}_i} + R p_i n_i = 0, \quad \frac{dn_i}{dt} + \mu_n \frac{r_i e_i n_\alpha - r_{i-1} e_{i-1} n_\beta}{s_i \bar{r}_i} + R p_i n_i = 0 \quad (5.164)$$

with  $i = 1, 2, \dots, M$ . These relations assume a constant mobility  $\mu_p$  and  $\mu_n$  of the positive and negative charges. Respectively, and their recombination through a constant recombination coefficient  $R$ . In (5.164),  $\alpha = i$  and  $\beta = i - 1$  under positive electric field  $e_i$  whereas  $\alpha = i + 1$  and  $\beta = i$  under negative electric field  $e_i$ . Additionally, Dirichlet boundary conditions are assumed, i.e.  $p_0 = p_{M+1} = n_0 = n_{M+1} = 0$ . Once the space-charge densities  $p_i(t)$  and  $n_i(t)$  are known, the total space-charge  $q'_{sp}(t)$  in (5.161) is computed as the following

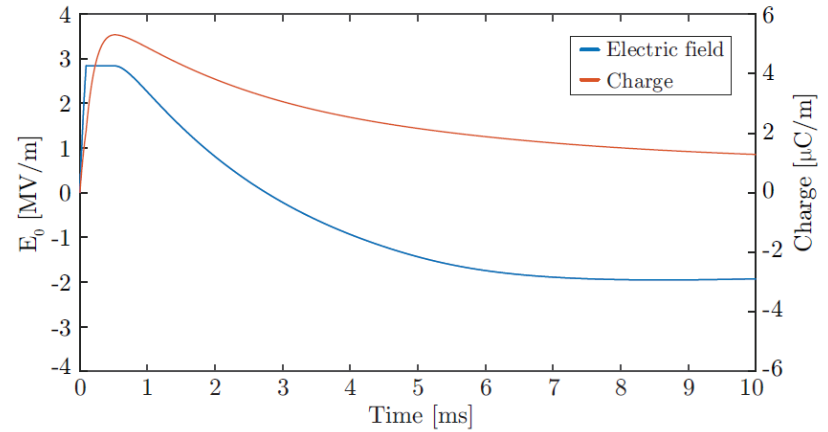
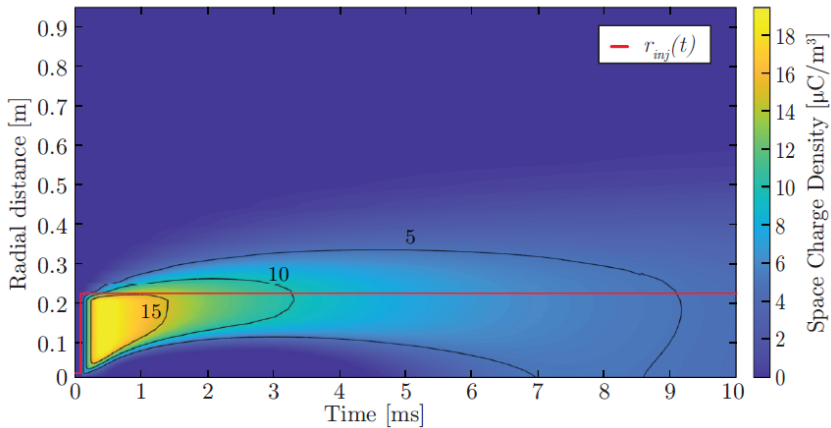
$$q'_{sp}(t) = \pi q_e \sum_{i=1}^M [p_i(t) - n_i(t)] (r_i^2 - r_{i-1}^2) \quad (5.165)$$

Finally, the total per unit length  $q'(t)$  needed for plotting the **q-v hysteretic loop** is computed as  $q'(t) = C'_{geo} v(t) + q'_{ind}(t) + q'_{sp}(t)$ . From the numerical derivative  $dv/dt$ , the **dynamic capacitance**  $C'_{dyn}$  is computed.

The trend of the space-charge density  $\rho_{sp}$  is shown, when a voltage source is applied to a conductor of radius  $r_0 = 1.32$  cm at height  $h = 7.5$  m over a perfectly conducting ground. The waveform of the voltage source is given by the following expression:

$$v(t) = \frac{V_{MAX}}{\eta} (e^{-\frac{t}{T_2}} - e^{-\frac{t}{T_1}}) \quad (5.166)$$

where  $V_{MAX} = 2V_{inc}$ ,  $V_{inc} = 263.25$  kV,  $\eta = 78\%$ ,  $T_1 = 167$  us and  $T_2 = 2648$  us, peak time  $T_p = 493$  us, rise time  $T_r = 250$  us ( $T_h = 2500$  us).



### Malik's Model

This model is to simulate the dynamic behavior of  $C_{dyn}'$  with  $v(t)$  greater than  $V_{inc}$  with an apparent increase in conductor radius  $r_0$ , which is replaced by the radius  $r_c(t) > r_0$ . This latter corresponds to the external boundary of the whole space-charge around the conductor and it must not be confused with  $r_{inj}$  of the previous model, defining only the ionization area.

This model is developed for a single conductor above a conducting ground plant at height  $h$  with a time delay  $\tau$  (ranging from 0.1us to 0.5us) in the formation of corona charge w.r.t. the instantaneous value of the voltage applied to the conductor. The time-dependent per unit length charge  $q'(t)$  is given by

$$q'(t + \tau) = 2\pi\epsilon_0\alpha E_{inc} r_c(t) \frac{2h - r_c(t)}{2h} + C'_{geo}[v(t + \tau) - v(t)] \quad (5.167)$$

given that the radius  $r_c(t)$  in the presence of corona can be determined by

$$r_c(t) \left\{ 1 + \frac{2h - r_c(t)}{2h} \ln \frac{2h - r_c(t)}{r_c(t)} \right\} = r_0 + \frac{v(t)}{\alpha E_{inc}} \quad (5.168)$$

In (5.167) and (5.168),  $\alpha < 1$  is a multiplicative factor considering the reduction of E-field in corona area after the inception. The main assumption of this model is to consider the E-field inside the corona sheath ( $r_0 \leq r \leq r_c$ ) constant and equal to  $\alpha E_{inc}$ ; consequently the surface E-field  $e_0(t)$  (oppositely to the [Kaptzov's assumption](#)) undergoes an abrupt discontinuity when the corona discharge starts, which can result in a discontinuity in the  $q-v$  relation. Comparison with (5.168) shows that the parameter  $\alpha$  introduces a step discontinuity between  $r_0$  and  $r_c(t)$  at  $t_{inc}$ , where the lower is  $\alpha$ , the larger is the step discontinuity, and the wider is the resulting corona hysteretic loop.

### Cooray's Model

Cooray describes the physics of corona phenomenon, identifying 4 different stages. In the first stage, the voltage  $v(t)$  applied to the conductor increases progressively; hence, a proportional relation is assumed between  $q'(t)$  and  $v(t)$ , with  $C'_{geo}$  being the proportionality constant. As the voltage reaches the inception threshold  $V_{inc}$ , the discharge starts in stage 2. For a positive (negative) voltage surge, a positive (negative) spatial charge progressively settles around the conductor; this phenomenon is considered through a time-dependent

a time-dependent increasing radius  $r_c(t)$ . Denoting with  $r_c(t)$ , the external radius of the corona charge distribution, the corresponding E-field  $e(t, r_c)$  is forced to the value  $E_c$ , which depends on the atmospheric conditions, conductor characteristics, and the applied voltage polarity. A time-dependent expression is adopted for the E-field at the conductor surface  $e_0(t)$ : it decays exponentially from its inception value  $E_{inc}$  to  $E_c$ , which is assumed to be the minimum field value to guarantee streamer propagation. The expression reads as follows.

$$e_0(t) = E_c + (E_{inc} - E_c)e^{-\frac{(t-t_{inc})}{\tau_d}} \quad (5.169)$$

In (5.169),  $\tau_d$  is the time constant defining the E-field decay, and  $t_{inc}$  denotes the corona inception time. The distribution of corona space-charge  $q'_{sp+}$  is assumed to be dependent on the inverse of the radial distance  $r$  from the conductor central axis (i.e.  $\rho_{sp+}r^{-1}$ ).

Noted that unlike previous model, any time delay in the spatial charge formation is neglected. Based on these assumptions, the following relation can be derived from trivial electrostatic consideration, given  $h \gg r_0$  and angular symmetry.

$$q'(t) = q'_0(t) + q'_{sp+}(t), \quad e_c(t) = E_c = \frac{q'_0(t) + q'_{sp+}(t)}{2\pi\epsilon_0 r_c(t)}, \quad e_0(t) = \frac{q'_0(t)}{2\pi\epsilon_0 r_0} \quad (5.170)$$

where the total charge  $q'(t)$  is the sum of the charge on conductor surface  $q'_0(t)$  and the corona spatial charge  $q'_{sp+}(t)$  with

$$q'_{sp+}(t) = \int_{r_0}^{r_c} \frac{\rho_{sp+}(t)}{r} 2\pi r dr = 2\pi\rho_{sp+}(t)[r_c(t) - r_0] \quad (5.171)$$

where  $2h \gg r_0$ ,  $r_c(t)$  and  $\rho_{sp+}(t)r^{-1}$  represents the radial distribution assumed for the per unit length space charge density in C/m<sup>3</sup>.

From (5.170) and (5.171), it is obtained that

$$\rho_{sp+}(t) = \frac{\epsilon_0[r_c(t)e_c(t) - r_0e_0(t)]}{r_c(t) - r_0} \quad (5.172)$$

Considering both the conductor and its perfect image located at depth  $h$  below the ground surface, the instantaneous voltage is given by

$$v(t) = \frac{q'_0}{2\pi\epsilon_0} \ln\left(\frac{2h}{r_0}\right) + \frac{\rho_{sp+}(t)}{\epsilon_0} (r_c - r_0) \ln\left(\frac{2h}{r_c}\right) + \frac{\rho_{sp+}(t)}{\epsilon_0} (r_c - r_0) - \frac{\rho_{sp+}(t)}{\epsilon_0} r_0 \ln\left(\frac{r_c}{r_0}\right) \quad (5.173)$$

where the time-dependence of  $r_c(t)$  is dropped for conciseness. Putting (5.172) into (5.173), the non-linear equation (5.173) can be solved with iterative method with unknown  $r_c(t)$ , then the total charge can be obtained with (5.170).

After the inception, the ionized area is supposed to expand as long as the sign of the voltage derivative is positive. The third stage of the model begins when the maximum voltage is reached and the voltage derivative changes sign. The model assumes that the corona sheath radius and the charge density are fixed to their maximum value  $r_c^M$  and  $\rho_{sp+}^M$  respectively due to the slow mobility of the space charges. The voltage decrease is associated with the initial progressive reduction and a subsequent change in sign of  $q'_0(t)$ , until  $e_0(t) = E_{ib}$ , i.e. the electric field causing the inception of back-corona and the development of negative space charges.

The **back corona** is the fourth stage. A second ionizing process begins in the radial direction from  $r_0$ , neutralizing progressively the previously settled positive charge and setting new negative space-charge  $q'_{sp-}(t)$ . The new negative charge is assumed to be

distributed in the area between  $r_0$  and the increasing radius  $r_{cb}(t)$  with the same distribution as in (5.171). The electric field is assumed constant and equal to  $E_{ib}$  in the back-corona area, i.e.  $r_0 \leq r \leq r_{cb}(t)$ . Hence, the negative charge density can be readily obtained as  $\rho_{sp-} = \varepsilon_0 E_{ib}$ . Finally, the voltage of the conductor may be expressed as

$$v(t) = \frac{q'_0}{2\pi\varepsilon_0} \ln\left(\frac{2h}{r_0}\right) + \frac{\rho_{sp-}(t)}{\varepsilon_0} (r_{cb} - r_0) \ln\left(\frac{2h}{r_{cb}}\right) + \frac{\rho_{sp-}(t)}{\varepsilon_0} \left[ (r_{cb} - r_0) - r_0 \ln\left(\frac{r_{cb}}{r_0}\right) \right] \\ + \frac{\rho_{sp+}^M}{\varepsilon_0} (r_{cm} - r_{cb}) \ln\left(\frac{2h}{r_{cm}}\right) + \frac{\rho_{sp+}^M}{\varepsilon_0} \left[ (r_{cm} - r_{cb}) - r_{cb} \ln\left(\frac{r_{cm}}{r_{cb}}\right) \right] \quad (5.174)$$

Equation (5.174) can be solved to find  $r_{cb}(t)$ ; once the radius is known the total charge is computed as  $q'(t) = q'_0(t) + q'_{sp+}(t) + q'_{sp-}(t)$ . The last remark concerns the transition between first and second stage. Let's focus on the corona inception time  $t_{inc}$ . If we assume a continuous function  $r_c(t)$  at time  $t_{inc}$ , i.e.  $r_c(t) \rightarrow r_0, t \rightarrow t_{inc}$  from (5.170),

$$q'_{sp+} = 2\pi\varepsilon_0(E_c r_c - E_{inc} r_0) \rightarrow 2\pi\varepsilon_0 r_0(E_c - E_{inc}) \neq 0 \quad (5.175)$$

For other empirical formula,

Inoue's Model:

$$C'_{dyn}(v) = C'_{geo} + \alpha\kappa \frac{[v(t) - V_{inc}]^{\alpha-1}}{v(t)}, \quad \kappa = \sigma_k \sqrt{\frac{r_0}{2h}} \quad (5.176)$$

Gary's Model:

$$q'(t) = C'_{geo} V_{inc} \left[ \frac{v(t)}{V_{inc}} \right]^B, \quad C'_{dyn}(v) = C'_{geo} B \left[ \frac{v(t)}{V_{inc}} \right]^{B-1}, \quad B = \begin{cases} 2.924 r_0^{0.153} & \text{positive polarity} \\ 1.121 + 6.8r_0 & \text{negative polarity} \end{cases} \quad (5.177)$$

Sivaev and Podporkin's Model:  $\kappa_1 = 1.17, \kappa_2 = 0.87$  and  $\alpha = 0.08$  and  $0.036$  for positive and negative impulse

$$q'(t) = C'_{geo} V_{inc} \left[ \frac{v(t)}{V_{inc}} \right]^{\left( \kappa_1 + \frac{v(t)}{V_{inc}} ah^{-\kappa_2} \right)}, \quad C'_{dyn}(v) = h^{-\kappa_2} \frac{C'_{geo}}{V_{inc}} \left[ \frac{v(t)}{V_{inc}} \right]^{\kappa_1 + \frac{v(t)}{V_{inc}} ah^{-\kappa_2-1}} \left\{ \kappa_1 h^{\kappa_2} V_{inc} + av(t) \left\{ 1 + \ln \frac{v(t)}{V_{inc}} \right\} \right\} \\ v(t) \rightarrow V_{inc}, C'_{dyn}(t) \rightarrow \kappa_1 C'_{geo} + a C'_{geo} h^{-\kappa_2} \quad (5.178)$$

Maccioni-Araneo's Model:

$$\Delta C(t) = 2\pi\varepsilon_0 \left[ \frac{1}{\ln\left(\frac{2h}{r_c(t)}\right)} - \frac{1}{\ln\left(\frac{2h}{r_0}\right)} \right] \Delta l, \quad v(t) = r_c(t) E_{inc} \ln\left(\frac{2h}{r_c(t)}\right) \quad (5.179)$$

Given the current generator  $i_{\Delta C}(t) = d[\Delta C(t)v(t)]/dt$

$$i_{\Delta C}(t) = \begin{cases} 0 & v(t) < V_{inc} \text{ or } \frac{dv}{dt} < 0 \\ v(t) \frac{d\Delta C}{dt} + \Delta C(t) \frac{dv(t)}{dt}, & v(t) \geq V_{inc} \text{ and } \frac{dv}{dt} > 0 \end{cases} \quad (5.180)$$

## Question 2

Townsend breakdown is based on the generation of successive secondary avalanches to produce breakdown. Consider a parallel plate capacitor with gas as insulating material and separated by distance  $d$ . A thickness  $dx$  at a distance  $x$  is from the cathode.

- (a) To explain the exponential rise, Townsend introduced a coefficient  $\alpha$  and is defined as the number of electrons produced by an electron per unit length of path in direction of field. When  $n$  electrons move through a distance  $dx$ , they produce another  $dn$  electrons due to collision. Given at  $x = 0$ ,  $n = n_0$ . Prove that

$$n(x) = n_0 e^{\alpha d} \quad (5.181)$$

Explain the physical meaning of  $e^{\alpha d}$  at  $x = d$ .

- (b) Given the number of electrons emitted from the cathode ( $n_0$ ), the number of electrons from cathode due to positive ion bombardment ( $n_+$ ) and the number of electrons reaching the anode ( $n$ ). Consider Townsend's second ionization coefficient  $\nu$ , which is defined as the number of electrons released from the cathode per incident positive ion, i.e.

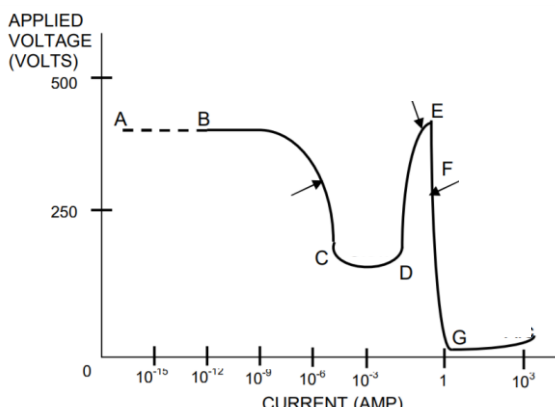
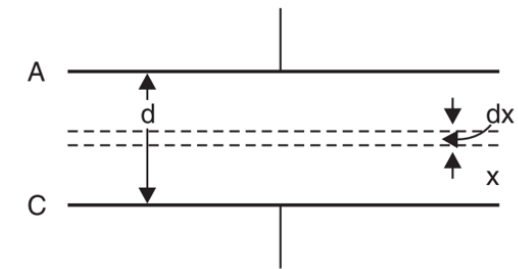
$$n_+ = \nu[n - (n_0 + n_+)], \quad n = (n_0 + n_+)e^{\alpha d} \quad (5.182)$$

Prove Townsend Criterion for Gas Breakdown:

$$I = \frac{I_0 e^{\alpha d}}{1 - \nu(e^{\alpha d} - 1)} \quad (5.183)$$

Describe the physical meaning for  $\nu e^{\alpha d} = 1$ ,  $\nu e^{\alpha d} > 1$ , and  $\nu e^{\alpha d} < 1$  and sketch the breakdown voltage [kV] – pressure x spacing characteristics based on Paschen's Law.

- (c) Sketch the discharge current – voltage diagram and explain its physical meaning and highlight the limitation of Townsend Theory.
- (d) Other than Townsend breakdown (a.k.a Avalanche breakdown), another breakdown mechanism is Streamer Theory. Explain the theory with the aids of the following diagram – DC Voltage – Current Characteristics at Discharge with Electrode without Sharp Edge



From experimental results, q-u curve is modelled for further transient simulation with Corona Effect.

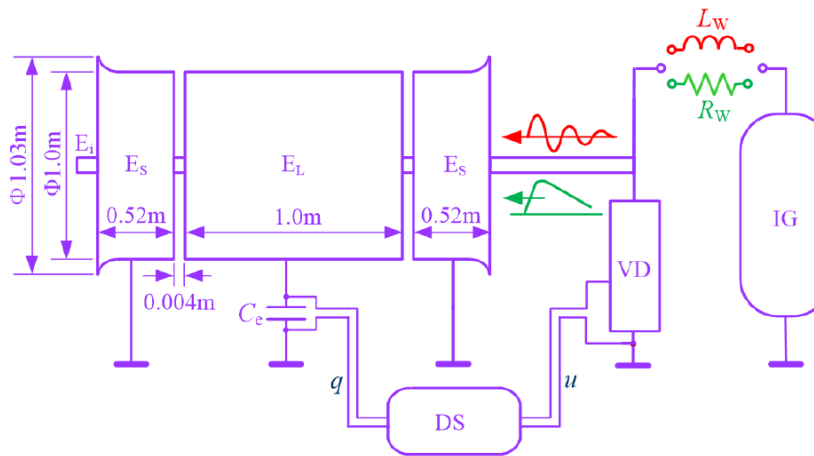
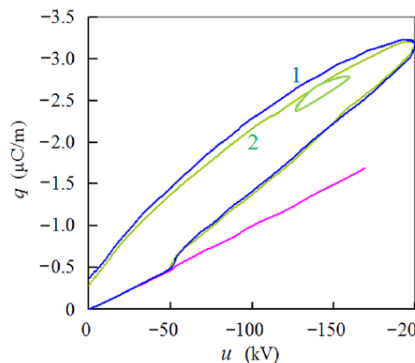
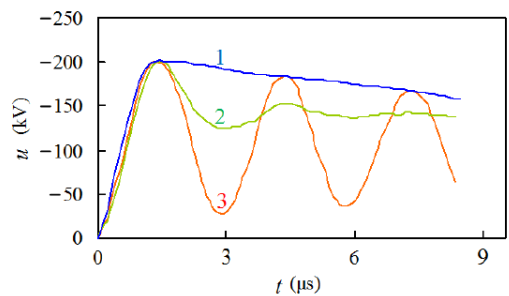


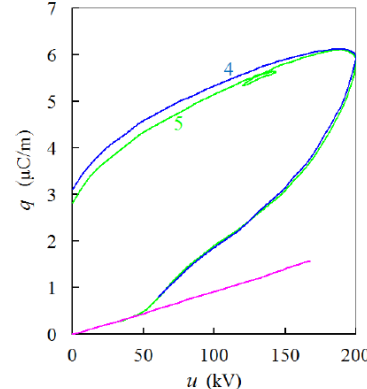
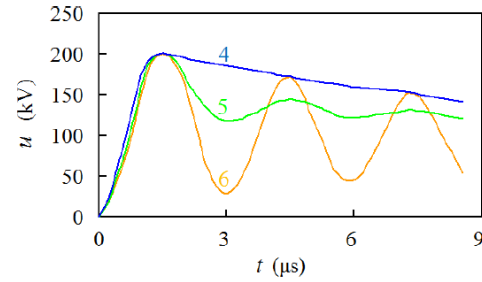
**Figure 2.** Diagram of experimental system ( $E_i$ —inner electrode;  $E_L$ —longer outer electrode;  $E_s$ —shorter outer electrode; DS—digital oscilloscope; VD—voltage divider; IG—impulse generator).

### Negative Surge:

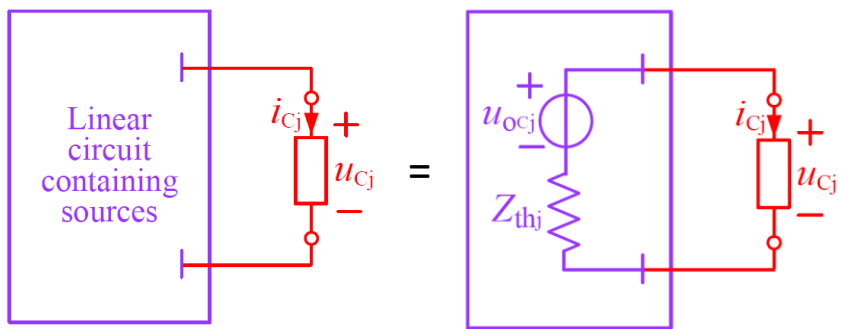
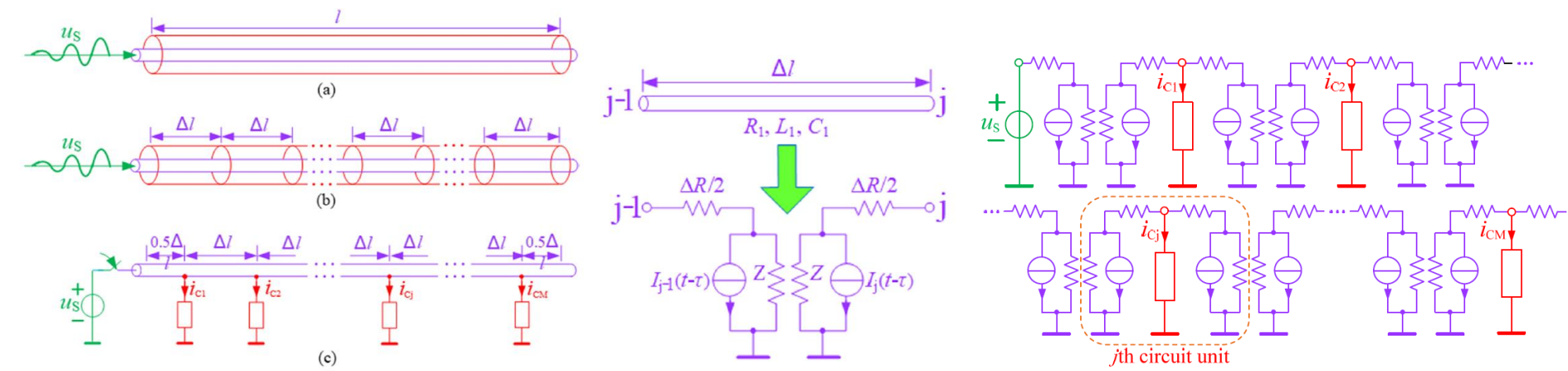
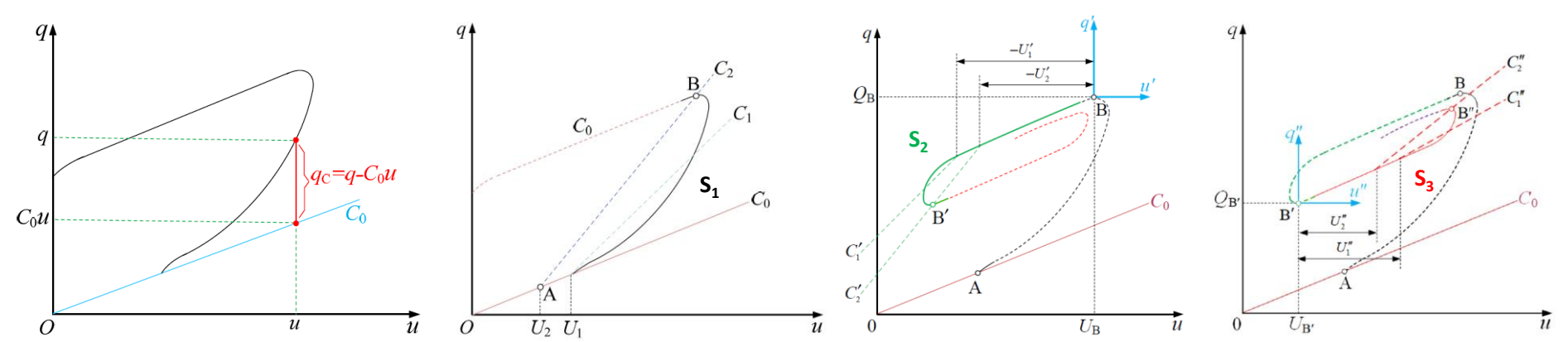


(a)

### Positive Surge:



(b)



Thevenin's equivalent circuit can be represented with

$$U_{ocj} - Z_{thj} i_{cj} = u_{cj} \quad (j = 1, 2, \dots, M) \quad (5.184)$$

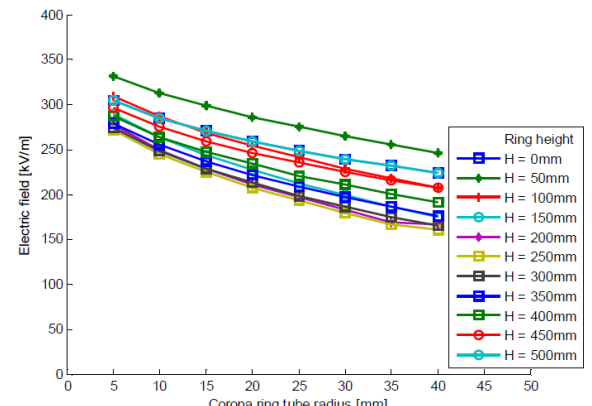
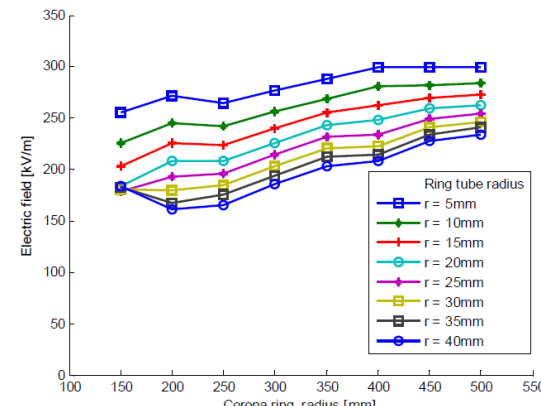
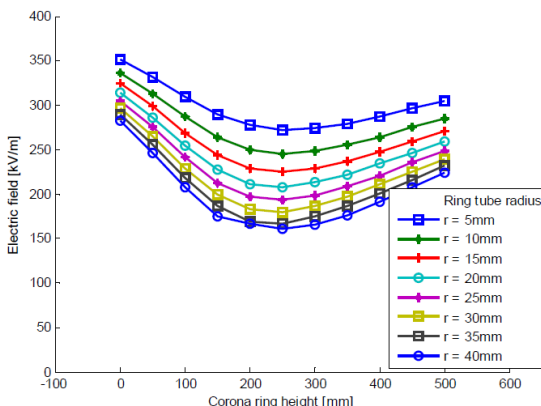
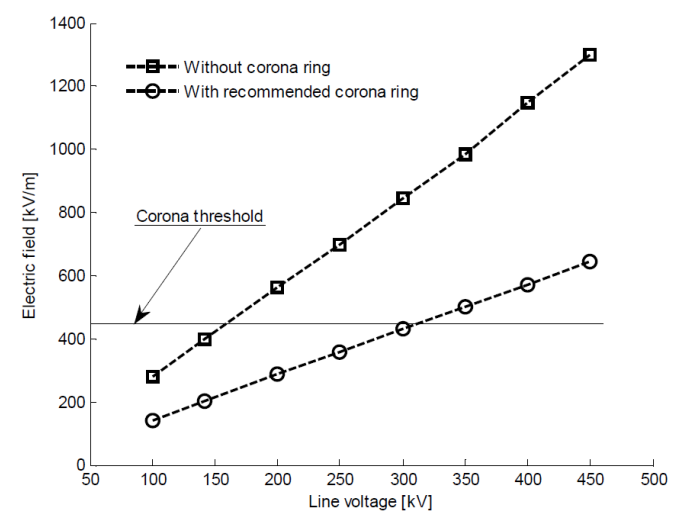
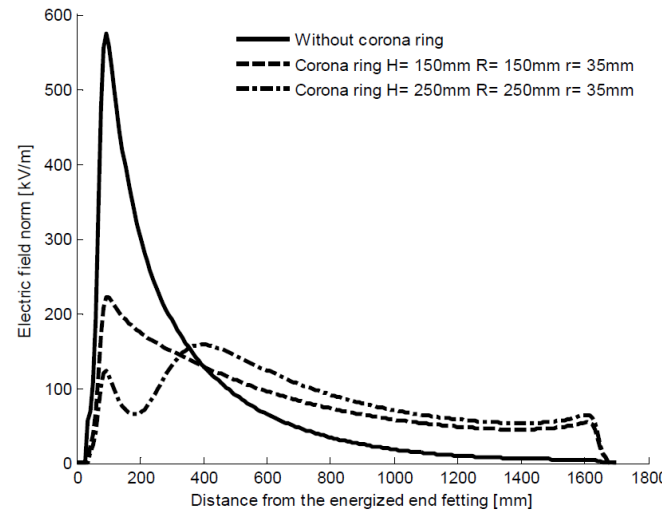
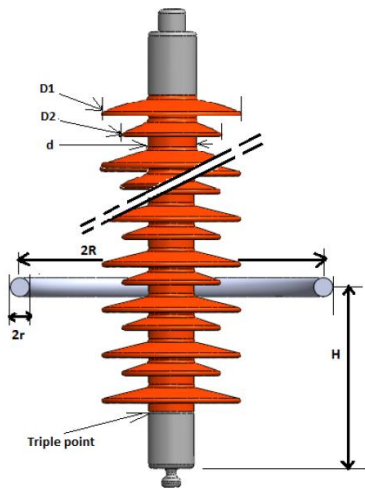
where  $i_{cj}$  is found with the  $q$ - $u$  curve.

$$i_{cj} = \frac{\beta}{1 + \beta \frac{\Delta t}{2}} [(C_2 - C_0)(u_{cj} - U_2) - q_{CP}(t - \Delta t)] \quad (5.185)$$

$$u_{cj} = \frac{1}{1 + \Gamma} \left[ u_{oc} + \Gamma U_2 - \frac{\Gamma}{C_2 - C_0} q_{CP}(t - \Delta t) \right], \quad \Gamma = \frac{\beta Z_{thj} (C_2 - C_0)}{1 + \beta \frac{\Delta t}{2}}$$

As the performance of high voltage insulator strings closely depends on **designs and locations of corona ring**, the effects of the corona ring radius, the ring tube radius and the ring vertical position are examined. The minimization of the electric field necessitates the optimization of corona ring.

High levels of E-field are possibly responsible for audible noise, electromagnetic pollution, partial discharges and premature aging of insulation. High local electric field can provoke the apparition of discharges on high voltage insulator surface, in which can degrade the polymeric materials and lead to erosion of the material. E-field distribution on the surface and within insulators string depends on numerous parameters including **applied voltage**, **insulator design** (shape- creepage vs clearance, conductivity and hydrophobicity), **tower configuration**, **corona ring**, **phase spacing**. The following aims to optimize the diameter, tube radius and position (height) of the corona ring with **particle swarm optimization (PSO)**.



Ring height  
■ H = 0mm  
■ H = 50mm  
■ H = 100mm  
■ H = 150mm  
■ H = 200mm  
■ H = 250mm  
■ H = 300mm  
■ H = 350mm  
■ H = 400mm  
■ H = 450mm  
■ H = 500mm

The goal of optimization design of corona ring structure is to reduce the electric field magnitude and then the corona discharges on the surface of composite insulator string near the energized end fitting. In order to reduce discharge activities, it is necessary to maintain the electrical field intensity lower than the threshold value of 450 kV/m. It is also to design the corona rings more compact and smaller. To interpolate the E-field, a 7-th order polynomial function is accurate enough, since it gives low RMSE value (= 2.2533) and high coefficient of determination ( $R^2 = 0.9963$ ), i.e.

$$E(H, R, r) = \sum_{i,j,k} a_{ijk} H^i R^j r^k \quad (5.186)$$

The objective function consisting a mathematical relation between the electric field magnitude and corona ring parameters minimizing the electric field, i.e.

$$\min E(H, R, r) \text{ subj. to } \begin{cases} H_{min} \leq H \leq H_{max} \\ R_{min} \leq R \leq R_{max} \\ r_{min} \leq r \leq r_{max} \end{cases} \quad (5.187)$$

The PSO algorithm for d-dimensional problem formulation can be described as follows.

Let  $P_i = (P_{i1}, P_{i2}, \dots, P_{id})$ . The particle position vector in d-dimension space and  $V_i = (V_{i1}, V_{i2}, \dots, V_{id})$ , the velocity vector of i-th particle in the search space. The best previous position of the i-th particle is stored and represented by  $P_{best\_i} = (P_{best\_1}, P_{best\_2}, \dots, P_{best\_d})$ . All  $P_{best\_i}$  are evaluated by using a fitness function. The best particle position among all of the  $P_{best\_i}$  becomes  $G_{best}$ . The velocity of each particle is dynamically adjusted according to its personal previous best solution  $P_{best\_ik}$  and the previous global solution  $G_{best\_ik}$  of the entire swarm. The position and velocity of i-th particle are updated with

$$\begin{aligned} V_i(k+1) &= w(k)V_i(k) + c_1 r_1(k)(P_{best}(k) - P_i(k)) + c_2 r_2(k)(G_{best}(k) - P_i(k)) \\ P_i(k+1) &= P_i(k) + V_i(k+1) \end{aligned} \quad (5.188)$$

where  $V_i(k)$  and  $V_i(k+1)$  are the velocities of the i-th particle of k-th and (k+1)-th iteration respectively.  $C_1$  and  $C_2$  are two positive constants, called acceleration factors,  $r_1(k)$  and  $r_2(k)$  are random values between 0 and 1 and  $w(k)$  is the momentum parameter which can change the search ability.

In general, the population size can change dynamically at each iteration with

$$P_{size}(i+1) = \text{round} \left( \left( \frac{E_{avr}(i) - E_{gbest}(i)}{E_{avr}(1) - E_{gbest}(1)} \right) \times P_{size max} \right) + P_{size min} \quad (5.189)$$

where  $E_{avr}(i)$  is an average objective function value of the observed iteration i,  $E_{gbest}(i)$  is an objective function value of the global best particle of the observed iteration i,  $P_{size max}$  and  $P_{size min}$  are the maximum and minimum (predefined) population size respectively.

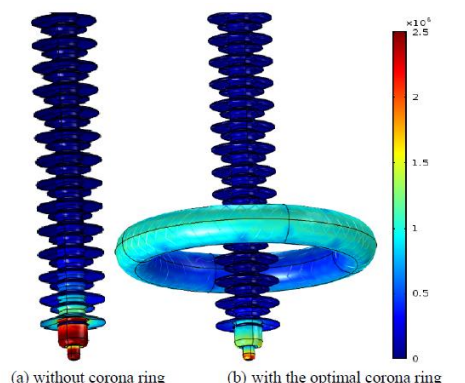
### Particle swarm optimization pseudo-code

```

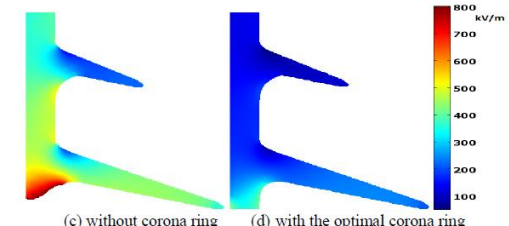
Initialize variables
Initialize swarm and velocities
Evaluate initial population
Initialize local minimum for each particle
Finding best particle in initial population

Start iterations
while iter < maxit
    iter = iter + 1
    for j = 1: popsize
        update velocity according (3)
        update particle positions according (4)
    end
    for j = 1: popsize
        evaluate the new swarm according (2)
        update the best local position for each particle
    end
    keep the best solution
    rank the solution
    adjust population size according (5)
end while

```



(a) without corona ring      (b) with the optimal corona ring



(c) without corona ring      (d) with the optimal corona ring

### 5.3 OHL Application in HVDC

With the rise of HVDC applications in current years, due to the increasing maturity of LCC-HVDC and MMC VSC-HVDC for higher transmission capacity and efficiency in long lines, current research topic includes the replacement of HVAC lines to HVDC lines and parallel run in HVAC with HVDC. The challenges hidden behind is the re-assessment of clearance and creepage distance under power frequency and lightning overvoltage. In this section, transient overvoltage (TOV) on OHL-HVDC with space charge and corona effect, lightning overvoltage in system with mixed underground cable – overhead line (UGC-OHL) are introduced. Topics such as converting HVAC to HVDC lines, optimal placement of HVDC substation, E-field consideration with crossed lines, interference from HVAC lines and HVDC protection for lightning are introduced.

Space charge around a HVDC transmission line may not only lead to EM environmental problems and corona loss, but also affect the occurrence of impulse corona and then the transient overvoltage propagation. Lightning not only always strikes the DC conductor with **opposite polarity**, but its overvoltage propagation is also different from AC lines. This is because the space charges of the HVDC transmission line will affect the occurrence and development of lightning impulse corona. The **dynamic capacitance** was obtained by measuring the q-v curve through impulse corona characteristic test in corona cage.

When the **space charges** fill the entire space, as is the case for HVDC transmission lines, because the current densities in the space are different everywhere, whether  $C_d$  obtained by the q-u curve is still suitable for the transmission line equations needs further derivation.

Conventional **Transmission Line Model**:

$$\begin{cases} -\frac{\partial u(t, z)}{\partial z} = L \frac{\partial i(t, z)}{\partial t} + R_0 i(t, z) \\ -\frac{\partial i(t, z)}{\partial z} = C_d \frac{\partial u(t, z)}{\partial t} + G_0 u(t, z) \end{cases} \quad (5.190)$$

During impulse corona, the capacitance is no longer the geometric capacitance  $C_{geo}$ , but the dynamic capacitance  $C_d$ . The equations in (5.190) ignore the frequency dependent characteristics due to **skin effect**, but this does not affect the derivation of the equations with background space charges. The space charges have no effect on the first equation of (5.190) because  $L$  is only related to the current in the conductor, and  $R_0$  is a characteristic of the conductor itself. However, for the second equation of (5.190), since corona develops in the radial direction, the parameters are affected by the space charges generated by either **DC corona** or **impulse corona**.

Conservation of Charge:

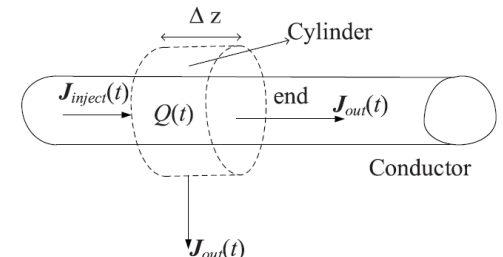
$$Q_{inject}(t) = Q(t) + Q_{out}(t) \quad (5.191)$$

Partial Derivative of (5.191) over time:

$$\iint_{end} \mathbf{J}_{inject}(t) \cdot d\mathbf{S} = \frac{\partial Q(t)}{\partial t} + \iint_{end} \mathbf{J}_{out}(t) \cdot d\mathbf{S} + \iint_{cylinder} \mathbf{J}_{out}(t) \cdot d\mathbf{S} \quad (5.192)$$

where

$$\iint_{end} \mathbf{J}_{inject}(t) \cdot d\mathbf{S} = i(t, z), \quad \iint_{end} \mathbf{J}_{out}(t) \cdot d\mathbf{S} = i(t, z + \Delta z) \quad (5.193)$$



For the cylinder term:

$$\iint_{cylinder} \mathbf{J}_{out}(t) \cdot d\mathbf{S} = \iint_{cylinder} \gamma \mathbf{E}(t) \cdot d\mathbf{S} + \iint_{cylinder} \mathbf{J}_{corona}(t) \cdot d\mathbf{S} \quad (5.194)$$

The first term on the right side with  $\gamma \mathbf{E}(t)$  is the conduction current, where  $\gamma$  is the electrical conductivity of air and  $\mathbf{E}(t)$  is the electric field on the surface of the conductor; and the second term on the right is the charges outflow due to corona discharge. Here, the effect of the second term is much greater than that of the first term when corona discharge occurs.

In (5.192), the effect of the distributed capacitance of the line is characterized by  $\partial Q(t)/\partial t$ . According to Gauss's Law, the amount of charge surrounded by the cylinder is

$$Q(t) = \epsilon \iint_{cylinder} \mathbf{E}(t) \cdot d\mathbf{S} \quad (5.195)$$

Here,  $\mathbf{E}(t)$  is determined by both the charge of the line and the space charge.

Corona discharge produces a lot of new substances, and hence the corresponding permittivity and resistivity may change. But compared with the widely distributed space charge, the corona layer around the conductor is very thin, and the area where the new substances are concentrated is small. Therefore, they are assumed unchanged. In future works, **corona products** and the change of  $\epsilon$  and  $\rho$  can be further studied. Let  $C(t)$  represents the ratio of  $Q(t)$  to the voltage,  $G_0(t)$  represents the ratio of leakage current to the voltage, and  $G(t)$  represents the ratio of corona discharge current to the voltage, i.e.

$$C(t) = \frac{\epsilon \lim_{\Delta z \rightarrow 0} \iint_S \mathbf{E}(t) \cdot d\mathbf{S}}{u(t, z)}; \quad G_0(t) = \frac{\lim_{\Delta z \rightarrow 0} \frac{1}{\Delta z} \iint_S \gamma \mathbf{E}(t) \cdot d\mathbf{S}}{u(t, z)}; \quad G(t) = \frac{\lim_{\Delta z \rightarrow 0} \frac{1}{\Delta z} \iint_S \mathbf{J}_{corona}(t) \cdot d\mathbf{S}}{u(t, z)} \quad (5.196)$$

Substitute (5.193) – (5.196) into (5.192) and dividing both sides by  $\Delta z$  yields:

$$\frac{\partial i(t, z)}{\partial z} + \frac{\partial}{\partial t} (C(t)u(t, z)) + (G_0(t) + G(t))u(t, z) = 0 \quad (5.197)$$

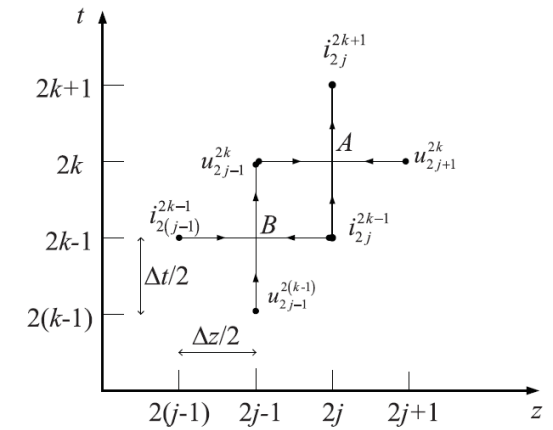
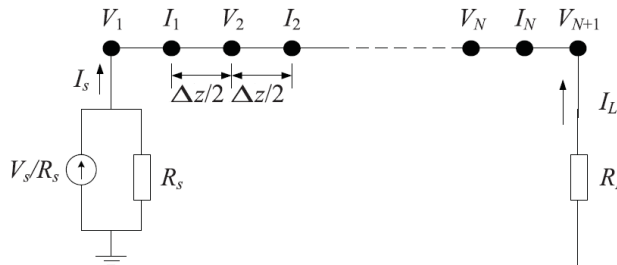
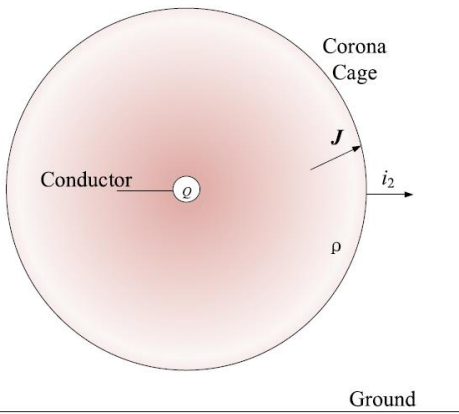
Because the E-field is affected by the space charge,  $C(t)$  and  $G_0(t)$  are parameters corresponding to space charge distribution. In addition, the definition of  $G(t)$  indicates that  $\mathbf{J}_{corona}(t)$  is controlled by the electric field on the conductor surface, so  $G(t)$  is also affected by the space charges. Therefore, the parameters of the transmission line equation are closely related to the space charge distribution.

Given the partial derivative of  $C(t)u(t, z)$  with respect to time can be written as

$$\frac{\partial}{\partial t} (C(t)u(t, z)) = \frac{\partial Q(t)}{\partial t} = \frac{\partial Q(t)}{\partial u(t, z)} \frac{\partial u(t, z)}{\partial t} = C'(t) \frac{\partial u(t, z)}{\partial t} \quad (5.198)$$

Hence, the second equation of (5.190) with any kinds of space charge should be

$$\frac{\partial i(t, z)}{\partial t} + C'(t) \frac{\partial u(t, z)}{\partial t} + (G_0(t) + G(t))u(t, z) = 0 \quad (5.199)$$



The parameter  $C_d$  in conventional transmission line equation is usually obtained by the q-u curve measured through impulse corona characteristics test in corona cage. The charge  $q$  is the time integral of the current  $i_2$  on the corona cage when there are distributed space charges as shown in the figure, i.e.

$$q = \int i_2 dt \quad (5.200)$$

where  $\rho$  is the space charge density generated by the DC corona and impulse corona.  $i_2$  can be expressed as

$$i_2 = \iint_{S'} \mathbf{J} \cdot d\mathbf{S}' + \iint_{S'} \frac{\partial \mathbf{D}}{\partial t} \cdot d\mathbf{S}' = \iint_{S'} \mathbf{J} \cdot d\mathbf{S}' + \frac{\partial q_{sum}}{\partial t} = i_{J2} + \frac{\partial q_{sum}}{\partial t} \quad (5.201)$$

where  $\mathbf{J}$  is the ion current density at the wall of the corona cage,  $q_{sum}$  is the sum of the charge  $Q$  on the conductor and the total space charge  $q_{space}$ ,  $i_{J2}$  is the ion current flowing on the corona cage, and  $S'$  is the surface of the corona cage. It can be seen from (5.200) and (5.201) that  $q$  is not equal to  $q_{sum}$ . The conventional dynamic capacitance  $C_d$  is

$$C_d = \frac{\partial q}{\partial u} = \frac{\partial q}{\partial t} \frac{\partial t}{\partial u} = i_{J2} \frac{\partial t}{\partial u} + \frac{\partial q_{sum}}{\partial t} \frac{\partial t}{\partial u} = i_{J2} \frac{\partial t}{\partial u} + \frac{\partial Q}{\partial t} \frac{\partial t}{\partial u} + \frac{\partial q_{space}}{\partial t} \frac{\partial t}{\partial u} = i_{J2} \frac{\partial t}{\partial u} + C' + \frac{\partial q_{space}}{\partial t} \frac{\partial t}{\partial u} \quad (5.202)$$

The total space charge  $q_{space}$  can be expressed as  $q_{space} = q_{corona} + q_0 - q_J$  where  $q_{corona}$  is the corona charge injected into the space from the conductor surface generated by impulse corona,  $q_0$  is the DC background space charge and  $q_J$  is the charge flowing out of the corona cage. Since the derivation of the charge  $q_J$  flowing out of the corona cage w.r.t time is the ion current  $i_{J2}$ , then

$$\frac{\partial q_{space}}{\partial t} \frac{\partial t}{\partial u} = \frac{\partial q_{corona}}{\partial t} \frac{\partial t}{\partial u} + \frac{\partial q_0}{\partial t} \frac{\partial t}{\partial u} - \frac{\partial q_J}{\partial t} \frac{\partial t}{\partial u} = \frac{\partial q_{corona}}{\partial t} \frac{\partial t}{\partial u} - \frac{\partial q_J}{\partial t} \frac{\partial t}{\partial u} = i_{corona} \frac{\partial t}{\partial u} - i_{J2} \frac{\partial t}{\partial u} \quad (5.204)$$

Substitute (5.203) into (5.201),

$$C_d = C' + i_{corona} \frac{\partial t}{\partial u} = C' + Gu \frac{\partial t}{\partial u} \quad (5.205)$$

Substitute (5.205) into (5.190),

$$\frac{\partial i}{\partial z} + C' \frac{\partial u}{\partial t} + Gu + G_0 u = 0 \quad (5.206)$$

Therefore, the transmission line equations proposed is equivalent to the traditional transmission line equations, with the parameters conveniently obtained through the EM numerical simulation.

Transmission Line Equation with Distributed Space Charge:

$$\begin{cases} \frac{\partial u(t, z)}{\partial z} + L \frac{\partial i(t, z)}{\partial t} + R_0 i(t, z) = 0 \\ \frac{\partial i(t, z)}{\partial z} + C'(t) \frac{\partial u(t, z)}{\partial t} + (G_0(t) + G(t))u(z, t) = 0 \end{cases} \quad (5.207)$$

#### With both space charge and impulse corona:

With Kaptzov's assumption, the E-field on the surface of the conductor keeps the same as the electric field  $E_c$  at the onset of corona discharge. Accordingly, charge  $Q(t)$  is a constant because it is the integral of the E-field along the surface of the conductor. Hence the partial derivative of  $Q(t)$  w.r.t. the voltage is 0, and then  $C'(t) = 0$ . In addition,  $G(t)$  is not equal to 0, then the line equation can be simplified as

$$\begin{cases} \frac{\partial u(t, z)}{\partial z} + L \frac{\partial i(t, z)}{\partial t} + R_0 i(t, z) = 0 \\ \frac{\partial i(t, z)}{\partial z} + (G_0(t) + G(t))u(z, t) = 0 \end{cases} \quad (5.208)$$

#### With space charge but no impulse corona

Charged particles can still exist in space in the absence of impulse corona, for example, when applying impulse voltage with opposite polarity in the presence of background space charges, and when the impulse voltage decrease during the tail time. Accordingly,  $G(t)=0$ , and the line equation is simplified as:

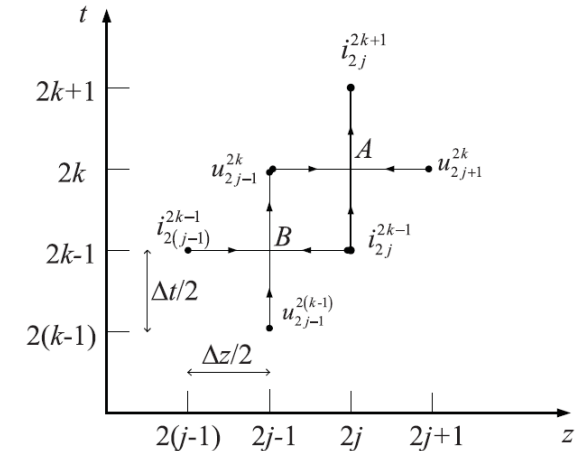
$$\begin{cases} \frac{\partial u(t, z)}{\partial z} + L \frac{\partial i(t, z)}{\partial t} + R_0 i(t, z) = 0 \\ \frac{\partial i(t, z)}{\partial z} + C'(t) \frac{\partial u(t, z)}{\partial t} + G_0(t)u(z, t) = 0 \end{cases} \quad (5.209)$$

Considering the three cases,  $C'(t)$  and  $G(t)$  can be expressed as

$$C'(t) = \begin{cases} C_0 & \rho(t) = 0, E(t) < E_c \\ 0 & \rho(t) \neq 0, E(t) \geq E_c \\ \frac{\partial Q(t)}{\partial u(t, z)} & \rho(t) \neq 0, E(t) < E_c \end{cases}, \quad G(t) = \begin{cases} 0 & \rho(t) = 0, E(t) < E_c \\ \frac{i_j(t)}{u(t, z)} & \rho(t) \neq 0, E(t) \geq E_c \\ 0 & \rho(t) \neq 0, E(t) < E_c \end{cases} \quad (5.210)$$

FDTD (Finite Difference – Time Domain) method is commonly used for solving transmission line equation. It is to separate the line into small segment with length  $\Delta z$ . In the figure,  $V_s$  and  $I_s$  are the voltage and current at the injection point, and  $R_s$  is the equivalent resistance at the injection point,  $I_L$  is load current and  $R_L$  is load resistance.  $V_i$  ( $i = 1, 2, \dots, N, N+1$ ) and  $I_i$  ( $i = 1, 2, \dots, N$ ) are the voltage and current at each calculation point. In time domain, the time interval between every two adjacent voltage calculation points is  $\Delta t$ , and the time interval between each voltage calculation point and its adjacent current calculation point is  $\Delta t/2$ . The method uses center difference formulation to guarantee second-order calculation accuracy:

$$\begin{cases} \frac{\partial u}{\partial z} = \frac{u_{2j+1}^{2k} - u_{2j-1}^{2k}}{\Delta z} \\ \frac{\partial i}{\partial t} = \frac{i_{2j}^{2k+1} - i_{2j}^{2k-1}}{\Delta t} \end{cases} \quad \begin{cases} \frac{\partial i}{\partial z} = \frac{i_{2j}^{2k-1} - i_{2(j-1)}^{2k-1}}{\Delta z} \\ \frac{\partial u}{\partial t} = \frac{u_{2j-1}^{2k} - u_{2(j-1)}^{2(k-1)}}{\Delta t} \end{cases} \quad (5.211)$$



For lines without space charge and impulse corona: (5.211) into (5.190)

$$\begin{cases} \frac{u_{2j+1}^{2k} - u_{2j-1}^{2k}}{\Delta z} + L \frac{i_{2j}^{2k+1} - i_{2j}^{2k-1}}{\Delta t} + \frac{R_0}{2} (i_{2j}^{2k+1} + i_{2j}^{2k-1}) = 0 \\ \frac{i_{2j}^{2k-1} - i_{2(j-1)}^{2k-1}}{\Delta z} + C_0 \frac{u_{2j-1}^{2k} - u_{2(j-1)}^{2(k-1)}}{\Delta t} + \frac{G_0}{2} (u_{2j-1}^{2k} + u_{2(j-1)}^{2(k-1)}) = 0 \end{cases} \rightarrow \begin{cases} u_{2j-1}^{2k} = \left( \frac{G_0}{2} + \frac{C_0}{\Delta t} \right)^{-1} \left[ \left( \frac{C_0}{\Delta t} - \frac{G_0}{2} \right) u_{2j-1}^{2(k-1)} - \frac{i_{2j}^{2k-1} - i_{2(j-1)}^{2k-1}}{\Delta z} \right] \\ i_{2j}^{2k+1} = \left( \frac{R_0}{2} + \frac{L}{\Delta t} \right)^{-1} \left[ \left( \frac{L}{\Delta t} - \frac{R_0}{2} \right) i_{2j}^{2k-1} - \frac{u_{2j+1}^{2k} - u_{2j-1}^{2k}}{\Delta z} \right] \end{cases} \quad (5.212)$$

For lines with space charge and impulse corona: (5.211) into (5.208)

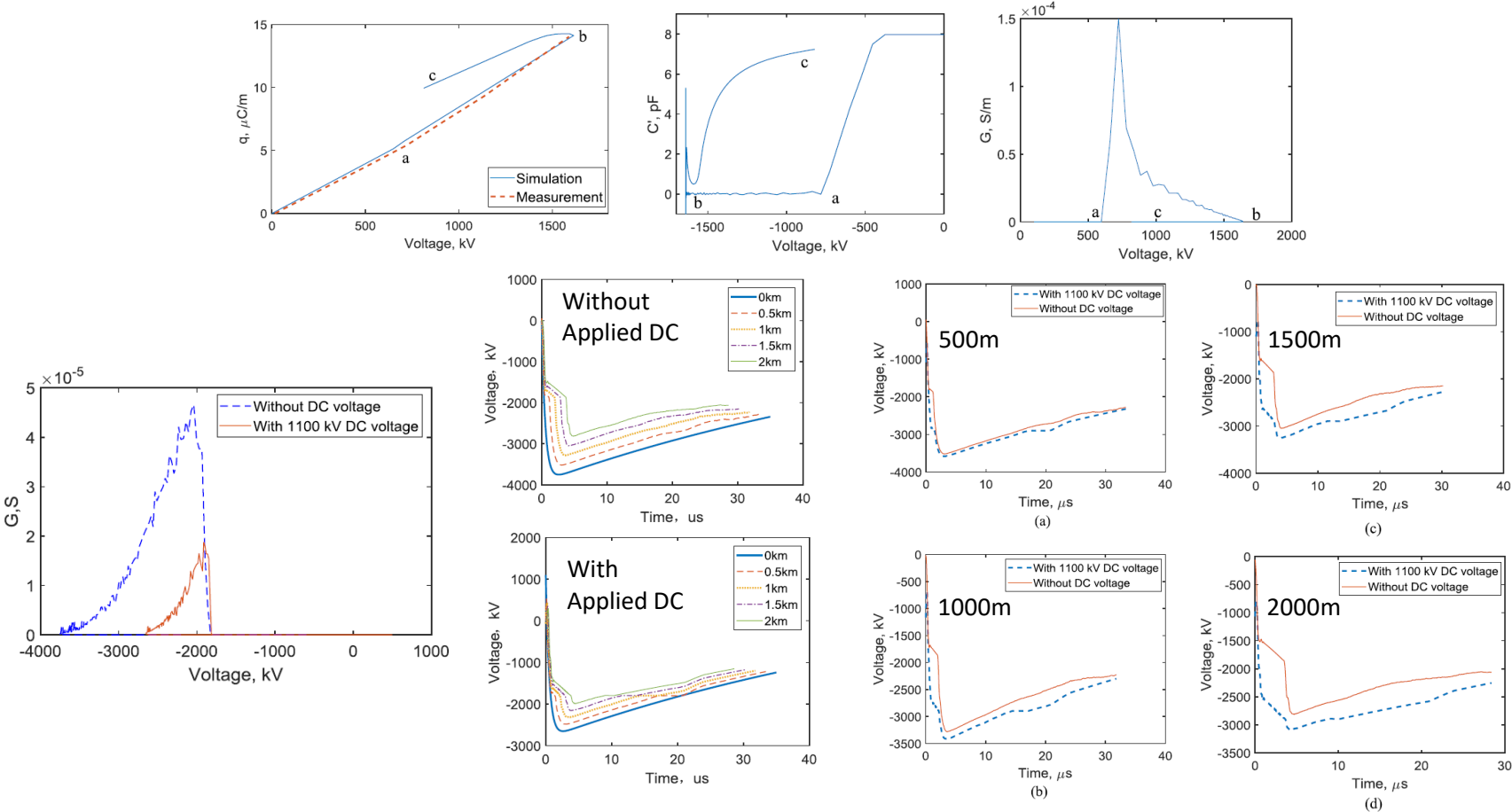
$$\begin{cases} \frac{u_{2j+1}^{2k} - u_{2j-1}^{2k}}{\Delta z} + L \frac{i_{2j}^{2k+1} - i_{2j}^{2k-1}}{\Delta t} + \frac{R_0}{2} (i_{2j}^{2k+1} + i_{2j}^{2k-1}) = 0 \\ \frac{i_{2j}^{2k-1} - i_{2(j-1)}^{2k-1}}{\Delta z} + \frac{\left( (G_0 + G(u_{2j-1}^{2k})) u_{2j-1}^{2k} + (G_0 + G(u_{2(j-1)}^{2(k-1)})) u_{2(j-1)}^{2(k-1)} \right)}{2} = 0 \end{cases} \quad (5.213)$$

$$\rightarrow \begin{cases} u_{2j-1}^{2k} = \left( \frac{G_0 + G(u_{2j-1}^{2k})}{2} \right)^{-1} \times \left( -\frac{G_0 + G(u_{2j-1}^{2k})}{2} u_{2j-1}^{2(k-1)} - \frac{i_{2j}^{2k-1} - i_{2(j-1)}^{2k-1}}{\Delta z} \right) \\ i_{2j}^{2k+1} = \left( \frac{R_0}{2} + \frac{L}{\Delta t} \right)^{-1} \times \left( \frac{L}{\Delta t} - \frac{R_0}{2} \right) i_{2j}^{2k-1} - \frac{u_{2j+1}^{2k} - u_{2j-1}^{2k}}{\Delta z} \end{cases}$$

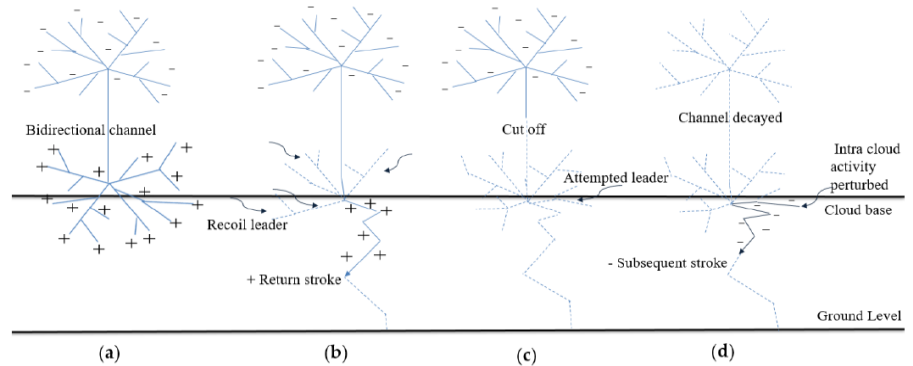
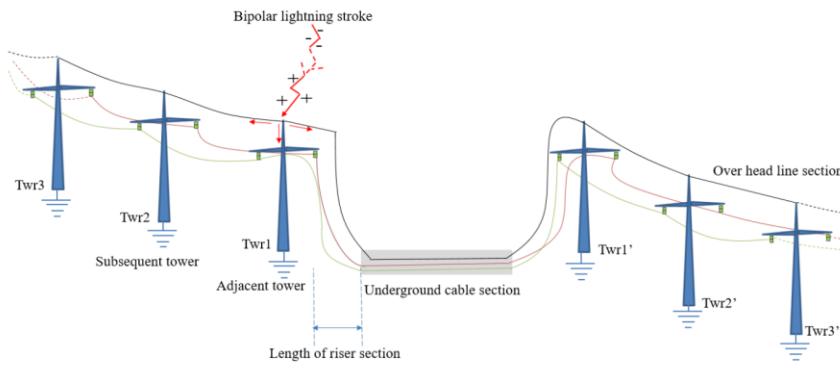
The polarity of the **background DC space charge** has no effect on the derivation of the transmission line equation. Because the lightning is mostly **negative polarity**, the probability of striking the positive polarity wire is greater.

The onset voltage of the impulse corona can be determined not only from the q-u curve but also from C-u curve and G-u curve. From the figures, the voltage corresponding to point "a" is the impulse corona onset voltage, and the voltage corresponding to point "b" is the peak of the impulse voltage. In the "0a" part of the curves, there is no space charge generated by impulse corona. So  $q$  increases linearly with  $u$ ,  $C'(t)$  is equal to the geometric capacitance, and  $G(t) = 0$ . In the "ab" part of the curves, corona occurs. The slope of q-u curve increases and  $G(t)$  is not equal to zero. But due to the Kaptzov's assumption, the charge  $Q(t)$  on transmission line keeps constant, so  $C'(t) = 0$ . In the "bc" part of the curves, corona disappears but the space charges still exist. The slope of q-u curve is approximately the geometric capacitance,  $C'(t)$  gradual recovers to the geometric capacitance and  $G(t) = 0$ .

The voltage on the transmission line is a superposition of the DC voltage and the lightning overvoltage. Therefore, the lightning overvoltage must reach a higher voltage to generate impulse corona discharge with an applied opposite DC voltage. Therefore, the corona discharge losses are relatively small, and the waveform attenuation is slower than those without the applied opposite DC voltage.



**Bipolar lightning strokes** are associated with multiple polarity electrical discharge with no current intervals in between, making their behavior quite peculiar. **Fast front analysis** of a mixed high voltage direct current (HVDC) transmission link can evaluate the factors that influence the line transients due to **shielding failures** and **back-flashovers** (BFOs), considering both overvoltage and **repeated polarity reversal** at the cable sending terminal. A detailed modeling of a bipolar lightning stroke, **frequency-dependent HVDC overhead**, and underground transmission line sections. Noticeable findings include the occurrence of only a positive polarity insulator BFO for the adjacent and subsequent tower, despite the dual polarity of the lightning stroke with relatively small values for the lightning parameters. The influence of traveling waves on the insulator flashover performance of the line varies with parameters such as **the riser section length**, the **tower grounding impedance**, and the **location of the lightning stroke**.



For lightning on mixed lines,

1. Transients due to bipolar strokes have usually asymmetrical magnitude characteristics and have several zero crossings.
2. Transients in transmission lines due to a unipolar direct lightning stroke with multiple flashovers and changing contact points within the **riser section** pertain to similar surge characteristics as that of the transients produced due to bipolar lightning strokes
3. Transmission lines that carrying high power over long distances usually passes through various terrain configurations with varying footing resistance of towers.
4. Unlike a unipolar lightning stroke, when a bipolar lightning stroke hits the OHL section, it can cause overvoltage and polarity reversal simultaneously inside the cable section.

### Line Insulation Modelling:

It is modelled as stray capacitance parallel to CB, which operates with leader progression model (LPM) as discussed below.

Given  $t_b$  = time to break down,  $t_i$  = corona inception time ( $\approx 0$ ),  $t_s$  and  $t_l$  are streamer and leader progression time.

$$t_b = t_i + t_s + t_l \quad (5.214)$$

The streamer begins to grow and crosses the gap after  $t_s$  if the voltage still increases after corona inception.  $t_s$  is given by:

$$\frac{1}{t_s} \int_0^{t_s} U(t) dt = M, \quad M = \begin{cases} 450g + 150 & \text{negative polarity} \\ 400g + 50 & \text{positive polarity} \end{cases} \quad (5.215)$$

where  $g$  = gap length.

The leader will start to grow from both sides after  $t_s$  until the voltage gradient across the un-bridge gap is larger than the critical inception gradient  $E_0$ . The leader progression velocity in  $\text{ms}^{-1}$  proposed by CIGRE is given by

$$v = \frac{dl}{dt} = k_l U(t) \left[ \frac{U(t)}{g - l} - E_0 \right] \quad (5.216)$$

where  $l$  is leader length in m,  $k_l$  is the leader coefficient, and  $E_0$  and  $k_l$  for arc horns and cap pin insulator are as given in the table.

Configuration	Polarity	$k$	$E_0$
		$\text{m}^2 \text{kV}^2 \text{s}^{-1}$	$\text{kVm}^{-1}$
arc horns	+	0.8	600
	-	1.0	670
cap and pin insulators	+	1.2	520
	-	1.3	600

For a given tower, surge impedance for the base, top and crossarm parts of the tower is given by:

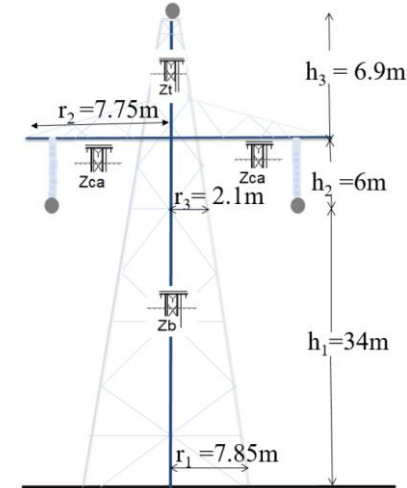
$$Z_b = 60 \ln \cot \left( 0.5 \tan^{-1} \frac{r_1 + r_2}{h_1} \right), Z_t = 60 \ln \cot \left( 0.5 \tan^{-1} \frac{r_2 + r_3}{h_3} \right), Z_{ca} = 60 \ln \left( \frac{2h_2}{r_2} \right) \quad (5.217)$$

A voltage surge produced with lightning partially running through OHGW, while the rest of it propagates towards the tower structure. Low value of tower footing impedance are desired in tower grounding, but the magnitude itself is strongly dependent on **seasonal variation, geography and soil conductivity**.

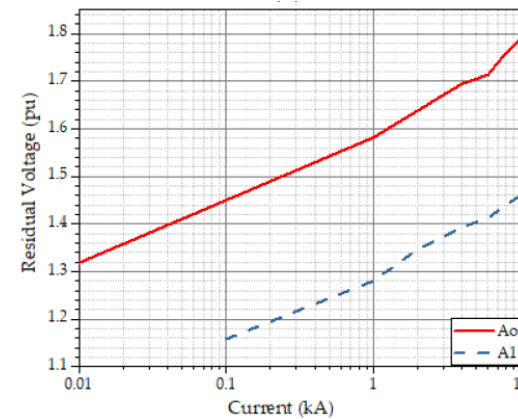
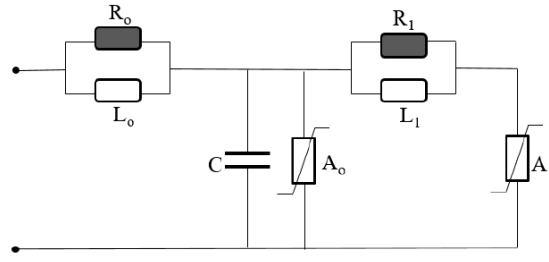
The **current dependent resistance model** is given by

$$R_T = \frac{R_0}{\sqrt{1 + \frac{I}{I_g}}}, \quad I_g = \frac{\rho E_0}{2\pi R_0^2} \quad (5.218)$$

where  $R_T$  is **footing resistance**;  $R_T$  at low frequency and current is given by  $R_0$ ;  $I_g$  is limiting current to start soil ionization;  $I$  is the lightning current from the footing resistance,  $E_0$  is the soil ionization gradient given by 300  $\text{kV/m}$ , and the typical grounding resistance is  $10\Omega$  and the corresponding soil resistivity  $\rho = 300\Omega\text{m}$ .



In the case of mixed HVDC transmission line, excessive lightning overvoltage stress on the OHL section can cause permanent failure of cable insulation. To prevent such failure, the cable section is often protected by surge arresters. A frequency-dependent surge arrester with maximum continuous operation voltage (MCOV) of 1.5 pu for the rated system voltage can be modelled with the following equivalent circuit. The lightning impulse protective level (LIPL) is 2.25 pu for 10kA, an 8 x 20 us discharge current impulse offering a protective margin of 20%. The surge arrester is 7m in height and has one parallel-connected metal oxide block, composed of an RLC circuit and two non-linear resistance  $A_0$  and  $A_1$ .

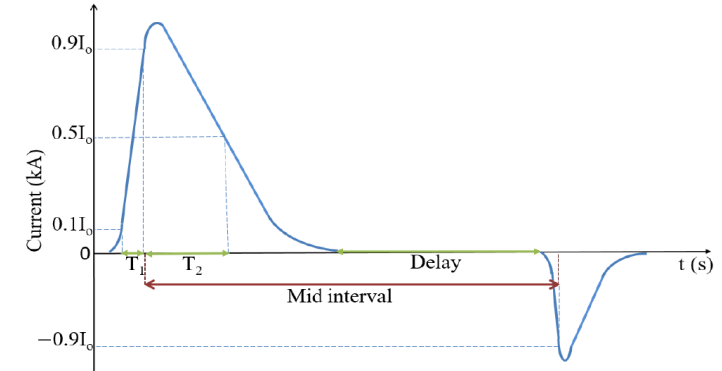


The bipolar lightning source model has its positive peak current higher than its negative peak current in most cases, and **76% of bipolar lightning strokes change their polarity from positive to negative**. Bipolar lightning flashes have been divided into a four-step. To dimension the bipolar lightning stroke, the following parameters are needed.

- two peak current magnitudes of lightning strokes (positive and negative);
- two rise and decay times;
- the mid-interval between the first and the subsequent stroke;

$$i(t) = \frac{I_0}{\eta} e^{-\frac{t}{T_2}} \left( \frac{\left(\frac{t}{T_1}\right)^n}{1 + \left(\frac{t}{T_1}\right)^n} \right) \quad (5.219)$$

given that  $\eta$  is a correction factor,  $I_0$  is the peak current,  $T_1$  and  $T_2$  are the rise time and decay time respectively.

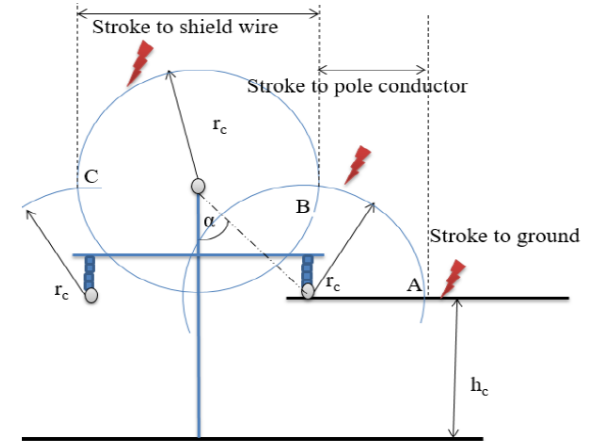


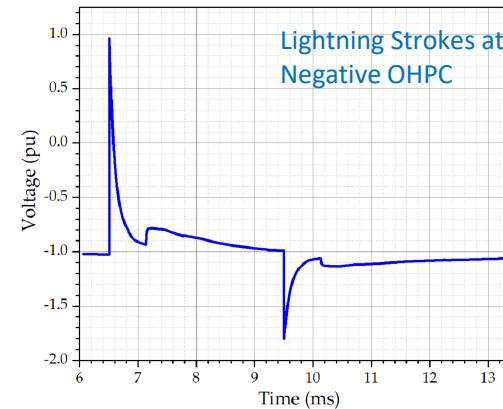
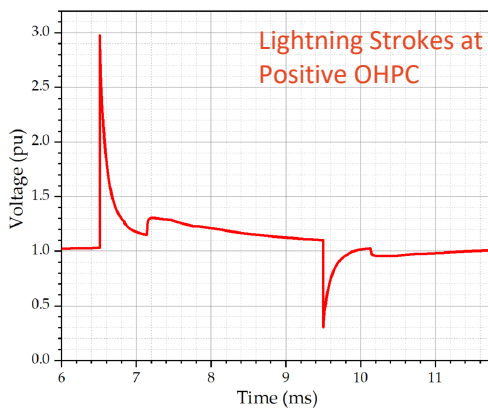
Waveform Constants	Stroke on OHGW		Stroke on OHPC	
	1st Stroke	2nd Stroke	1st Stroke	2nd Stroke
$I_0$ (kA)	70	-57	36	-15
$\eta$	0.89	0.98	0.89	0.99
$T_1$ ( $\mu$ s)	12	3	8	1.9
$T_2$ ( $\mu$ s)	210	77.5	85	90
$n$	7	85	69	58

### Case Study 1: Overhead Pole Conductor (OHPC)

Note that the maximum shielding failure current can be found with:

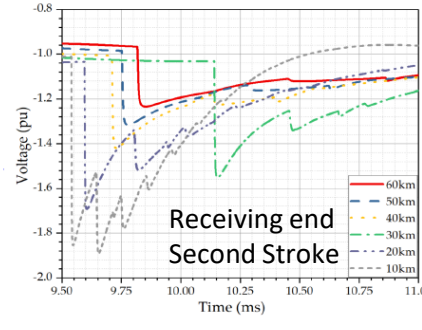
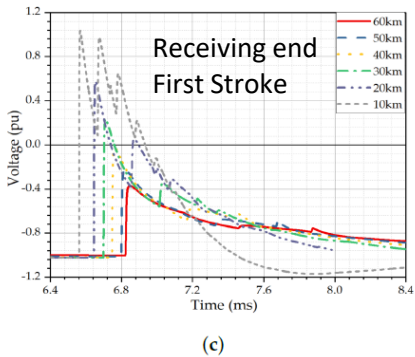
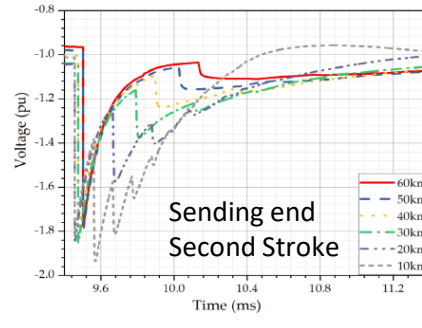
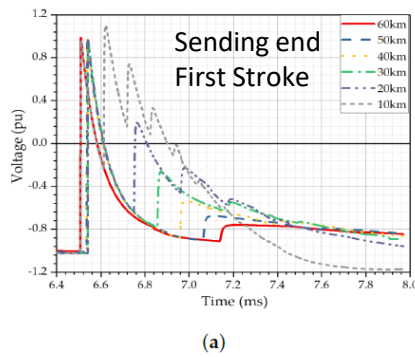
$$I_{MSF} = \left[ \frac{\gamma(h_c + h_g)}{2} \right]^{\frac{1}{Y}}, \quad \gamma = \frac{1}{0.36 + 0.17 \ln(43 - h_c)} \quad (5.220)$$



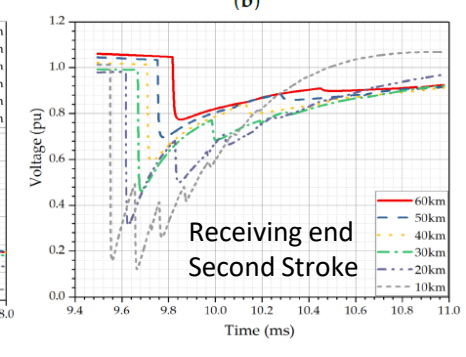
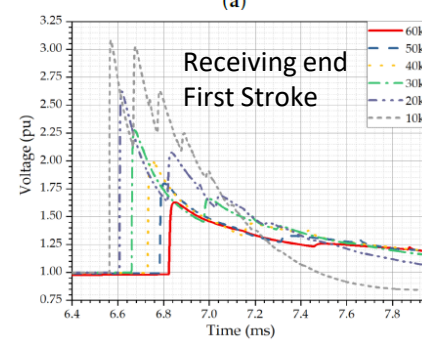
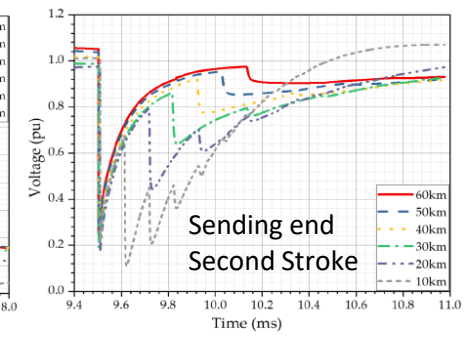
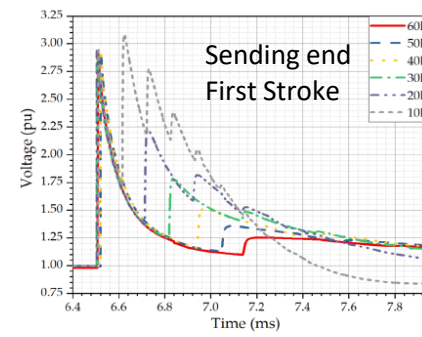


where  $\alpha$  is the **shielding angle**, constant X and Y = 10 and 0.65 respectively,  $h_c$  is the conductor height in m and  $h_g$  is the ground wire height in m. As a result of SF, when the bipolar stroke hits the positive OHPC of transition tower; overvoltage increases up to 3 pu due to the first stroke, and minor polarity reversal is seen due to the subsequent stroke. In case of bipolar lightning stroke to negative pole, critical voltage polarity reversal is seen due to the first stroke, while the subsequent stroke causes overvoltage.

#### Shielding Failure (SF) at **negative pole**



#### Shielding Failure (SF) at **positive pole**



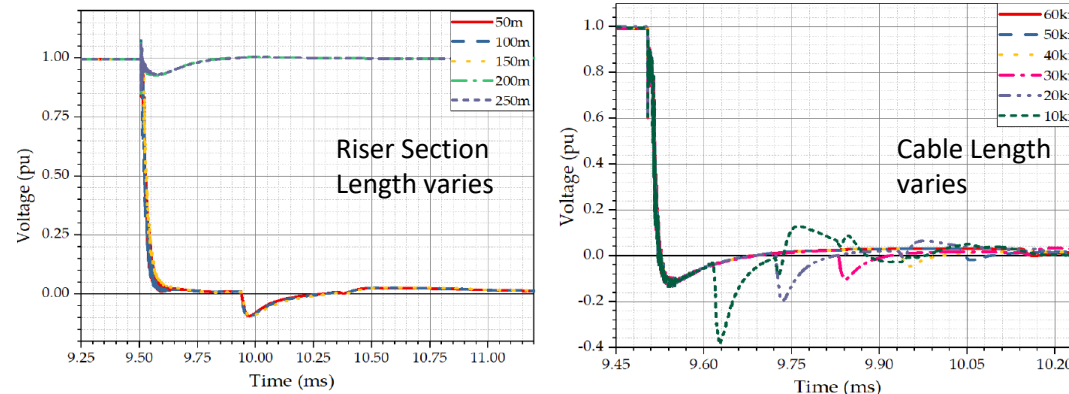
It is noted that:

1. When lightning hits the negative OHPC, **critical polarity reversal** takes place due to the first lightning stroke (-1 pu to 1 pu at 60 km cable length), while the subsequent stroke causes overvoltage in UGC.
2. The cable will accumulate **space charge** due to this polarity reversal, accompanying enhancement in the local fields in its insulation, which will have a severe impact on its electrical strength.
3. The voltage levels at the cable terminals in the cases of overvoltage produced due to **subsequent stroke** stay within a safe range, but there exists a potential threat of **cable insulation breakdown** due to polarity reversal. At the receiving end of long cable sections, polarity reversal due to the first stroke is sufficiently reduced compared to the overvoltage due to the subsequent stroke.
4. In shorter cables, the subsequent stroke arrives before the voltage returns to the system rated voltage after the first stroke, where the system voltage takes longer to normalize because the propagation constant of the cable is short compared to the tail time of the lightning stroke; this causes a constructive superposition of the forward and backward traveling waves.
5. **Direct stroke** onto the positive pole conductor resulted in a buildup of overvoltage due to the first stroke and the small **polarity reversal** in the case of the subsequent stroke. The overvoltage due to the first stroke at cable terminals is above the LIWL of the cable. Therefore, the application of SA is unavoidable for the protection of the cable insulation from permanent failure.
6. Overvoltage produced at cable terminals due to the first stroke is more alarming, as it is above the threshold level of cable insulation. After the application of SA, the overvoltage at the cable terminals is decreased along with the threat of cable insulation failure. However, the overvoltage is still above the LIPL of the SA.

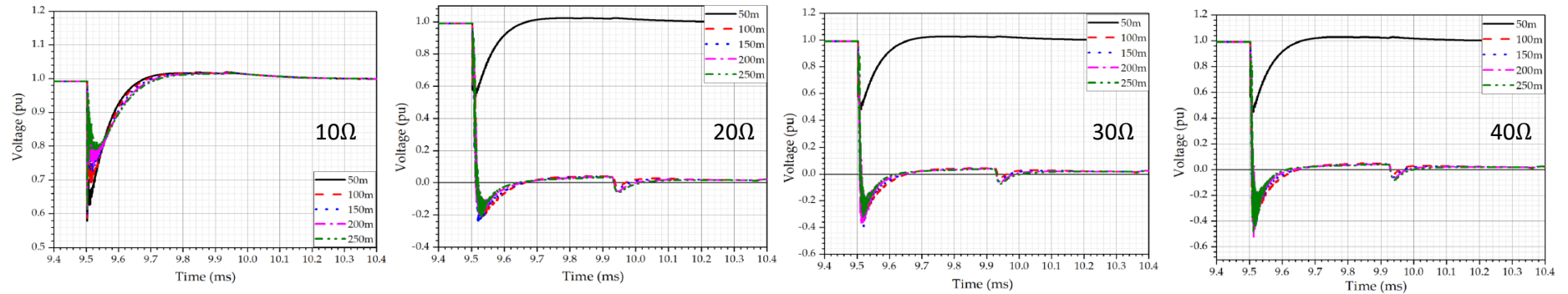
### Case Study 2: Strokes on OPGW

In response to the direct stroke at the top of the adjacent and subsequent towers at the cable entrance, BFO took place due to the negative subsequent stroke of bipolar lightning. This is because of the short front time of the negative subsequent stroke compared to the positive first stroke. In comparison to the negative OHPC, the positive OHPC was already under more stress due to the sequence of polarity of lightning strokes and due to the short front time of the subsequent stroke added to the impulse overvoltage.

Cable Positive Pole-to-Ground Overvoltage due to BFO at different location:



### Case Study 3: Effect of Tower Footing Impedance



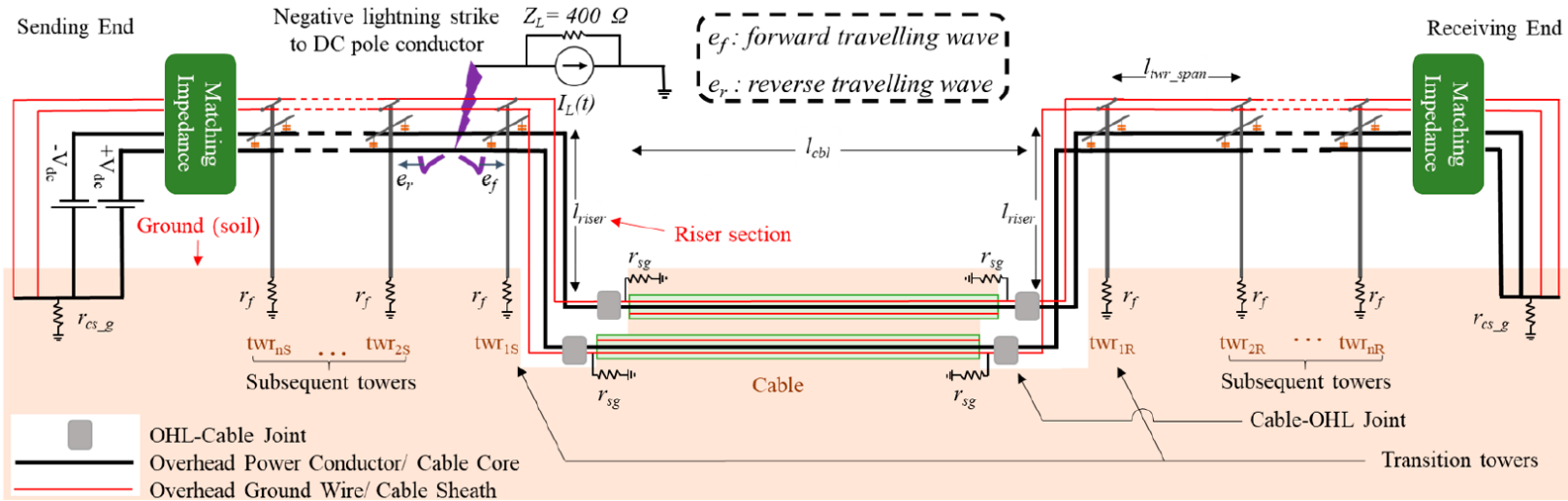
With an increase in the **tower footing resistance**, the magnitude and frequency of the opposite polarity reflected wave from the tower base will decrease, but this effect is compensated by the shorter riser section length, which offers a smaller travel time and attenuation for the reflection wave at the cable entrance to reach the adjacent tower. Thus, increasing the footing resistance of the tower adjacent to the cable entrance with a shorter riser section will not result in BFO.

These reflected waves will attenuate the voltage stress at the lightning strike location, which is at the adjacent tower and will prevent insulation failure. Similarly, despite the varying riser section lengths, no ground fault occurred with a smaller footing resistance of the adjacent tower. However, BFO will occur inevitably in cases where the riser section length increases along with the footing resistance of the adjacent tower; both of these sufficiently reduce the magnitude of the reflected waves and cause BFO.

#### Summary:

1. **Insulation coordination strategy** for underground cables is based upon the standard industry test waveshape (10 kA, 8/20 s), and in adverse situations at an unprotected cable terminal, the surge doubles. In case of bipolar lightning strokes even with minimal lightning stroke parameters, the voltage surge at the cable terminals exceeds the assumed margin of the worst-case scenario for cable insulation.
2. Insulator flashover at OHLs produces lightning overvoltage, which originate multiple reflecting waves from the tower base and cable entrance, leading to an increase in cable insulation failure risk, due to dual polarity reversal along with bipolar lightning strokes.
3. In **bipolar stroke** on OHGW, voltage stress caused insulator flashover of positive pole due to subsequent lightning stroke and contribution of reflected waves from the first stroke. In unipolar lightning strokes, BFO occurs only under exceptional lightning and grounding conditions.
4. BFO occurred at the adjacent tower due to **subsequent stroke** when the footing resistance of tower and riser section length were both large. At smaller riser section lengths, no BFO took place despite varying footing resistance due to reflection waves from the cable entrance, the adjacent tower and its neighboring tower base. Strong backward reflected waves from the cable entrance at shorter riser section lengths compensate for the effect of increased footing resistance of the adjacent tower and no BFO occurs despite the rising footing resistance. At the subsequent tower with riser section length > 150m, no BFO occurs due to sufficient attenuation of backward waves from the cable entrance.
5. **Shielding failure** of positive OHPC caused overvoltage at the cable terminals, which was above the LIPL of cable and energy dissipated by SA increased with decreasing cable length.
6. Small **propagation time** in shorter cable enable the constructive superposition of forward and backward travelling waves.

Another modelling has been performed for unipolar lightning.

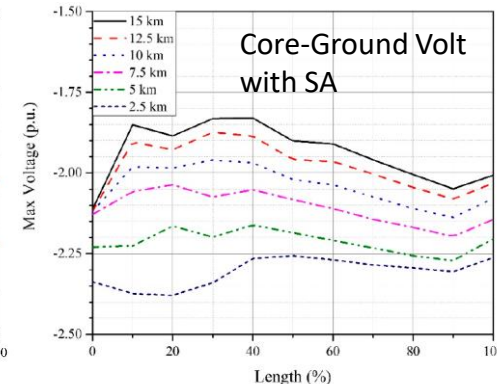
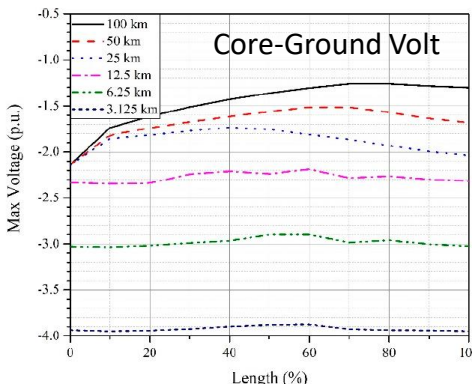
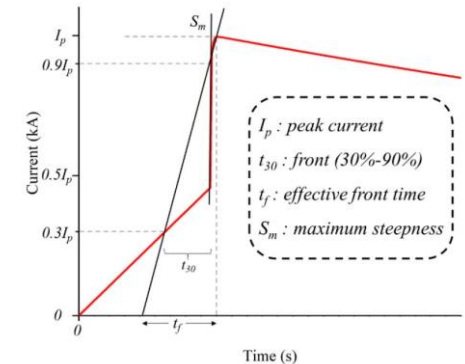


A lightning current waveform with upward concave front can be modelled as

$$i(t) = \begin{cases} At + Bt^n, & t < t_n \\ I_1 e^{-\frac{(t-t_n)}{t_1}} - I_2 e^{-\frac{(t-t_n)}{t_2}}, & t > t_n \end{cases} \quad (5.221)$$

Summary:

- Max core-ground OV increases with a decrease in length of cable. It is due to positive reflection coefficient at the receiving end of cable. For cable shorter than 16km, OV is expected to exceed the LIPL of the cable. Hence, SA should be installed.
- Max sheath-ground OV is independent of cable length due to negative reflection at the receiving end boundary.
- Sheath-ground OV can exceed the LIWL of the jacket significantly for high sheath-grounding impedance ( $> 1.2\Omega$ )
- Sending end subsequent tower "twr<sub>2S</sub>" is most vulnerable to flashover in case of OHPC as well as OHGW strikes. The flashover due to OHGW can be prevented by limiting footing impedance of twr<sub>2S</sub> to  $6\Omega$ .



Different technological options are available to enhance transmission capacity of existing HVAC lines, by means of **current uprating** or **voltage upgrading**. The current uprating options may include the deployment of conventional (series compensators, phase shift transformers) or advanced (FACTS, real-time thermal monitoring) control device or reconductoring with high-temp-low-sag (HTLS) conductors. Beyond all these HVAC options, the transmission capacity increase of existing HVAC lines can be achieved by the conversion of HVAC to HVDC.

An approximate but very practical approach is the one involving the concept of **insulation ratio**  $i_R$ , i.e. the ratio between insulation length required for each AC phase and that required for each DC pole, which is expressed by

$$i_R = k \frac{k_1 E_a}{k_2 V_d} \quad (5.221)$$

where

$k$  = ratio between continuous working DC and AC withstand voltage (determines creepage length of insulators) =  $\sqrt{2}$

$k_1$  = per unit overvoltage for AC lines insulated (determines conductor clearances) = 2.5

$k_2$  = per unit overvoltage for DC lines insulated = 1.7

$E_a$  = phase-to-ground voltage for AC lines

$V_d$  = pole-to-ground voltage of DC lines

$k$  is strongly dependent on the environmental condition. The ratio between  $k_1$  and  $k_2$  can be computed by starting from the clearance  $d_{ac}$  between the active parts and tower in the AC lines, two formulations can be found in literature.

$$\frac{k_1}{k_2} = \frac{d_{ac}}{0.08 + \left( \frac{\sqrt{3}}{\sqrt{2}} V_d - 8.7 \right) \times 0.0051}, \quad \frac{k_1}{k_2} = d_{ac} \left( \frac{1.25 V_d \text{ pu}}{500 K_d} \right)^{-1.667} \quad (5.222)$$

where

pu = peak switching overvoltage (in per unit) expected for the DC line;

$K_d$  = 1.15 for monopolar DC; = 1.25 for bipolar DC

$V_d$  = pole-to-ground voltage of DC lines in [kV]

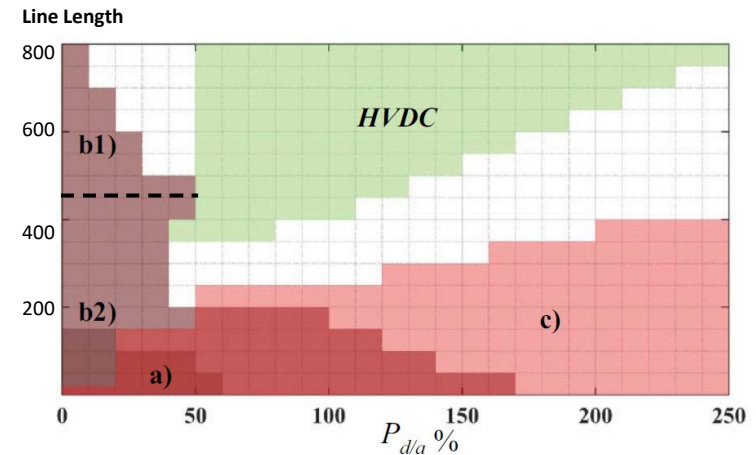
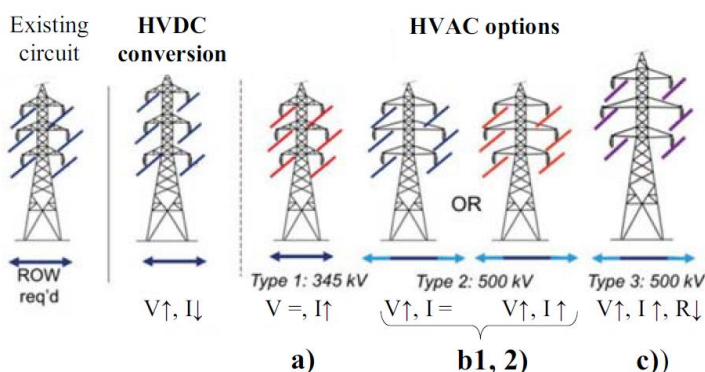
From (5.221), if  $i_R = 1$ , the AC OHL can be converted into a DC line without modifying the insulation lengths. In this situation, the same current, line resistance and power factor = 1 can have a first approximation on the transmittable power ratio  $P_{d/a}$  between transmittable power in DC and that in AC, which is given by

$$P_{d/a} = \frac{P_d}{P_a} = \frac{V_d}{E_a} = k \frac{k_1}{k_2} \quad (5.223)$$

	$k$	$P_{d/a}$	$p\%$
Clean Environment (theoretical limit)	$\sqrt{2}$	2.08	48%
Very light pollution	0.999	1.47	68%
Light pollution	0.909	1.33	74%
Medium pollution	0.83	1.22	81%
Heavy pollution	0.714	1.05	95%
Very heavy pollution	0.625	0.91	108%

Moreover, since it is assumed to have same line current for both AC and DC cases, the line percentage loss ratio  $p\%$  between AC operation and DC one is given by

$$p\% = \frac{p_{d\%}}{p_{a\%}} = \frac{k_2}{k_1} \frac{1}{k} \quad (100) \quad (5.224)$$



### Optimization Problem:

Given total investment cost (TIC) and total operation cost (TOC)

$$\min Z = \sum_{t \in \Omega_T} \left( \left( \frac{1}{(1+r)^{t-1}} \right) TIC_t \right) + \left( \left( \frac{1}{(1+r)^t} \right) TOC_t \right) \quad (5.225)$$

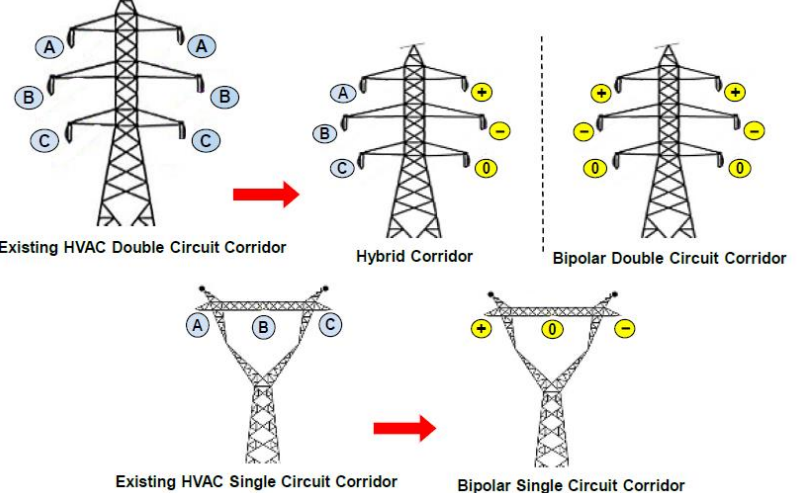
Constraint:

- Generation Constraint:  $P_j^{\min} I_{j,d,h}^t \leq P_j^t \leq P_j^{\max} I_{j,d,h}^t \quad \forall j \in \Omega_G, t \in \Omega_T, d \in \Omega_D, h \in \Omega_H$  (5.226)

- Reserve Constraint  $0 \leq R_{j,d,h}^t \leq P_{j,d,h}^t \quad \forall j \in \Omega_G, t \in \Omega_T, d \in \Omega_D, h \in \Omega_H$  (5.227)

- Coupling of HVAC to VSC-HVDC & Flow Constraint:  $\sum_{v \in \Omega_v} Kc_l^v (1 - \beta \sum_{c \in \Omega_c} Yd_{l,c}^t) Pv c_{v,l,d,h}^t = 2\alpha \sum_{c \in \Omega_c} Yd_{l,c}^t \quad (5.228)$

$$-Kc_l^v P_l^{\max} \sum_{c \in \Omega_c} Yd_{l,c}^t \leq Pv c_{v,l,d,h}^t \leq Kc_l^v P_l^{\max} \sum_{c \in \Omega_c} Yd_{l,c}^t$$



#### 4. Power Balance

$$P_{i,d,h}^t + Pw_{i,d,h}^t + Ps_{i,d,h}^t - (Ld_i^{PK} LF_h^d (1 + LG)^t) = \sum_{l \in \Omega_{EL}} A_l^i Pe_{l,d,h}^t + \sum_{l \in \Omega_{NL}^{AC}, c \in \Omega_C} K_l^i Pl_{l,c,d,h}^t + Kcb_v^i Pv_{v,l,d,h}^t \quad (5.229)$$

Similarly, the optimization of converter location and converter sizing are solved for transfer of HVAC lines to HVDC lines.

The optimization problem can be solved with different objectives such as minimization of investment and operation costs, or maximization of social welfare, i.e.

$$\min_{u_l, P_{cap,l}^{DC}, P_{g,0}, R_{g,0}^{up}, R_{g,0}^{dn}, p_{d,c}^{lsd}, p_{w,c}^{spl}} \sum_{l \in \Omega_{LC}} C_l^{DC}(P_{cap,l}^{DC}, u_l) + (\underbrace{\sum_{g \in \Omega_G} (C_g^p(P_{g,0}) + C_g^{r,up}(R_{g,0}^{up}) + C_g^{r,dn}(R_{g,0}^{dn}))}_{\text{Cost of Gen Unit } g \text{ over year}} + \underbrace{\sum_{i \in \Omega_I} \sum_{c \in \Omega_C} C_i^{lsd}(P_{i,c}^{lsd})}_{\text{Cost of Load Shedding}} + \underbrace{\sum_{w \in \Omega_W} \sum_{c \in \Omega_C} C_w^{spl}(P_{w,c}^{spl})}_{\text{Cost of Wind Spillage}}) \quad (5.229)$$

Variables include:

$P_{l,c}^{AC}, P_{l,c}^{DC}$  = AC/DC Power Flow at Line  $l$  and Contingency  $c$  [MW]

$P_{cap,l}^{DC}$  = Power Rating of HVDC Converter in Line  $l$  [MW]

$P_{g,0}, P_{g,c}$  = Generating Unit Output Power at Operating Point and After Contingency  $c$  [MW]

$P_{i,c}^{lsd}$  = Load Shedding at bus  $i$  and contingency  $c$  [MW]

$p_{w,c}^{spl}$  = Wind Spillage at Wind Farm  $w$  and Contingency  $c$  [MW]

$R_{g,0}^{up}, R_{g,0}^{dn}$  = Upward / Downward Reserve of Generating Unit  $g$  [MW]

$u_l \in \{0, 1\}$  = Binary Variable for Converting a Circuit from AC to DC in line  $l$

$\Delta\theta_l$  = Voltage Angle Difference between Two Nodes of Line  $l$ .

subj. to

1. Power Flow Equality Constraints  $A_{ig}P_{g,c} - P_i + A_{il}(P_{l,c}^{AC} + P_{l,c}^{DC}) + A_{iw}(P_w - P_{w,c}^{spl}) + P_{i,c}^{lsd} = 0$  (5.230)

2. AC Transmission Line Flow  $-(2 - u_l - L1_{l,c}^{AC})M_l \leq P_{l,c}^{AC} - B_l\Delta\theta_{l,c} \leq (2 - u_l - L1_{l,c}^{AC})M_l$   $-u_l L1_{l,c}^{AC} \bar{P}_l \leq P_{l,c}^{AC} \leq u_l L1_{l,c}^{AC} \bar{P}_l$  (5.231)

3. DC Transmission Line Flow  $(1 - u_l)P_{cap,l}^{DC} \leq P_{cap,l}^{DC} \leq (1 - u_l)\bar{P}_{cap,l}^{DC}$   $-L1_{l,c}^{DC} P_{cap,l}^{DC} \leq P_{l,c}^{DC} \leq L1_{l,c}^{DC} P_{cap,l}^{DC}$  (5.232)

4. Output Limits of Generating Unit  $0 \leq P_{g,0} \leq \bar{P}_g; 0 \leq R_{g,0}^{up} \leq \bar{P}_g - P_{g,0}; 0 \leq R_{g,0}^{dn} \leq P_{g,0}$  (5.233)

5. Limits for Security Actions  $0 \leq P_{w,c}^{spl} \leq P_w; 0 \leq P_{i,c}^{lsd} \leq P_i$  (5.234)

With the large-scale implementations of HVDC transmission technology, the environmental impacts of electromagnetic field near HVdc projects have become a focus of public attention. In contrast to the HVAC power lines, the electric field near HVDC lines is greatly influenced by the **space charges** generated by **corona discharge**. The electric field considering the **flowing space charges** is named as **ion-flow field**. An accurate and efficient prediction method for ion-flow field is needed during the design of HVDC lines.

### Mathematical Model for Ion-Flow Field

#### 1. Governing Equation for Potential $\varphi$ (Poisson's Equation)

$$\nabla^2 \varphi = -(\rho^+ - \rho^-)/\epsilon \quad (5.235)$$

given that  $\rho^+$  and  $\rho^-$  are positive and negative space charge respectively.

#### 2. Relationship between Electric Field and Electric Potential

$$\mathbf{E} = -\nabla \varphi \quad (5.236)$$

#### 3. Boundary Condition (Dirichlet Condition):

$$\begin{cases} \varphi \Big|_{\Gamma_L} = U \\ \varphi \Big|_{\Gamma_G} = 0 \end{cases} \quad (5.237)$$

where  $\Gamma_L$  and  $\Gamma_G$  are the boundary on transmission lines and ground respectively.

#### 4. Charge Transport Equation

$$\begin{cases} \nabla \cdot (\rho^+ k^+ \mathbf{E}) = -R_i \rho^+ \rho^- / e \\ \nabla \cdot (\rho^- k^- \mathbf{E}) = +R_i \rho^+ \rho^- / e \end{cases} \quad (5.238)$$

where  $k$  is ion mobility rate;  $R_i$  is ion recombination rate; and  $e$  is the charge of an electron.

#### 5. Boundary Condition (Dirichlet Condition) for (5.238)

$$\rho \Big|_{\Gamma_L} = \rho_L \quad (5.239)$$

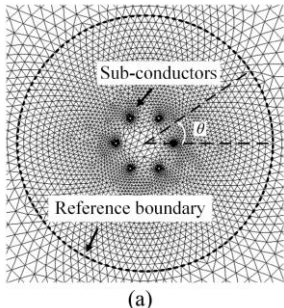
where  $\rho_L$  is the space charge density on  $\Gamma_L$ .

**Kaptzov's hypothesis**, i.e. E-field on the conductor surface remains on the corona onset electric field after the corona discharge has been stable, is applied to determine the value of  $\rho_L$ .

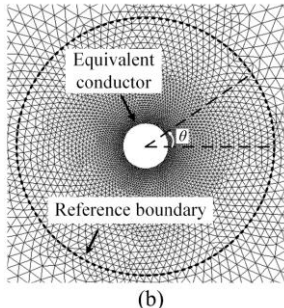
Recall Peek's Equation: [Note – Conversion factor is included to transfer bundled conductor to single conductor]

$$\begin{cases} E_{oneq+} = m_{eq+} E'_{oneq+} = m_{eq+} \times 33.7(1 + 0.240/\sqrt{r_{eq}}) \\ E_{oneq-} = m_{eq-} E'_{oneq-} = m_{eq-} \times 31.0(1 + 0.308/\sqrt{r_{eq}}) \end{cases} \quad (5.240)$$

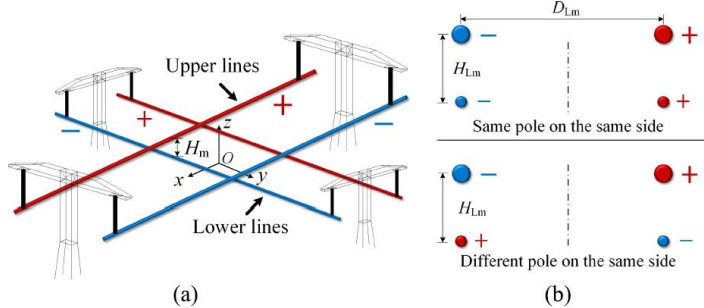
Where  $E'_{oneq}$  and  $E_{oneq}$  are corona onset electric fields on the “smooth” and “rough” equivalent conductor, respectively.



(a)

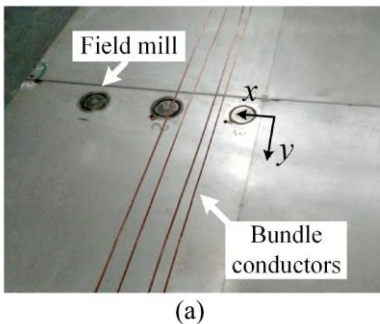
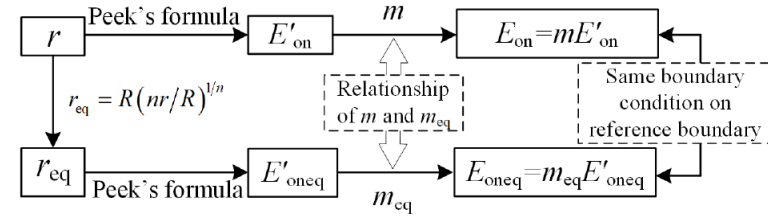


(b)

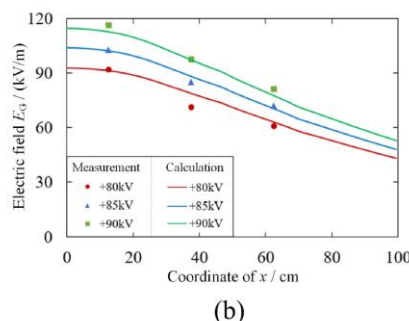


(a)

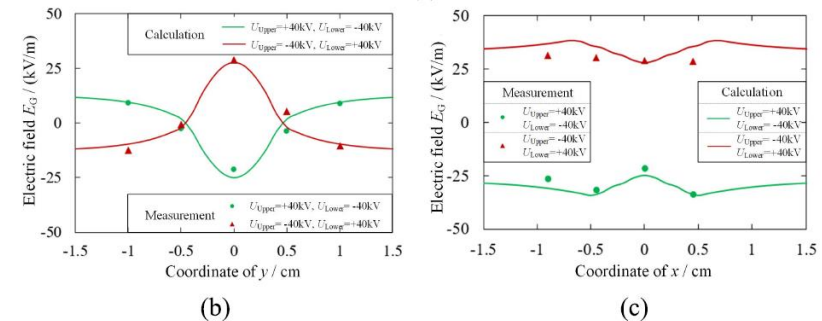
(b)



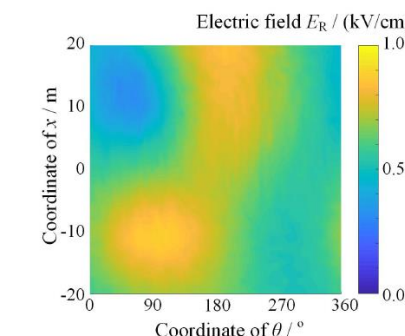
(a)



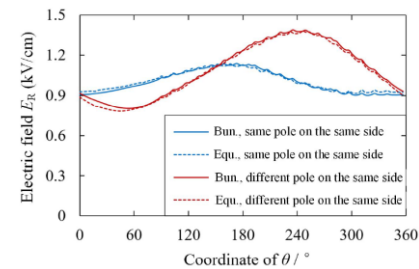
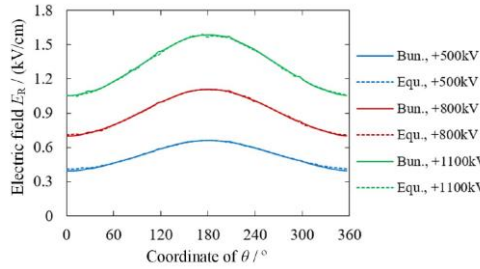
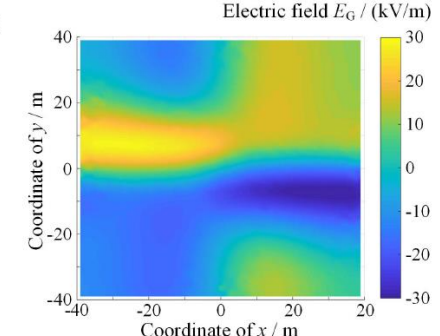
(b)



### Boundary of Lower Lines

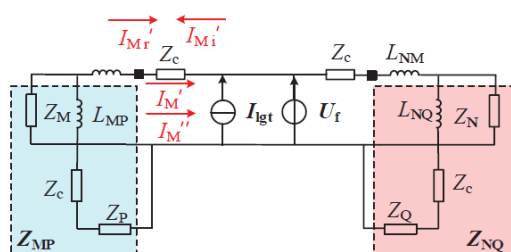
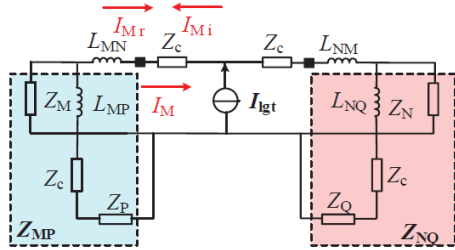
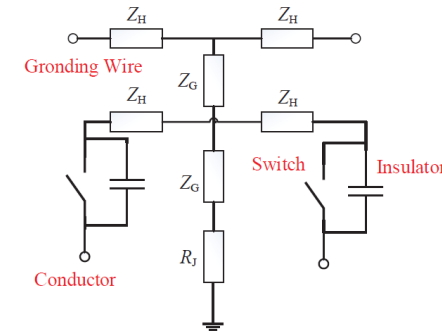
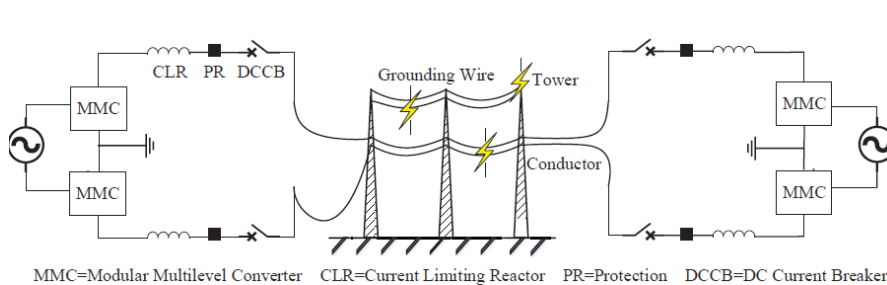


### On Ground



Due to the small damping effect in HVDC system, fault current develops very fast, requiring the protection (CB + Converter) to discriminate fault correctly within 1~2ms. Traveling wave characteristic is suitable for fast discrimination, but it can be easily affected by the high-frequency disturbance. For VSC-HVDC systems in OHL, lightning disturbance is the main reason for line protection mal-operation. Therefore, it is necessary to accurately distinguish lightning disturbances from faults, ensuring safety and stability of the system.

Traditional methods include time-domain (integral value, rate of change, mean value, variance), frequency-domain ([wavelet transform](#), [Hilbert-Huang transform](#) to calculate energy content in different frequency) or AI based methods (BR-CNN, SAE, SVM). Time-domain methods is based on setting a threshold, yet the threshold is often relying on Morphological Analysis and Correlation Analysis, in which extraction-based method increases the time delay, which is contradiction to the ultra-speed protection requirement; Frequency-domain methods heavily depends on the mother wavelet. Improper selection will affect extraction results. AI-based method requires high quantity in data with good data symmetry for further simulation. A method based on [rise-fall-time-ratio](#) (RFTR) of 1-mode current is proposed with travelling wave.



### Lightning Disturbance

Given  $I_{igt}$  = lightning current source,  $I_M$  is current measured for CD,  $I_{mi}$  is incident wave,  $I_{mr}$  is reflected wave,  $Z_c$  is line characteristic impedance,  $L_{MN}$ ,  $NM$ ,  $MP$ ,  $NQ$  are current limiting reactors and  $Z_{M, N, P, Q}$  are converter station impedance

$$I_M = I_{Mi} + I_{Mr} = (1 + \beta_M)I_{Mi} = (1 + \beta_M) \frac{Z_{LN}}{Z_{LM} + Z_{LN}} I_{igt} \quad (5.241)$$

$$Z_{LM} = Z_c + sL_{MN} + Z_{MP}, \quad Z_{LN} = Z_c + sL_{NM} + Z_{NQ}$$

### Characteristics Analysis of 1-mode Current

$$\begin{pmatrix} I_1 \\ I_0 \end{pmatrix} = \frac{1}{\sqrt{2}} \begin{pmatrix} 1 & -1 \\ 1 & 1 \end{pmatrix} \begin{pmatrix} I_p \\ I_n \end{pmatrix} \quad (5.242)$$

where  $I_p$  and  $I_n$  are positive pole and negative pole current respectively.

Back-Flash without flashover: when lightning strike the tower or the ground wire, the additional voltage  $\Delta U_{lgt}$  generated by lightning will add voltage  $\Delta U_p$  and  $\Delta U_n$  to the positive and negative conductor.

$$\Delta U_p = K_p \Delta U_{lgt}; \Delta U_n = K_n \Delta U_{lgt} \quad (5.243)$$

where  $K_p$  and  $K_n$  are the coupling coefficients of the tower (or ground wire) and the conductor.

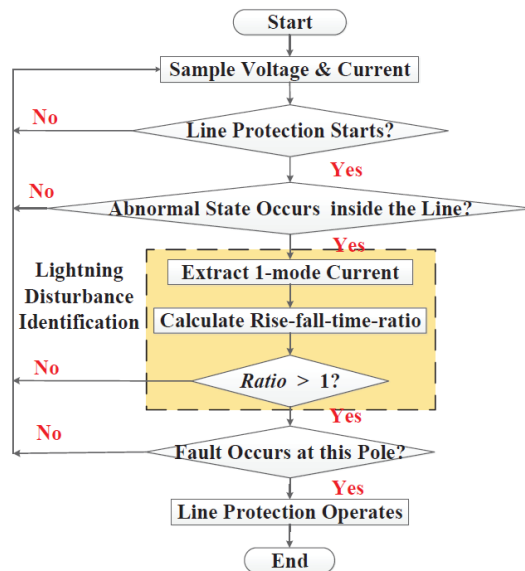
Before the DC control system responds, the additional current is given by

$$\Delta I_p = \frac{\Delta U_p}{Z_p}; \Delta I_n = \frac{\Delta U_n}{Z_n} \quad (5.244)$$

where  $Z_p$  and  $Z_n$  are system impedance of positive and negative pole. For symmetrical system,  $Z_p = Z_n$ .

Based on (5.242) – (5.244), the 1-mode component of additional current  $\Delta I_1$  can be obtained.

$$\Delta I_1 = \frac{1}{\sqrt{2}} \left( K_p \frac{\Delta U_{lgt}}{Z_p} - K_n \frac{\Delta U_{lgt}}{Z_n} \right) \approx \frac{1}{\sqrt{2}} (K_p - K_n) \frac{\Delta U_{lgt}}{Z_s} \quad (5.245)$$



Step 1: Line Protection Device Start

Step 2: Determine if it is a fault (or disturbance, and reset)

Step 3: Extract the 1-mode of additional current  $\Delta I_1$

Step 4: Calculate the ratio of rise time and fall time within a fixed time window –

$$T_{rise}(k) = \begin{cases} 1, & \Delta I_1(k) < \Delta I_1(k+1) \\ 0, & \Delta I_1(k) \geq \Delta I_1(k+1) \end{cases} \quad (5.246)$$

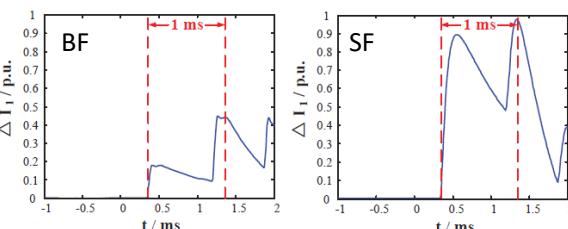
$$T_{fall}(k) = 1 - T_{rise}(k)$$

$$Ratio = \frac{\sum_{k=1}^N T_{rise}(k)}{\sum_{k=1}^N T_{fall}(k)}, \quad Ratio \begin{cases} < 1, & \text{disturbance} \\ > 1, & \text{fault} \end{cases} \quad (5.247)$$

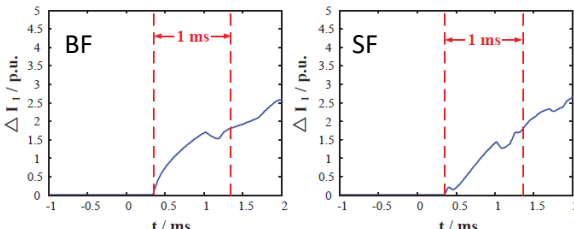
Step 5: Lightning Disturbance Identification determines whether a disturbance occurs according to the ratio. If yes, reset protection.

Step 6: Launch a trip command if no.

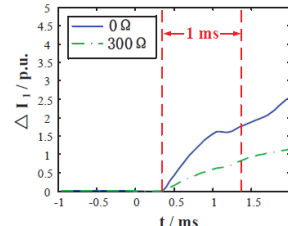
Lightning Disturbance (without Flashover)



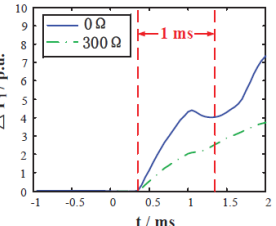
Lightning Fault (with Flashover)



(a) Pole-to-Ground Fault



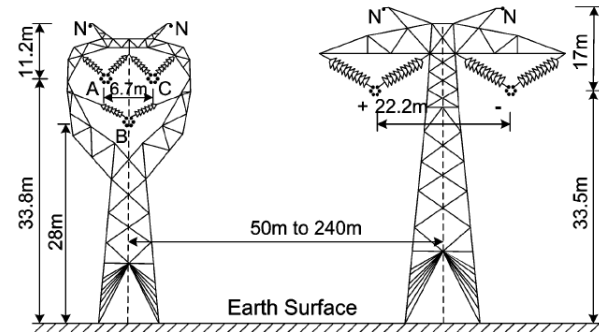
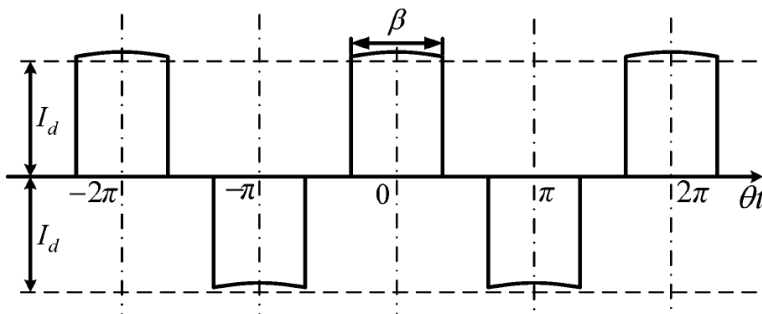
(b) Pole-to-Pole Fault



EM interference in a DC line, due to the capacitive and inductive coupling from a parallel AC line in close proximity is studied. Fundamental frequency current induced on the DC line would be converted to DC component and harmonic current components after it flows into the converting equipment which may cause saturation, noise and irregular operation of the converting transformer.

It is noted that

- If the separation distance between AC and DC lines is larger than 50 m, the induced voltage on dc line would NOT lead **the insulation of converting equipment breakdown** and the generated DC would not cause irregular operation of converting transformer.
- Whether for the induced transverse voltage or the induced longitudinal EMF, the **shielding effect** of ground wires is evident. Consequently, the ground wires should be provided in the parallel ac/dc transmission system.
- The **interference** generated in the case of typical horizontal arrangement of ac phase conductors is higher than that in the case of compact arrangement especially when the separation distance between ac and dc lines is near.
- The induced transverse voltage does not vary with the parallel length markedly, while the induced longitudinal EMF increases with the parallel length in approximate direct proportion. Long distance parallel AC/DC transmission lines should be avoided in practice.
- Both the induced transverse voltage and the induced longitudinal EMF are affected slightly by **soil resistivity**.



Per unit length Self-impedance  $Z_s$ : (Complex Depth method)

$$Z_s = j\omega \frac{\mu_0}{2\pi} \ln \frac{2(h+p)}{r}, \quad p = \frac{1}{\sqrt{j\omega\mu_0\sigma}} \quad (5.248)$$

where  $\sigma$  is soil conductivity,  $h$  is the height of conductor over ground,  $r$  is the radius of conductor.

In a common 3-phase 6-pulse converter bridge, current after inversion  $i_a$  is given by

$$i_a = \frac{2\sqrt{3}}{\pi} I_d \left[ \cos \theta t - \frac{1}{5} \cos 5\theta t + \frac{1}{7} \cos 7\theta t - \frac{1}{11} \cos 11\theta t + \dots \right] \quad (5.249)$$

where  $I_d$  is the DC current on DC line.

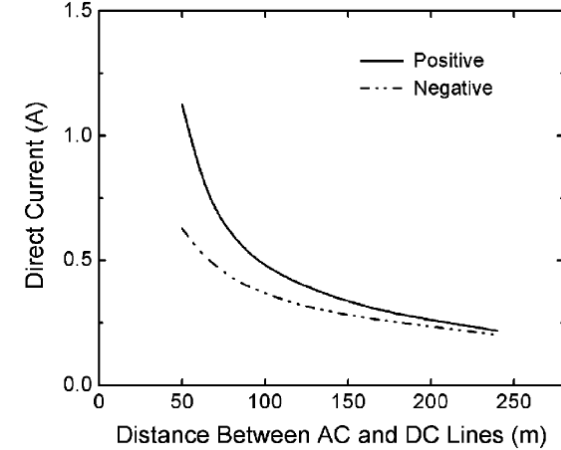
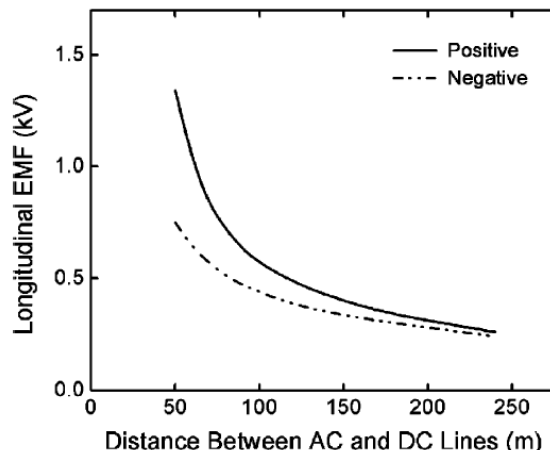
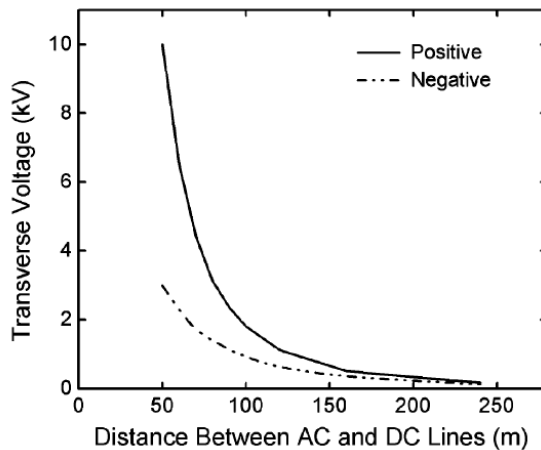
In parallel AC/DC transmission system, current through DC line is

$$i'_d = i_d + i_{ind} \cos(\theta t + \varphi) \quad (5.250)$$

With Fourier Transform and operating principle for 3-phase 6-pulse converter bridge, the DC component of the current generated after inversion can be given by

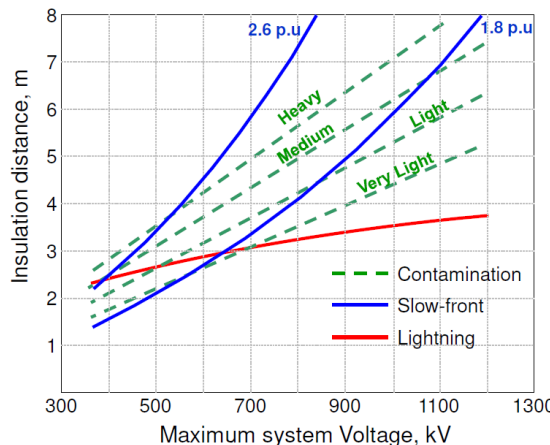
$$I_{dcc} = \frac{\sqrt{3}}{\pi} I_{ind} \cos \varphi \quad (5.251)$$

Considering the worst case, namely  $\cos \varphi = 1$ ,  $I_{dcc} \approx 0.552 I_{ind}$ .

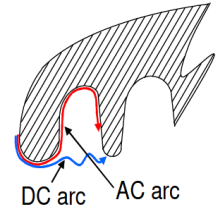
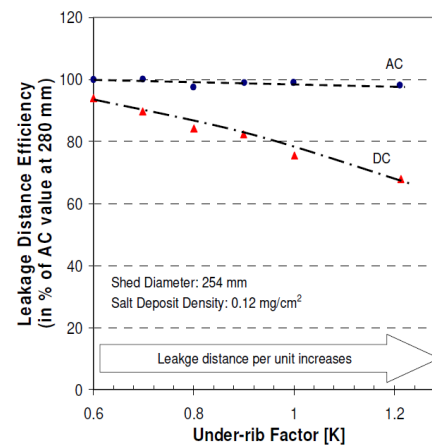
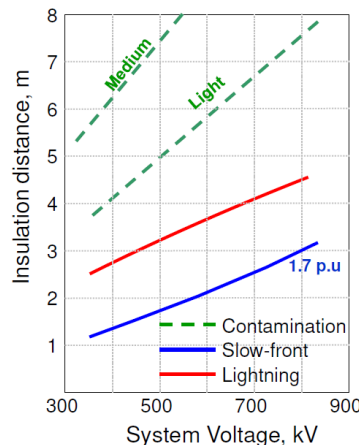


## Extra Material:

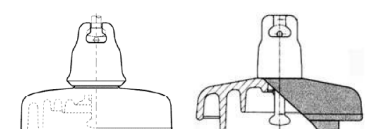
### AC Systems



### DC Systems



Need special DC insulator profiles



## 5.4 Ground Potential Rise (GPR)

Lightning is one of the main factors causing insulation failure and line outage, and it imposes high costs to power utilities for maintenance and replacement of damage equipment. Surge arrester and shield wires are main devices against lightning surge and minimize the probability of Back-Flashover (BFO) and Shielding Failure (SF). Yet, another concern for BFO and SF is the safety issue created by ground potential rise (GPR). Hence, other than the lightning parameters affecting resultant overvoltage, tower footing resistance is studied to avoid breaching the limit.

Given the occurrence of lightning parameter  $x$ .

$$p(x) = \frac{1}{\sigma_{\ln x} \sqrt{2\pi}} \exp \left\{ -\frac{1}{2} \left( \frac{\ln x - \ln \bar{x}}{\sigma_{\ln x}} \right)^2 \right\} \quad (5.252)$$

To represent the lightning current waveform, Heidler function is employed.

$$i(t) = \frac{I_p}{\eta} \frac{\left(\frac{t}{\tau_1}\right)^n}{1 + \left(\frac{t}{\tau_1}\right)^n} e^{-\frac{t}{\tau_2}} \quad (5.253)$$

where  $I_p$ ,  $n$ ,  $\eta$ ,  $\tau_1$ ,  $\tau_2$  are peak current, current steepness factor, peak current correction factor, time constants for rise time and decay time respectively.

Striking distance to conductor  $R_c$  and to ground  $R_g$  are found with

$$R_c = 10 I^{0.65}, R_g = 0.8615 I^{0.65} \quad (5.254)$$

For the transmission tower,

$$R_i = \Delta R_i h_i [\Omega], \quad L_i = 2\tau R_i [\mu H], \quad \Delta R_1 = \frac{2Z_{t1}}{h - h_2} \ln \left( \frac{1}{\alpha_1} \right), \quad \Delta R_2 = \frac{2Z_{t2}}{h} \ln \left( \frac{1}{\alpha_2} \right) \quad (5.255)$$

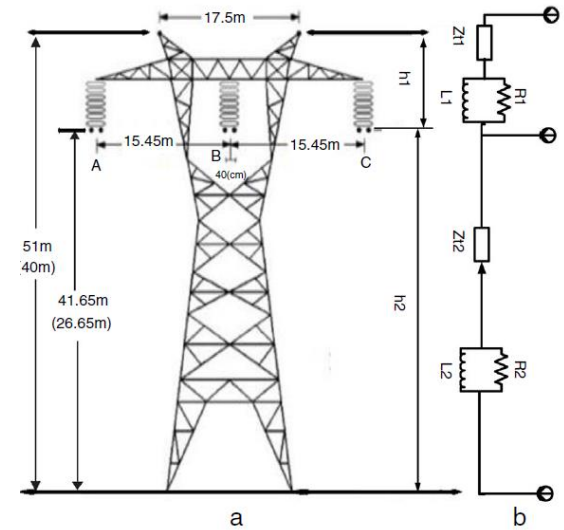
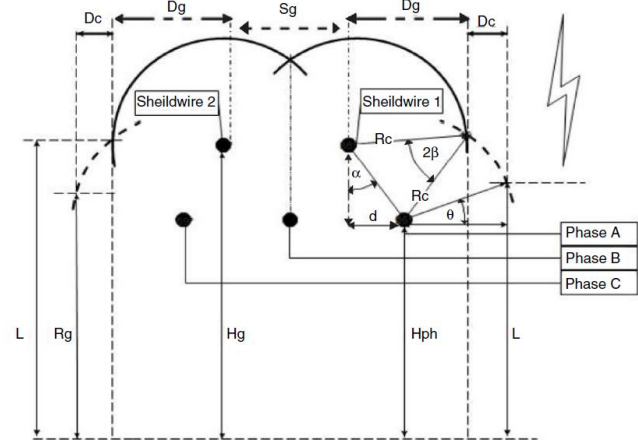
where  $\tau = h/c$  where  $c = 300m/\mu s$ , the light velocity in free space,  $h$  [m] is tower height,  $\alpha_1 = \alpha_2 = 0.89$ , the attenuation factor along the tower.

Integration model is employed for insulator strings:

$$DE = \int_{t_0}^t (V(t) - V_0)^k dt$$

(5.256)

where  $V_0$  [kV] is the required minimum voltage,  $DE$  [ $kV^k \mu s$ ] is the disruptive effect of applied Impulse voltage  $V(t)$  exceeds  $V_0$  and  $k$  is a factor according for the effect of applied voltage amplitude and time on  $DE$ .



Frequency dependent of soil electrical parameters based on Longmire and Smith's (1975) analytical formula is used.

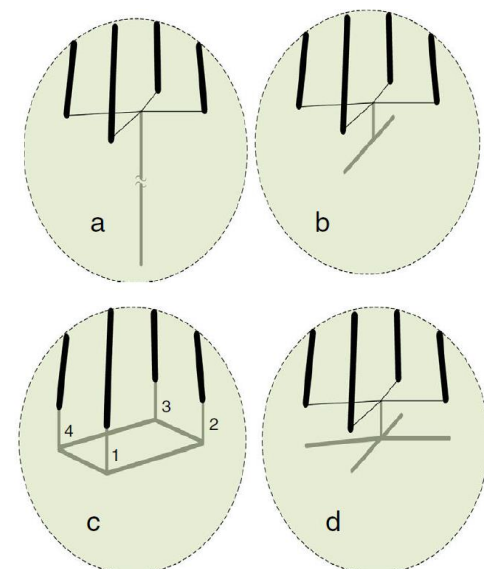
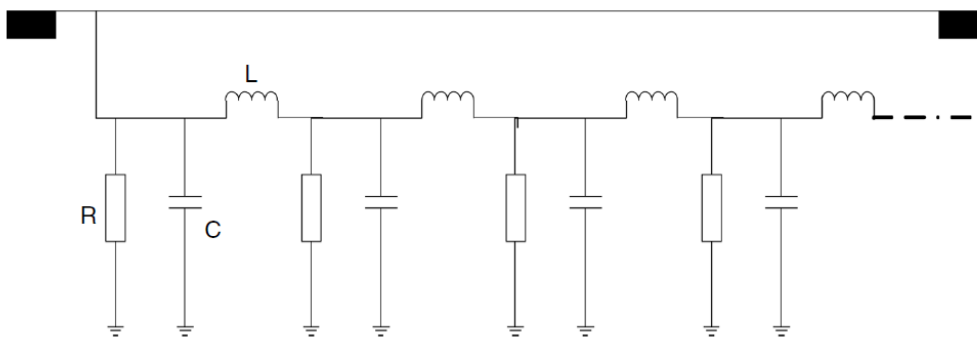
$$\rho_0 = 125 \left( \frac{p}{10} \right)^{-0.54} [\Omega\text{m}], \quad \varepsilon_\infty = 5 \quad (5.257)$$

$$\rho_f = \left( \rho_0^{-1} + 2\pi\varepsilon_0 \sum_{n=1}^{14} \frac{\left( a_n \left( \left( \frac{p}{10} \right)^{1.28} 10^{n-1} \right) \left( \frac{f}{\left( \frac{p}{10} \right)^{1.28} 10^{n-1}} \right)^2 \right) }{1 + \left( \frac{f}{\left( \frac{p}{10} \right)^{1.28} 10^{n-1}} \right)^2} \right)^{-1}, \quad \varepsilon_r(f) = \varepsilon_\infty + \sum_{n=1}^{14} \frac{a_n}{1 + \left( \frac{f}{\left( \frac{p}{10} \right)^{1.28} 10^{n-1}} \right)^2}$$

where  $\rho_0$  is low-frequency resistivity, p is water percentage in soil, f is frequency range which varies DC to 2MHz,  $\rho_f$  and  $\varepsilon_r(f)$  are soil resistivity and relative permittivity respectively.

Grounding system can be modeled in three different ways: the **wide-band model** assuming **constant** (CP wide-band) and **frequency-dependent** (FD wide-band) electrical parameters or a **simple resistor** (Static model). However, the soil ionization due to the high impulse current injected into the tower-footing grounding system is neglected.

Given the following equivalent circuit for grounding electrode, where R is non-linear resistance.



If transmission line is excited from one-side, while the far-end is opened, the grounding impedance is

$$Z(j\omega) = Z_c \coth \gamma l \quad (5.258)$$

where  $Z_c$  and  $\gamma$  are respectively characteristics impedance and propagation constant. The grounding electrode for vertical rod and horizontal rod are given by

$$(5.259)$$

$$Z_c = \frac{A_1}{2\pi} \sqrt{\frac{j\omega\mu_0\rho}{1+j\omega\varepsilon\rho}}, \quad \gamma = \sqrt{j\omega\mu_0 \left( \frac{1}{\rho} + j\omega\varepsilon \right)}; \quad Z_c = \frac{A_2}{2\pi} \sqrt{\frac{j\omega\mu_0\rho}{2(1+j\omega\varepsilon\rho)}}, \quad \gamma = \sqrt{j\omega\mu_0 \left( \frac{1}{\rho} + j\omega\varepsilon \right)/2}$$

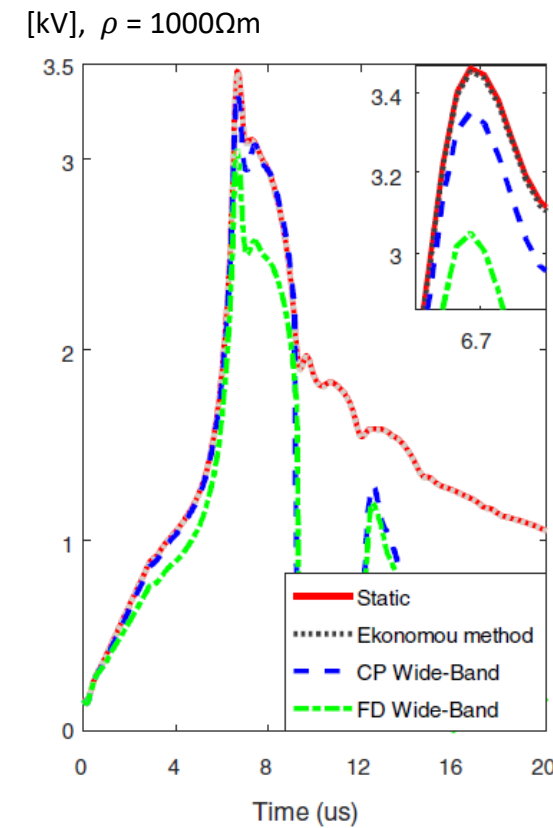
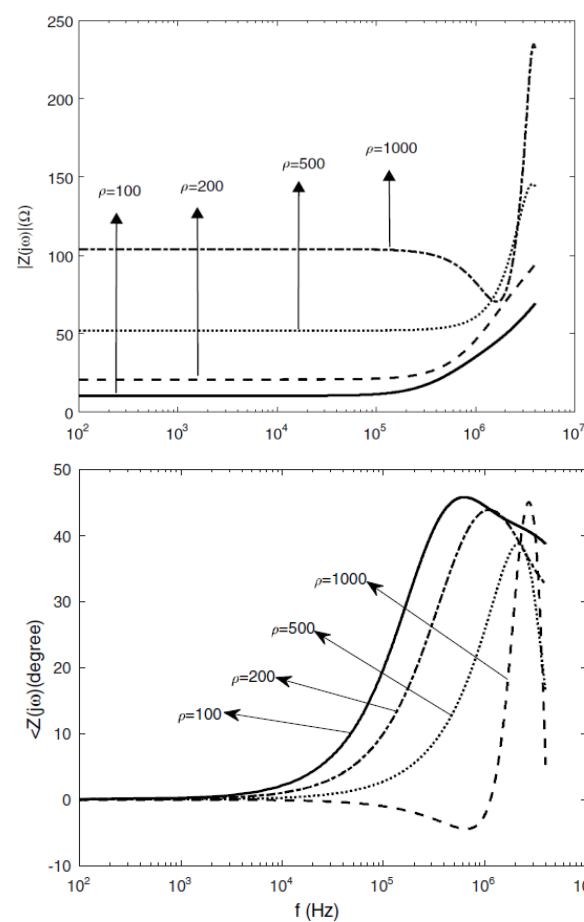
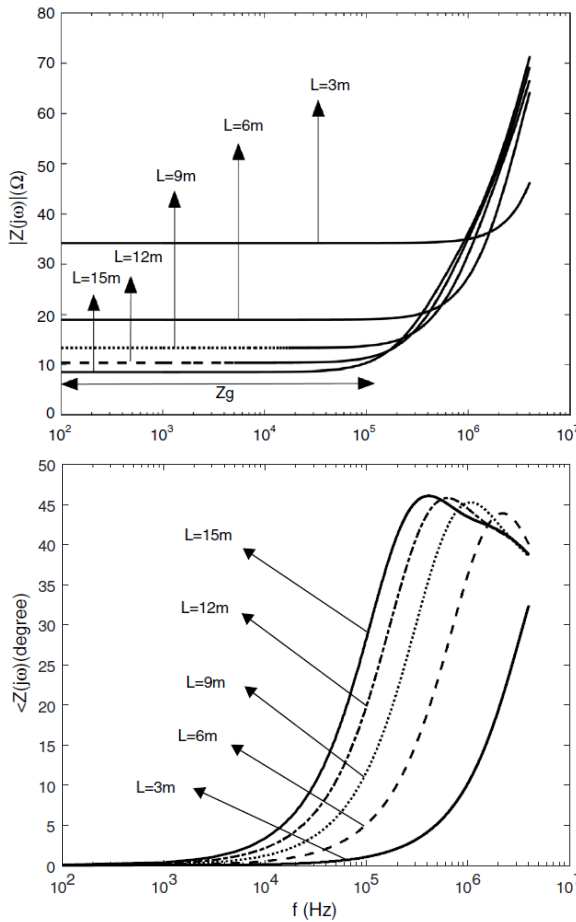
Soil resistance for the case of vertical and horizontal rode in  $f = 50\text{Hz}$  is

$$Z_g = \frac{\rho}{2\pi l} (A_1) - \text{Vertical Rod}; \quad Z_g = \frac{\rho}{\pi l} (A_2) - \text{Horizontal Rod} \quad (5.260)$$

where  $l$  [m],  $a$  [m],  $\rho$  [ $\Omega\text{m}$ ],  $d$  [m] are rod length, geometric radius of electrode, soil resistivity and grounding rode depth, respectively.

If conductor radius ( $a$ ) and grounding rod depth ( $d$ ) was ignored in comparison with the rod length ( $L$ ), i.e.  $L \gg a, d$ ; the grid resistance is

$$R = \frac{\rho}{\pi l} \left( \ln \frac{2L}{\sqrt{2ad}} - 1 \right) = \frac{\rho}{2\pi l} \left( \ln \frac{2L}{a} + \ln \frac{L}{d} - 2 + \frac{4d^2}{L} - \frac{d^2}{L} + \dots \right) \quad (5.261)$$



For Tower, its electromagnetic transient response can be described by **telegraph equation**:

$$\begin{cases} -\frac{\partial u(h, t)}{\partial h} = R(h)i(h, t) + L(h)\frac{\partial i(h, t)}{\partial h} \\ -\frac{\partial i(h, t)}{\partial h} = C(h)\frac{\partial u(h, t)}{\partial h} \end{cases} \quad (5.262)$$

where  $L(h)$ ,  $R(h)$  and  $C(h)$  are per unit length inductance, resistance and capacitance of conductor, respectively. They varies with the height of infinitesimal cylinder element. It is given that

$$L(h) = L_G(h) + L_E(h) + L_c(h), R(h) = R_E(h) + R_c(h) \quad (5.263)$$

where  $L_G(h)$  reflects the magnetic flux in air;  $L_E(h)$  reflects the earth is not an ideal conductive plane, and  $L_c(h)$  is the inner inductance of the conductor;  $R_E(h)$  reflects the limited conductivity of earth,  $R_c(h)$  is the internal resistance of the tower, accounting for the active power loss when the EM field penetrates inside the conductor. As for the capacitance  $C(h)$ , it is only composed of the geometric capacitance  $C_G(h)$ .

For the vertical parts  $L_3$  and  $L_6$  of the tower, which are perpendicular to the ground, the parameters at different heights are different; so the vertical body of the tower is modeled as a non-uniform transmission line. Since the cross-section radius of the vertical part is much smaller than its length, the lightning wave can be regarded as a spherical wave propagating on the tower. The propagation process of the spherical wave is similar to the transverse electromagnetic wave propagation process of the **double-cone antenna**.

With an infinitesimal element  $dh$  with a radius  $r_{eq}$  and height  $h$  above the ground on the cylindrical conductor of length  $H$ . The propagation of the spherical wave in the element can be regarded as double cone antenna shown.  $p$ , the **penetration depth** of wave propagating to the earth is calculated by

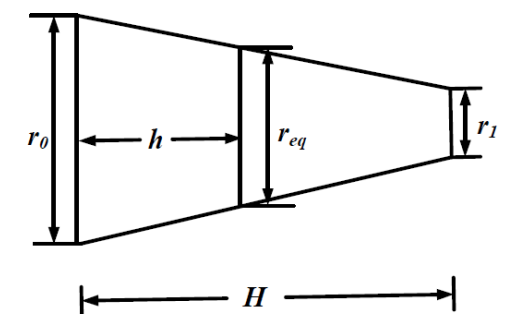
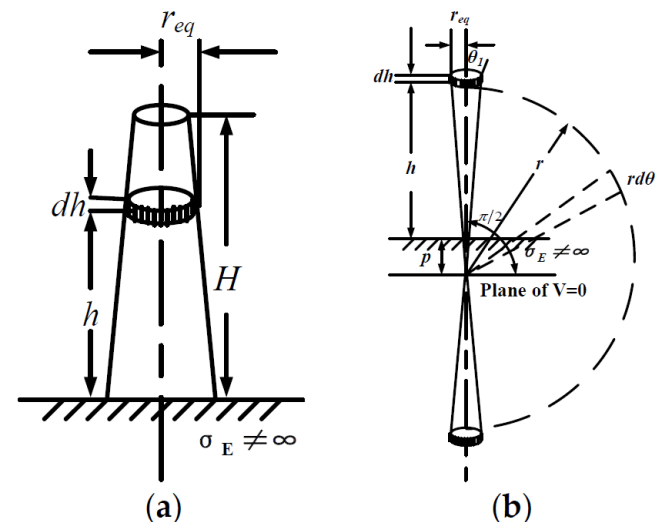
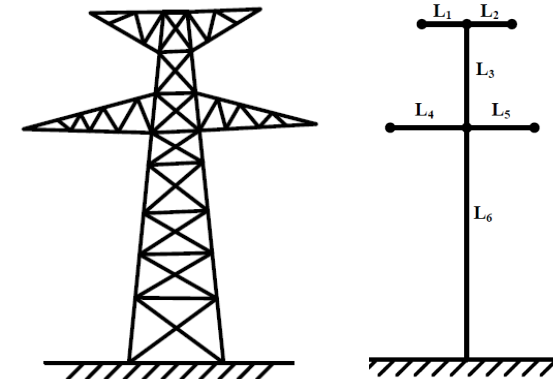
$$p = \frac{1}{\sqrt{j\omega\mu_E\sigma_E}} \quad (5.264)$$

where  $\omega$  is the angular frequency of the lightning current.

The main truss structure of the tower is usually trapezoidal, so the equivalent radius of the vertical infinitesimal element obtained by the proportional method:

$$r_{eq} = r_0 - \frac{r_0 - r_1}{H}h \quad (5.265)$$

where  $r_0$  is the equivalent radius of tower base, and  $r_1$  is that of tower top.



E-field and B-field strength of a transverse EM wave propagating in a bi-conical antenna can be expressed in a spherical coordinate system:

$$\begin{cases} H_\varphi = A_0 e^{-j\beta r} / (r \sin \theta) \\ E_\theta = H_\varphi \sqrt{\mu/\epsilon} \\ E_r = E_\varphi = H_\theta = H_r = 0 \\ \beta = \omega \sqrt{\mu \epsilon} \end{cases} \quad (5.266)$$

where  $A_0$  is the vector magnetic position,  $\beta$  is the phase constant,  $\mu, \epsilon$  are the magnetic permeability and dielectric constant of the medium above the ground plane respectively.

For a differential element, the voltage  $U$  can be obtained with

$$U = \int_{\theta_1}^{\pi/2} E_\theta r d\theta \quad (5.267)$$

where  $\theta_1$  is the half of the cone angle,  $\pi/2$  is the angle between the axis of the cone and the ground. From the Ampere loop theorem, the current flowing through the infinitesimal element is shown below.

$$I = \int_0^{2\pi} H_\varphi r_{eq} d\varphi \quad (5.268)$$

Substituting for simplification gives:

$$U = \sqrt{\frac{\mu}{\epsilon}} A_0 e^{-j\beta r} \ln \left[ \cot \frac{\theta_1}{2} \right], \quad I = 2\pi A_0 e^{-j\beta r} \quad (5.269)$$

With the geometric relationship

$$\cot \frac{\theta_1}{2} = \frac{\sqrt{(h+p)^2 + r_{eq}^2} + (h+p)}{r_{eq}} \quad (5.270)$$

Substituting (5.270) into (5.269),

$$Z_0 = Z_G + Z_E = \frac{1}{2\pi} \sqrt{\frac{\mu}{\epsilon}} \ln \frac{\sqrt{h^2 + r_{eq}^2} + h}{r_{eq}} + \frac{1}{2\pi} \sqrt{\frac{\mu}{\epsilon}} \ln \frac{\sqrt{(h+p)^2 + r_{eq}^2} + (h+p)}{\sqrt{h^2 + r_{eq}^2} + h} \quad (5.271)$$

In turn, geometric inductance  $L_G$  of the vertical conductor and geometric capacitance  $C_G$  is given

$$L_G = \sqrt{\mu \epsilon} Z_G, \quad C_G = \mu \epsilon (L_G)^{-1} \quad (5.272)$$

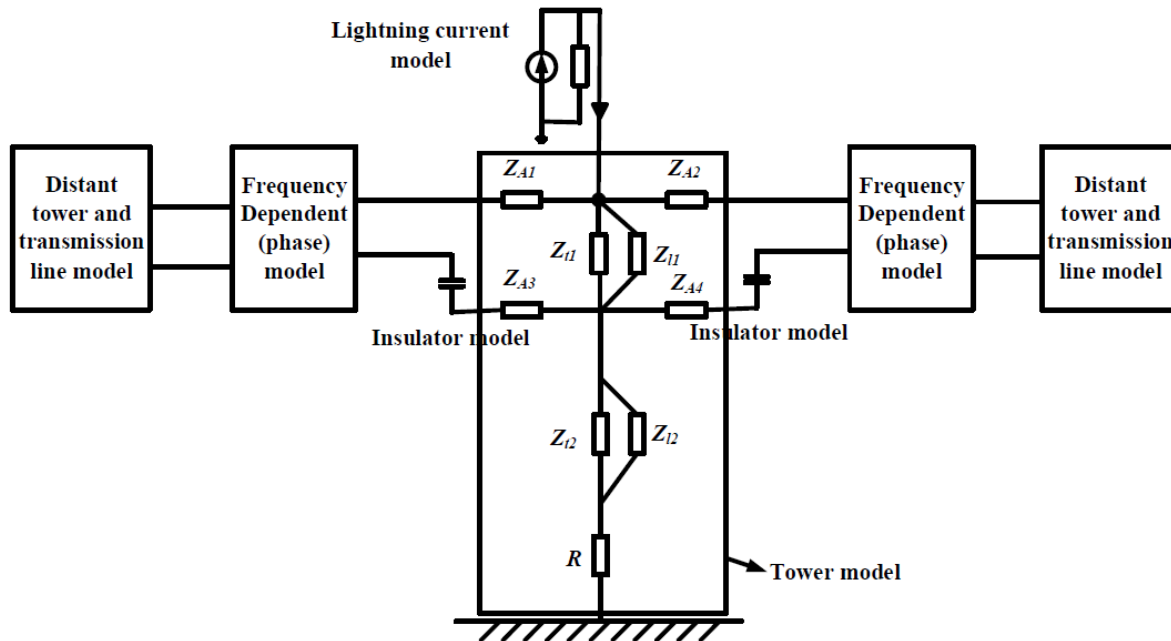
The generalized inductance and the ground inductance and ground resistance is given by

$$L_{EC} = \sqrt{\mu \epsilon} Z_E, \quad \begin{cases} L_E = \operatorname{Re}\{L_{EC}\} \\ R_E = -\omega \operatorname{Im}\{L_{EC}\} \end{cases} \quad (5.273)$$

Since conductor has a skin effect [self induced current for varying current] when flowing through a high-frequency current, the conductor itself has internal inductance and resistance, which is calculated by:

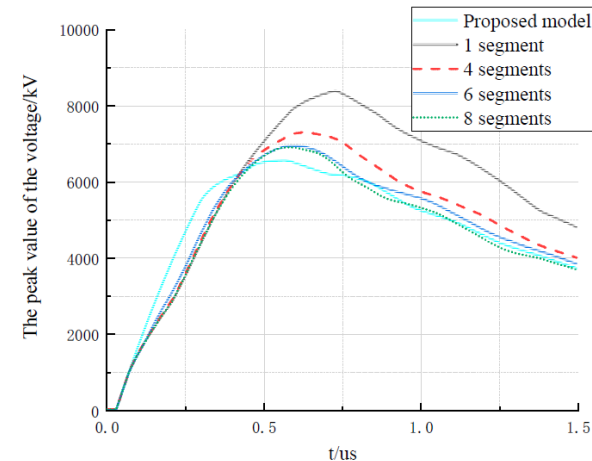
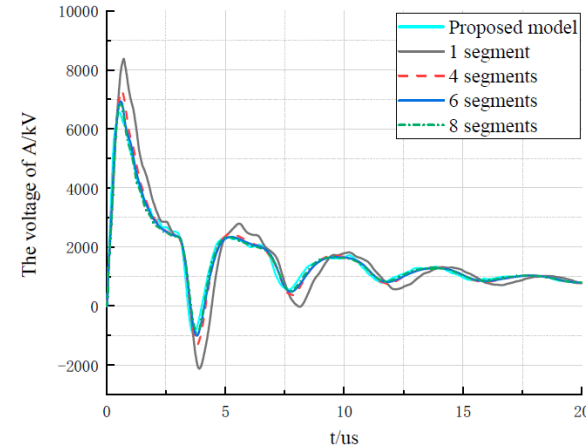
$$\left\{ \begin{array}{l} Z_C = \sqrt{j\omega\mu_c\rho}/2\pi r_{eq} \\ L_C = Im\{Z_C\}/\omega \\ R_C = Re\{Z_C\} \end{array} \right. \quad (5.274)$$

where  $\rho$  is the resistivity of conductor;  $\mu_c$  is magnetic permeability of the conductor.



### Summary:

- With increasing number of segment, the peak voltage at tower top gradually reduced, the peak time gradually decreased, i.e. larger rate-of-rise.
- Non-uniform line model built here is consistent with EM transient response of multi-segment multi-surge impedance model. The proposed model can reflect the changes of spatial structure of tower more realistically, and more suitable for lightning transient analysis for tower.
- Accuracy of tower model determines the reliability of lightning protection analysis. The structure of tower becomes more and more complicated, and the ordinary multi-surge impedance model is no longer applicable. The future modelling of tower should focus on its physical characteristics. The tower model should be able to reflect the E-field and B-field generated by the lightning current and tower's own structure.



## 5.5 Dynamic Line Rating (DLR)

Existing transmission capacity limitations in many power systems are increasingly impeding the grid integration of ever larger RES energy shares. While **network reinforcement** by adding new lines (building new towers, applying high temp low sag or adding lines onto tower to four circuit) is costly and often requires lengthy construction lead time, a short-term alleviation to the **capacity limitation problem** is to maximizing the limit dynamically by thermal modelling, real-time economic dispatch and state estimation.

**Steady-State Heat Transfer:**

$$P_J + P_S = P_C + P_R$$

Joule's Heat –	$P_J = I_{DC}^2 R_{DC} [1 + \alpha(T_{av} - 293K)]$	(5.275)
Solar Heat –	$P_S = \alpha_S S D$	
Convective Cooling –	$P_C = \pi \lambda_f (T_s - T_a) N u$	
Radiative Cooling –	$P_R = \pi D \varepsilon \sigma_B (T_s^4 - T_a^4)$	

where  $\alpha$  = resistance temperature coefficient,  $\alpha_S = 0.23$  for bridge stranded Al conductor to 0.95 for weathered conductor in industrial environment (0.5),  $\lambda_f$  = thermal conductivity of air,  $Nu$  = Nusselt number,  $\varepsilon$  is emissivity (0.5),  $\sigma_B$  = Stefan Boltzmann constant.

Assume coherent temperature distribution across conductor, the resulting DC current rating  $I_{DC}$  of heat balance is given by

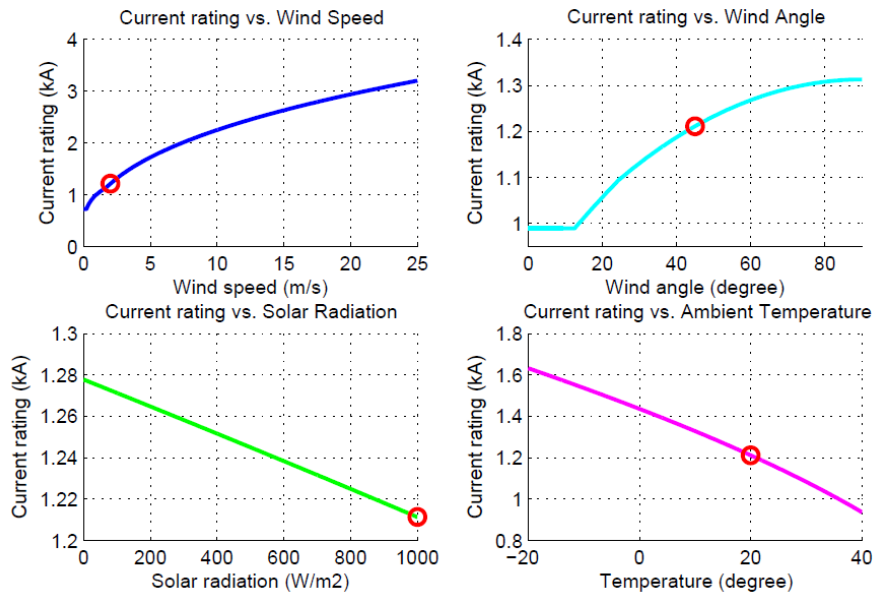
$$I_{DC} = \sqrt{\frac{P_C + P_R - P_S}{R_{DC} [1 + \alpha(T_{av} - 293K)]}} \quad (5.276)$$

The equivalent AC rating is given by

$$I_{AC} = \frac{I_{DC}}{\sqrt{1.0123 + 2.319 \times 10^{-5} I_{DC}}} \quad (5.277)$$

As shown in the figure,

- Wind speed ( $V$ ) has a much larger effect on  $I_{AC}$ , increased from 700A at  $V = 0$  m/s to 3300A at  $V = 25$  m/s
- Wind attack angle ( $\delta$ ) and ambient temperature ( $T_a$ ) also have quite an obvious effect on  $I_{AC}$ , with an increase of 35% and decrease of 41% respectively.
- The global solar radiation ( $S$ ) has a quite small effect on rating, only 5% drop going from 0 to 1000W/m<sup>2</sup> solar radiation.



Situation	Absolute	DLR Percentage	Influence on DLR
Heating Load Increase	0.14% per $1^\circ\text{C}$ drop	$\frac{0.1\% \Delta P_{DLR}}{1\% \Delta T}$	7 ×
Wind feed-in Increase	11.1% per $1\text{m/s}$ increase	$\frac{4\% \Delta P_{DLR}}{1\% \Delta V}$	300 ×
PV feed-in Increase	0.14% per $100\text{W/m}^2$ increase	$\frac{0.014\% \Delta P_{DLR}}{1\% \Delta S}$	1 ×

## Economic Dispatch Model:

$$\min J(k) = \sum_{l=k+N-1}^{l=k} (x(l) - x_{ref})^T Q_x (x(l) - x_{ref}) R_u u(l) + \delta u(l)^T \delta R_u \delta u(l) \quad (5.278)$$

such that

$$\begin{aligned} x(l+1) &= Ax(l) + Bu(l) \\ 0 \leq x^{min} &\leq x(l) \leq x^{max} \leq 1 \\ u^{min} &\leq u(l) \leq u^{max} \\ \delta u^{min} &\leq \delta u(l) \leq \delta u^{max} \\ P_{line}^{min}(l) &\leq P_{line}(l) \leq P_{line}^{max}(l) \end{aligned}$$

where N is the prediction step number,  $x$  and  $x_{ref}$  are state variable and their reference value,  $u$  is the node variable,  $Q_x, R_u, \delta R_u$  are optimization parameters.

The research on power transmission lines requires transmission line parameters, including **series resistance**, **series reactance** and **shunt susceptance** as vital inputs to various power system analyses and applications, such as the power flow analysis and the protective relaying application. Accurate estimate of line parameters may also be employed for transmission line thermal condition monitoring. With increasing application of **Phasor Measurement Unit** (PMU), it provides controllability and observability with time-synchronized phasors from large network.

Given –

$V_{P1i}, V_{P2i}$  : i-th positive sequence voltage phasors at bus P1 and bus P2

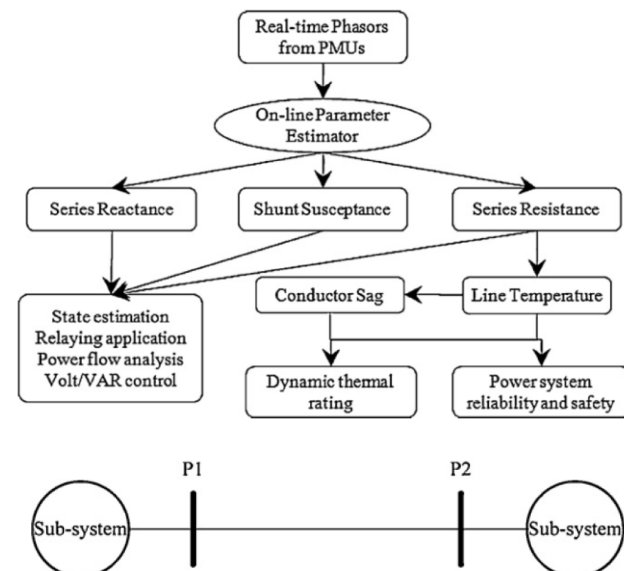
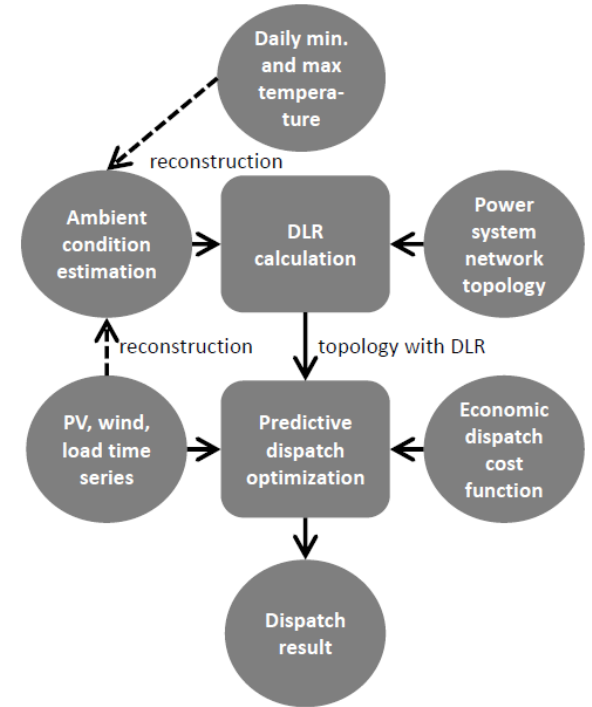
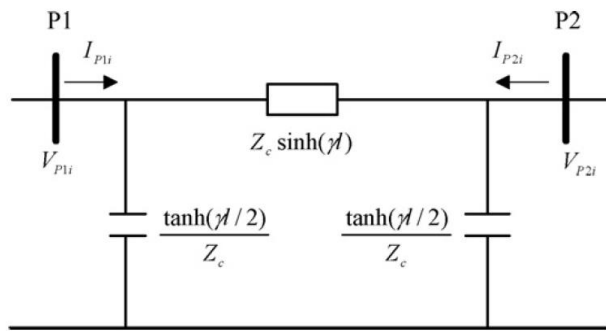
$I_{P1i}, I_{P2i}$  : i-th positive sequence current phasors at bus P1 and P2

$i = 1, 2, \dots, N$ ; where N is total number of measurement sets

$Z_c$  : characteristics impedance of the line

$\gamma$  : propagation constant of the line

$l$  : the total length of the line (known);



Assume the synchronous phasors are adopted, the following equations can be obtained.

$$V_{P1i} - Z_c \sinh \gamma l I_{P1i} + \sinh \gamma l \tanh\left(\frac{\gamma l}{2}\right) V_{P1i} - V_{P2i} = 0 \quad (5.279)$$

$$I_{P1i} - \frac{\tanh\left(\frac{\gamma l}{2}\right) V_{P1i}}{Z_c} + I_{P2i} - \frac{\tanh\left(\frac{\gamma l}{2}\right) V_{P2i}}{Z_c} = 0 \quad (5.280)$$

$$Z_c = \sqrt{z_1/y_1} \quad \gamma = \sqrt{z_1 y_1} \quad (5.281)$$

In order to detect potential synchronization errors, the synchronization angle can also be modelled in the line equations.

$$V_{P1i} - Z_c \sinh \gamma l I_{P1i} + \sinh \gamma l \tanh\left(\frac{\gamma l}{2}\right) V_{P1i} - V_{P2i} e^{j\delta} = 0 \quad (5.282)$$

$$I_{P1i} - \frac{\tanh\left(\frac{\gamma l}{2}\right) V_{P1i}}{Z_c} + I_{P2i} e^{j\delta} - \frac{\tanh\left(\frac{\gamma l}{2}\right) V_{P2i} e^{j\delta}}{Z_c} = 0 \quad (5.283)$$

where  $\delta$  denotes the synchronization angle between bus P<sub>1</sub> and P<sub>2</sub>.

Define the unknown variable vector as

$$X = [x_1, x_2, x_3, x_4]^T \quad (5.284)$$

where  $x_1, x_2, x_3$  are the positive sequence series resistance, series reactance and shunt susceptance per unit length, respectively;  $x_4$  is the synchronization angle. Set  $x_4 = 0$  when synchronous measurements are utilized.

By employing the defined variables, (5.282) can be re-written as

$$f_i(X) = V_{P1i} - Z_c \sinh \gamma l I_{P1i} + \sinh \gamma l \tanh\left(\frac{\gamma l}{2}\right) V_{P1i} - V_{P2i} e^{jx_4} \quad (5.285)$$

where  $i = 1, 2, \dots, N$ , representing the index of the total number of measurement set N;

$$Z_c = \sqrt{\frac{x_1 + jx_2}{jx_3}}, \quad \gamma = \sqrt{(x_1 + jx_2)(jx_3)} \quad (5.286)$$

Define the function vector  $F(X)$  as

$$F_{2i-1}(X) = \text{Re}\{f_i(X)\}, \quad F_{2i}(X) = \text{Im}\{f_i(X)\} \quad i = 1, 2, \dots, N \quad (5.287)$$

Then the unknown variable vector X can be derived iteratively with

$$H = \frac{\partial F(X_k)}{\partial X_k} \rightarrow X_{k+1} = X_k - (H^T H)^{-1} [H^T F(X_k)] \quad (5.288)$$

where H is composed of derivatives of the function vector w.r.t. X;  $X_k$  and  $X_{k+1}$  are variable vectors for k-th and (k+1)-th iteration.

For optimal estimation,

Define the voltage and current phasors along with the synchronization angle as known measurements:

$$M = [V_{P11}, I_{P11}, V_{P21}, I_{P21}, \dots, V_{P1N}, I_{P1N}, V_{P2N}, I_{P2N}, \delta] \quad (5.289)$$

Set  $\delta = 0$  when synchronous measurement are utilized. Modelling  $\delta$  in the line equations makes it possible to detect potential synchronization errors.

Define the measurement function as

$$Y_i(X) = x_{2i-1}e^{jx_{2i}}; \quad Y_{4N+1}(X) = x_{8N+4} \quad (5.290)$$

where  $i = 1, 2, \dots, N$ , representing the index of total number of measurement set  $N$ ; and the unknown variable vector  $X$  is defined as

$$X = [x_1, x_2, \dots, x_{8N}, x_{8N+1}, x_{8N+2}, x_{8N+3}, x_{8N+4}]^T \quad (5.291)$$

where  $x_1, x_2, \dots, x_{8N}$  are unknown variables, representing the  $4N$  complex measurement;  $x_{8N+1}, x_{8N+2}, x_{8N+3}$  are positive sequence series resistance, series reactance and shunt susceptance per unit length, respectively;  $x_{8N+4}$  denotes the synchronization angle.

Following the defined variable, (5.285) can be re-written as:

$$f_i(X) = x_{8i-7}e^{jx_{8i-6}} - Z_c \sinh \gamma l x_{8i-5}e^{jx_{8i-4}} + \sinh \gamma l \tanh\left(\frac{\gamma l}{2}\right) x_{8i-7}e^{jx_{8i-6}} - x_{8i-3}e^{jx_{8i-2}}e^{jx_{8N+4}} \quad (5.292)$$

where  $i = 1, 2, \dots, N$ ; representing the index of total measurement set  $N$ .

$$Z_c = \sqrt{\frac{x_{8N+1} + jx_{8N+2}}{jx_{8N+3}}}, \quad \gamma = \sqrt{(x_{8N+1} + jx_{8N+2})(jx_{8N+3})} \quad (5.293)$$

Introduce  $S$  as the measurement vector with elements shown below:

$$\begin{aligned} S_i &= 0, \quad i = 1, 2, \dots, 2N \\ S_{2i-1+2N} &= \text{abs}(M_i), \quad i = 1, 2, \dots, 4N \\ S_{2i+2N} &= \text{angle}(M_i), \quad i = 1, 2, \dots, 4N \\ S_{10N+1} &= M_{4N+1} \end{aligned} \quad (5.294)$$

Introduce  $F(X)$  as the function vector with elements shown below:

$$\begin{aligned} F_{2i-1}(X) &= \text{real}\{f_i(X)\}, \quad i = 1, 2, \dots, N \\ F_{2i}(X) &= \text{imag}\{f_i(X)\}, \quad i = 1, 2, \dots, N \\ F_{2i-1+2N}(X) &= \text{abs}\{Y_i(X)\} = x_{2i-1}, \quad i = 1, 2, \dots, 4N \\ F_{2i+2N}(X) &= \text{angle}\{Y_i(X)\} = x_{2i}, \quad i = 1, 2, \dots, 4N \\ F_{10N+1} &= Y_{4N+1}(X) = X_{8N+4} \end{aligned} \quad (5.295)$$

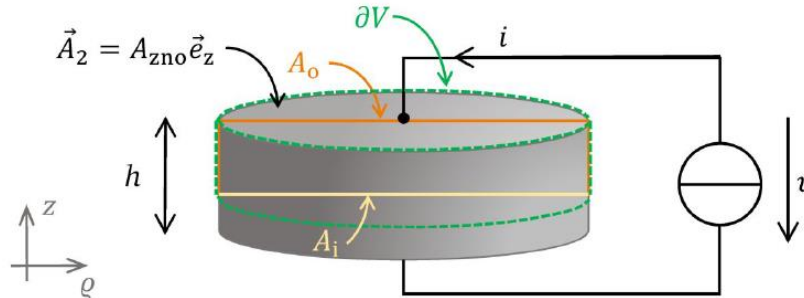
Given the measurement vector and function vector related by  $S = F(X) + \mu$ , the optimal estimate of  $X$  can be obtained by minimize

$$J = [S - F(X)]^T Q^{-1} [S - F(X)] \rightarrow H = \frac{\partial F(X_k)}{\partial X_k} \rightarrow X_{k+1} = X_k + (H^T W H)^{-1} [H^T W (S - F(X_k))] \quad (5.296)$$

where  $H$  is composed of derivatives of the function vector w.r.t.  $X$ ;  $W = Q^{-1}$  is the weighted matrix, where  $Q$  is the covariance matrix.

## 5.6 Surge Arrester – Electrothermal Modelling

Consider a ZnO element with volume  $V$ , height  $h$ , and cross section  $A_{\text{ZnO}}$  excited by voltage  $u$  with current  $i$ .



For sufficiently low frequency, E-field are irrotational and can be described by a scalar potential  $\varphi$ . The electro-quasistatic approximation of Maxwell Equations is motivated by the problem where capacitive-resistive effects are present, but the propagation effects of the EM wave through the region of interest are negligible.

Ampere's Law (Charge Conservation Equation):

$$\nabla \cdot \left( \frac{\partial}{\partial t} \vec{D} \right) + \nabla \cdot \vec{J} = \nabla \cdot (\nabla \times \vec{H}) = 0 \quad (5.297)$$

Constitutive Material Relations:

$$\vec{D} = \epsilon \vec{E}; \quad \vec{J} = \sigma \vec{E} \quad (5.298)$$

Definition of electric scalar potential:

$$\vec{E} = -\nabla \varphi \quad (5.299)$$

For surge arrester problems, the equation is strongly non-linear due to electrical characteristics of ZnO material. The relative permittivity and conductivity depend on the magnitude of E-field,  $|\vec{E}|$  and the temperature,  $T$ , i.e.  $\epsilon = f(|\vec{E}|, T)$  and  $\sigma = g(|\vec{E}|, T)$ , respectively. Finally the **electro-quasistatic** (EQS) equation is obtained as

$$\boxed{\nabla \cdot \left( \frac{\partial}{\partial t} \epsilon \nabla \varphi \right) + \nabla \cdot (\sigma \nabla \varphi) = 0} \quad (5.300)$$

(5.300) is subjected to boundary conditions specifying either the electric potential or the normal component of total current density at the boundary. Due to the resistive current, resistive loss or Joule's Losses

$$\dot{q}_p = \sigma(|\vec{E}|, T) \vec{E}^2 = \sigma(|\vec{E}|, T) |\nabla \varphi|^2 \quad (5.301)$$

Under the configuration,

$$\vec{A}_{\text{ZnO}} = \pi \rho_{\text{ZnO}}^2 \vec{e}_z; \quad u = - \int_{z_1}^{z_2} \vec{E}(\vec{r}, t) \cdot d\vec{z} = \varphi_1 - \varphi_2; \quad \left. \frac{\partial \varphi}{\partial n} \right|_{\rho=\rho_{\text{ZnO}}} = 0 \quad (5.302)$$

Equation (5.300) is integrated over an arbitrary volume  $V$ , which spans around the conductor surface  $\vec{A}_2$ . Apply the Gauss's Law, the integral reduces to the surface integral over  $dV$

$$\nabla \cdot \left( \frac{\partial}{\partial t} \varepsilon \nabla \varphi \right) + \nabla \cdot (\sigma \nabla \varphi) = 0 \rightarrow \int_{\partial V} \left[ \frac{\partial}{\partial t} \varepsilon (|\vec{E}(\vec{r}, t)|) \vec{E}(\vec{r}, t) + \sigma (|\vec{E}(\vec{r}, t)|) \vec{E}(\vec{r}, t) \right] \cdot d\vec{A} = 0 \quad (5.303)$$

Splitting the surface into outside  $\vec{A}_0$  and inside  $\vec{A}_i$  the ZnO domain.

$$\underbrace{\int_{A_0} \left[ \frac{\partial}{\partial t} \varepsilon (|\vec{E}|) \vec{E} + \sigma (|\vec{E}|) \vec{E} \right] \cdot d\vec{A}}_i - \int_{A_i} \left[ \frac{\partial}{\partial t} \varepsilon (|\vec{E}|) \vec{E} + \sigma (|\vec{E}|) \vec{E} \right] \cdot d\vec{A} \quad (5.304)$$

To show the derivation of C and R for a non-linear field and temperature dependent conductivity and permittivity,  $\sigma(|E|, T), \varepsilon(|E|, T)$ , no net charges are allowed inside the domain. It is assumed that the E-field inside ZnO resistor is homogeneous and points in vertical direction between the two electrodes,  $\vec{E} = -E \vec{e}_z$ . Thus, (5.302) can be simplified to

$$u = Eh \quad (5.305)$$

(5.304) is evaluated on a surface in z-direction,  $\vec{A}_i = A_{ZnO} \vec{e}_z$

$$\int_{A_{ZnO}} \left[ \frac{\partial}{\partial t} \varepsilon (|\vec{E}|, T) \vec{E} + \sigma (|\vec{E}|, T) \vec{E} \right] \cdot d\vec{A} = i \quad (5.306)$$

Due to uniform field, the integral can be simplified.

$$A_{ZnO} \left[ \frac{d}{dt} \varepsilon (|u|, T) \frac{u}{h} + \sigma (|u|, T) \frac{u}{h} \right] = i \quad (5.307)$$

$$\frac{d}{dt} C(|u|, T) u + \frac{1}{R(|u|, T)} u = i \quad (5.308)$$

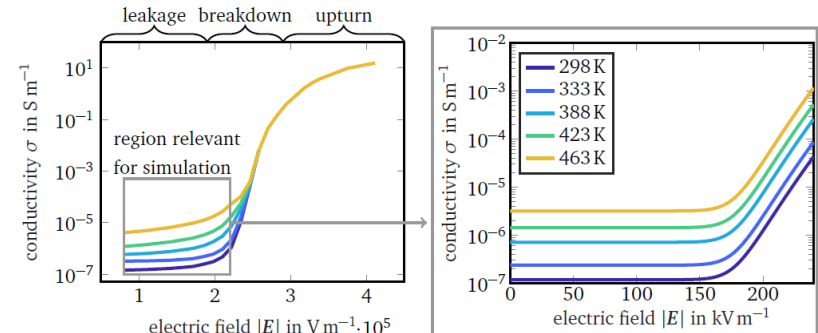
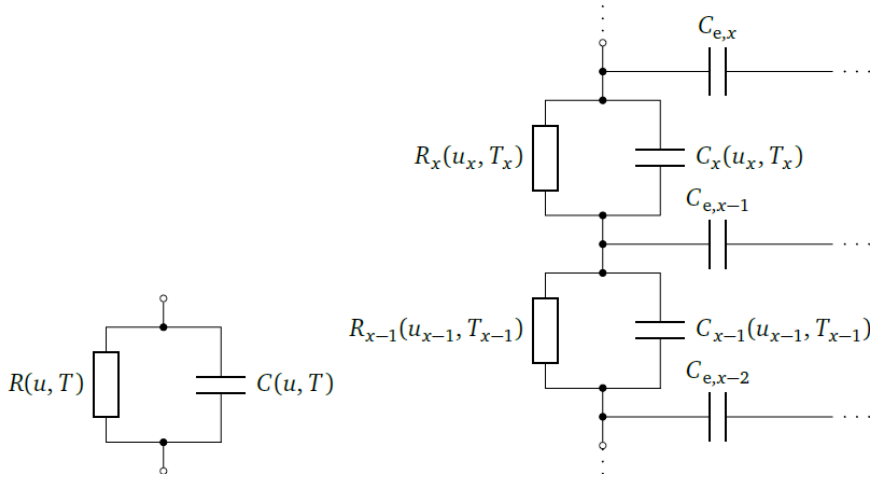
where  $C(u, T)$  and  $R(u, T)$  are defined by

$$C(|u|, T) = A_{ZnO} \varepsilon (|u|, T) h^{-1}; \quad R(u, T) = h (\sigma (|u|, T) A_{ZnO})^{-1} \quad (5.309)$$

The total current,  $i$ , splits into a capacitive,  $i_{cap}$ , and a resistive component,  $i_{res}$ , which are represented by the circuit element. Due to the nonlinearity of  $\varepsilon(u, T)$ , a differential capacitance  $C_d(u, T)$  can be introduced.

$$i_{cap} = \frac{d}{dt} (C(|u|, T) u) = \frac{du}{dt} \left( \frac{dC(u, T)}{du} u + C(u, T) \right) = C_d \frac{du}{dt} \quad (5.310)$$

The nonlinear and, in general, temperature,  $T$ , dependent EQS equation is interpreted as a parallel circuit of a nonlinear capacitance,  $C(u, T)$ , and a nonlinear resistance,  $R(u, T)$ . In a station class arrester, many ZnO resistors are stacked to a column of several meters in height. Thus, in the circuit representation, the external field effects must be taken into account by **parasitic stray capacitances**.



The non-linear conductivity and relative permeability of the ZnO in the region of interest can be approximated by:

$$\varepsilon(|\vec{E}|, T) = [e^{b_1|\vec{E}|} + b_2] e^{b_3 T - b_4}, \quad \sigma(|\vec{E}|, T) = \left( \left( \frac{\vec{E}}{a_1} \right)^\alpha + a_2 \right) \exp[(T - a_3)a_4] \quad (5.311)$$

The overall electrical behavior of a station class arrester is very complex, as it is determined by three aspects:

- The strongly nonlinear electric field dependence of the conductivity and permittivity of the ZnO material, which clips overvoltage.
- The strongly nonlinear temperature dependence of the ZnO material, which requires a detailed thermal model to update the operating point in the material distributions for a transient computation.
- The large axial dimensions which introduce an imbalance of the axial field stresses due to the stray capacitances.

The non-linear transient heat conduction equation describes the evolution of the temperature T, by

$$\frac{\partial c_v(T)T}{\partial t} - \nabla \cdot (\lambda(T)\nabla T) = \dot{q} = \frac{d\dot{Q}}{dA} \quad (5.312)$$

where  $c_v(T)$  and  $\lambda(T)$  are the temperature dependent specific heat capacity and thermal conductivity respectively.

The thermal heat flux density that is transferred from a surface at temperature  $T_1$  and to the surrounding fluid at temperature  $T_2$  due to convection can be approximated by

$$\dot{q} = \alpha_{th}(T_1 - T_2) = \alpha_{th}\Delta T \quad (5.313)$$

where  $\alpha_{th}$  is the heat transfer coefficient, which is found with **Nusselt number** Nu, describing the ratio of convective to conductive heat transfer normal to the solid to fluid boundary,

$$Nu = \frac{\alpha_{th}l_c}{\lambda} = \frac{\lambda_{eff}}{\lambda} \quad (5.314)$$

Herein, the **characteristics convection length** is  $l_c$ , the thermal conductivity of the fluid is  $\lambda$  and the effective thermal conductivity is  $\lambda_{eff}$ . The latter describe the total heat transfer in the fluid including convective effects. In general, Nusselt number for natural convection depends on fluid and flow properties and geometrical dimension of the problem,  $Nu = f(Gr, Pr)$ . **Grashof number**  $Gr$  and **Prandtl number**  $Pr$  describe the kinematic and intrinsic properties of the involved fluid, which is defined by

$$Gr = g\beta(T)\Delta T l_c^3 \nu(T)^{-2}; \quad Pr = \nu a^{-1} \quad (5.315)$$

where  $l_c$  is the characteristics length,  $\beta(T)$  is the **volumetric thermal expansion coefficient**,  $\nu$  is the kinematic viscosity,  $a = \lambda/\rho c_p$  is the thermal diffusivity. Finally, thermal energy is transferred by radiation emission and absorption from hot body surface with emissive heat flux per unit surface area,

$$\dot{q}_r = \varepsilon_{rad} C_S T^4 \rightarrow Q_{12} = A \varepsilon_{rad} C_S (T_1^4 - T_2^4) \quad (5.316)$$

where  $C_S$  is Stefan-Boltzmann Constant.

Consider the discretization of (5.300), the **nonlinear field- and temperature-dependent equation**, which is a **stiff problem** and requires special care for the selection of time integration scheme. Hence, an implicit time integration approach is adopted.

$$[\nabla \cdot (\varepsilon \nabla \varphi)]_{t^n}^{t^{n+1}} + \int_{t^n}^{t^{n+1}} \nabla \cdot (\sigma \nabla \varphi) dt = 0 \rightarrow \nabla \cdot (\varepsilon \nabla \varphi) \Big|^{t^{n+1}} - \nabla \cdot (\varepsilon \nabla \varphi) \Big|^{t^n} + \int_{t^n}^{t^{n+1}} \nabla \cdot (\sigma \nabla \varphi) dt = 0 \quad (5.317)$$

Discretize the equation in time with **backward Euler scheme**,

$$\nabla \cdot (\varepsilon \nabla \varphi) + \Delta t \nabla \cdot (\sigma \nabla \varphi) \Big|^{t^{n+1}} = \nabla \cdot (\varepsilon \nabla \varphi) \Big|^{t^n} \quad (5.318)$$

where  $\Delta t$  is the electric time step.

Similarly, the **nonlinear transient heat conduction equation** describes the time evolution of the temperature depending on the nonlinear material parameters, the volumetric heat capacity  $c_v(T)$  and thermal conductivity,  $\lambda(T)$ , respectively. For the time discretization, the same procedure as for the EQS is adopted. This yields,

$$c_v(T) - \Delta t_{th} \nabla \cdot (\lambda(T) \nabla T) - \Delta t_{th} \dot{q} \Big|^{t^{n+1}} = (c_v T) \Big|^{t^n} \quad (5.319)$$

where,  $\Delta t_{th}$  is the thermal time step.

A FEM study follows a fundamental scheme that starts with the discretization of computation domain  $\Omega$  into a set of mesh cells referred to as finite element. In each of these cells, the solution  $\varphi(r, t)$  is approximated by linear basis functions as

$$\varphi(r, t) \approx \sum_j w_j(r) u_j(t) \quad (5.320)$$

where  $w_j(r)$  are nodal FE shape functions (local piecewise linear hat functions) associated with the nodes of a triangular mesh constructed for the computational domain  $\Omega$  and  $u_j(t)$  are the degree of freedoms (DoFs). The **Ritz-Galerkin method** determines a solution for the DoFs such that the error, i.e. the residual, of the approximated and exact solution is minimized, The discretization of the resistive term of (5.300) is exemplarily shown. Starting with the conductivity term of EQS equation (5.300), the following transformations are performed.

$$\int_{\Omega} \nabla \cdot (\sigma \nabla \varphi) w_i d\Omega = \int_{\Omega} \nabla \cdot (\sigma \nabla \varphi w_i) d\Omega - \int_{\Omega} (\sigma \nabla \varphi \cdot \nabla w_i) d\Omega = \int_{\partial\Omega} \sigma \frac{\partial \varphi}{\partial n} w_i d\Gamma - \int_{\Omega} (\sigma \nabla \varphi \cdot \nabla w_i) d\Omega \quad (5.321)$$

The solution is approximated by the basis functions, as defined (5.320), and becomes

$$\approx \underbrace{\sum_j u_j \int_{\partial\Omega} \sigma \frac{\partial w_j}{\partial n} w_i d\Gamma}_{\text{Boundary Term}} - \underbrace{\sum_j u_j \int_{\Omega} (\sigma \nabla w_j \cdot \nabla w_i) d\Omega}_{= k_{ij}} \quad (5.322)$$

The first term is determined by the boundary conditions of the problem at hand. In the case of homogeneous Neumann boundary conditions, this term vanishes. At boundaries with Dirichlet boundary conditions the FE test functions,  $w_i$  are zero and boundary terms vanish as well. The second term corresponds to line  $i$  of the  $n \times n$  stiffness matrix  $\mathbf{K}_\sigma$ . Thus, neglecting the boundary terms, the **spatially discretized EQS system of equations** is obtained from (5.318) as,

$$(\mathbf{K}_\varepsilon + \Delta t \mathbf{K}_\sigma) \mathbf{u} \Big|^{t^{n+1}} = \mathbf{K}_\varepsilon \mathbf{u} \Big|^{t^n} \quad (5.323)$$

$$\mathbf{K}_\varepsilon^{n+1} \mathbf{u}^{n+1} - \mathbf{K}_\varepsilon^n \mathbf{u}^n + \Delta t \mathbf{K}_\sigma^{n+1} \mathbf{u}^{n+1} = 0 \quad (5.324)$$

where  $\mathbf{K}_\varepsilon$  is defined analogously using the permittivity,  $\varepsilon$ , instead of conductivity,  $\sigma$ . The superscripts indicate the time steps at which the variables are evaluated.

Similar procedures is applied for the FE-discretized transient heat conduction problem.

$$T(r, t) \approx \sum_j w_j(r) \theta_j(t) \quad (5.325)$$

where  $\theta_j(t)$  are the DoTs for the unknown temperature. The integral of the first term of (5.319) becomes

$$\int_{\Omega} (c_v T) w_i d\Omega \approx \sum_j \theta_j \underbrace{\int_{\Omega} c_v w_j w_i d\Omega}_{= m_{ij}} \quad (5.326)$$

This corresponds to line  $i$  of the mass matrix  $\mathbf{M}_{c_v}$ . The source term of electric losses yields a source term vector  $\dot{\mathbf{q}}$ . Finally, the discretized heat conduction equation is obtained

$$[(\mathbf{M}_{c_v} + \Delta t_{th} \mathbf{K}_\lambda) \boldsymbol{\theta} - \Delta t_{th} \dot{\mathbf{q}}] \Big|^{t^{n+1}} = \mathbf{M}_{c_v} \boldsymbol{\theta} \Big|^{t^n} \quad (5.327)$$

The **homogeneous Neumann boundary condition** is equivalent to the electrical case and resembles a thermal insulation. Additionally, the inhomogeneous Neumann boundary condition (i.e. a Robin-type boundary condition) is considered, resembling convection, or radiation, respectively. The Dirichlet boundary condition imposes a fixed temperature on the boundary cells of the computational domain. The Neumann boundary condition imposes a normal heat flux density  $\dot{q}_n$  on the boundary cells.

$$(\mathbf{M}_{C_v} + \Delta t_{th} (\mathbf{K}_\lambda + \mathbf{B})) \boldsymbol{\theta} - \Delta t_{th} (\dot{\mathbf{q}} + \mathbf{b}) \Big|^{t^{n+1}} = \mathbf{M}_{C_v} \boldsymbol{\theta} \Big|^{t^n} \quad (5.328)$$

$$\mathbf{M}_{C_v}^{n+1} \boldsymbol{\theta}^{n+1} - \mathbf{M}_{C_v}^n \boldsymbol{\theta}^n + \Delta t_{th} (\mathbf{K}_\sigma^{n+1} + \mathbf{B}^{n+1}) \boldsymbol{\theta}^{n+1} = \Delta t_{th} (\dot{\mathbf{q}}^{n+1} + \mathbf{b}^{n+1}) \quad (5.329)$$

Where each element of  $\mathbf{b}$  is obtained as

$$-\sum_j \theta_j \int_\Gamma \lambda \frac{\partial w_j}{\partial n} w_i d\Gamma = \int_\Gamma \dot{q}_n w_i d\Gamma \quad (5.330)$$

A convection or radiation boundary condition is regarded as a heat flux in the normal direction to the boundary surface. Both conditions are temperature-dependent. Thus, for the convective case, it is obtained that

$$\int_\Gamma \dot{q}_n w_i d\Gamma = \int_\Gamma \alpha_{th} (w_j \theta_j - \theta_0) w_i d\Gamma \quad (5.331)$$

where  $\theta_0$  is the constant ambient temperature. This is separated to contributions that enter  $\mathbf{B}$  and  $\mathbf{b}$ , respectively by

$$B_{ij} = \int_\Gamma \alpha_{th} w_i w_j \theta_j d\Gamma, \quad b_i = - \int_\Gamma \alpha_{th} w_i \theta_0 d\Gamma \quad (5.332)$$

The radiative boundary condition is obtained

$$\int_\Gamma \dot{q}_n w_i d\Gamma = \sum_j \varepsilon_{rad} C_s \left( (w_j \theta_j)^4 - \theta_0^4 \right) w_i d\Gamma \quad (5.333)$$

The discretized fully-coupled electrothermal problem is based on (5.324) and (5.329), and is given by:

$$\mathbf{K}_\epsilon^{n+1} \mathbf{u}^{n+1} - \mathbf{K}_\epsilon^n \mathbf{u}^n + \Delta t \mathbf{K}_\sigma^{n+1} \mathbf{u}^{n+1} = 0 \quad (5.324)$$

$$\mathbf{M}_{C_v}^{n+1} \boldsymbol{\theta}^{n+1} - \mathbf{M}_{C_v}^n \boldsymbol{\theta}^n + \Delta t_{th} (\mathbf{K}_\sigma^{n+1} + \mathbf{B}^{n+1}) \boldsymbol{\theta}^{n+1} = \Delta t_{th} (\dot{\mathbf{q}}^{n+1} + \mathbf{b}^{n+1}) \quad (5.329)$$

$$\rightarrow \begin{pmatrix} \mathbf{K}_\epsilon^{n+1} \mathbf{u}^{n+1} - \mathbf{K}_\epsilon^n \mathbf{u}^n \\ \mathbf{M}_{C_v}^{n+1} \boldsymbol{\theta}^{n+1} - \mathbf{M}_{C_v}^n \boldsymbol{\theta}^n \end{pmatrix} + \Delta t \begin{pmatrix} \mathbf{K}_\sigma^{n+1} \mathbf{u}^{n+1} \\ (\mathbf{K}_\sigma^{n+1} + \mathbf{B}^{n+1}) \boldsymbol{\theta}^{n+1} \end{pmatrix} = \begin{pmatrix} 0 \\ \Delta t (\dot{\mathbf{q}}^{n+1} + \mathbf{b}^{n+1}) \end{pmatrix} \quad (5.334)$$

The EQS and transient heat conduction equation are coupled by the power losses,  $\dot{\mathbf{q}}_p$ , which are evaluated based on the EQS electric field solution by

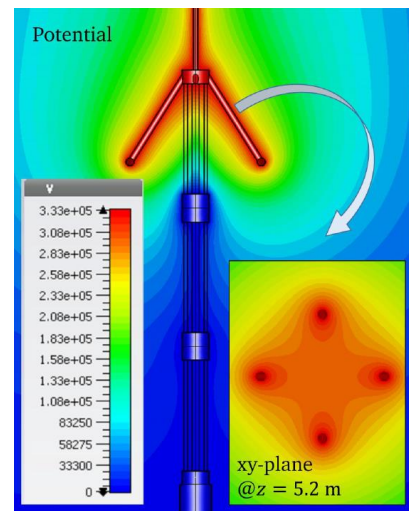
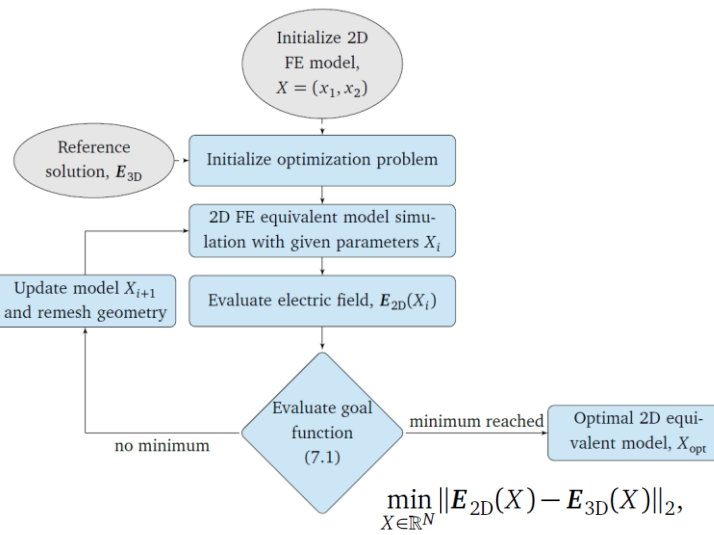
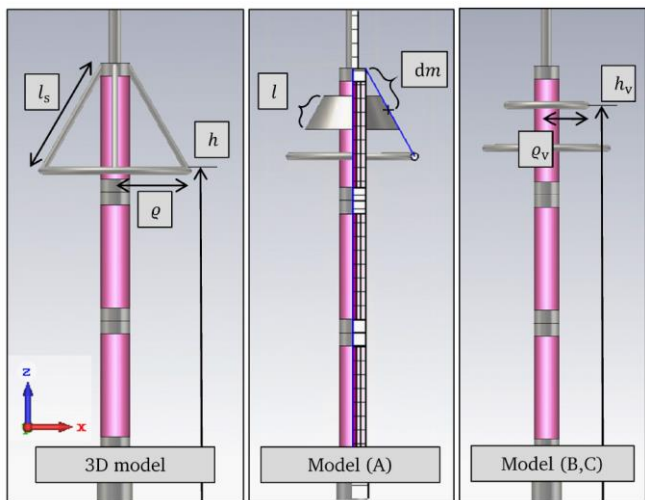
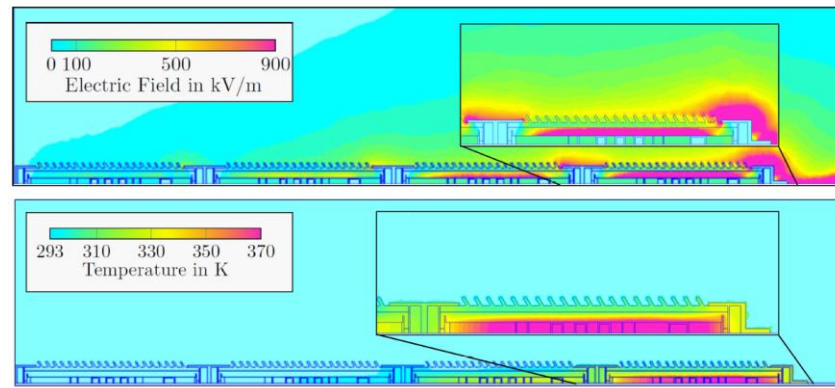
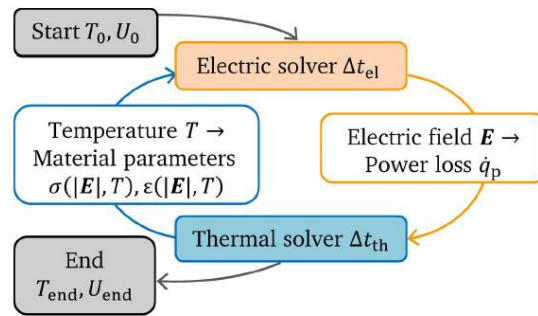
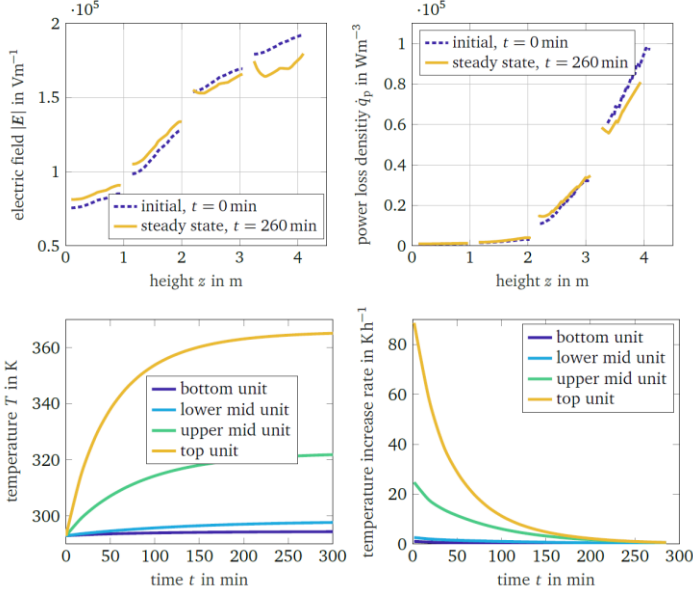
$$\dot{\mathbf{q}}_p = \sigma(|\mathbf{E}|, T) \mathbf{E}^2 \quad (5.335)$$

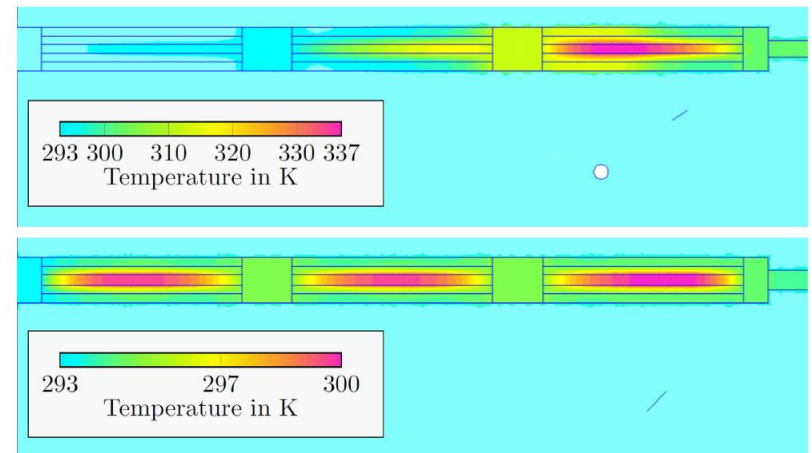
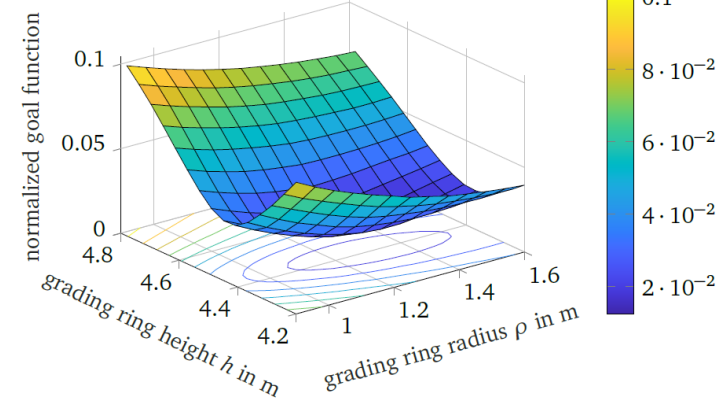
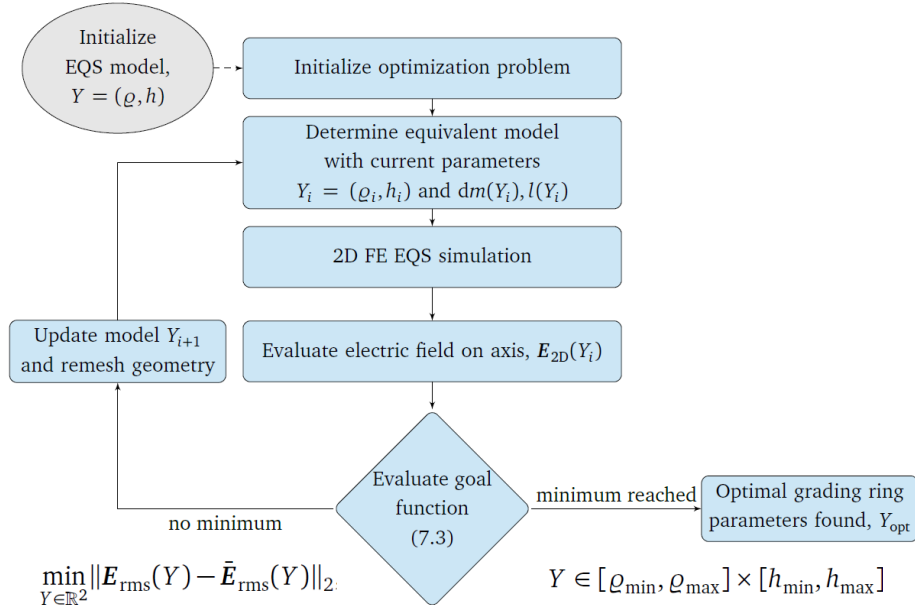
The term  $\dot{\mathbf{q}}$  on the right hand side of the thermal sub-problem is, then, composed of the power losses and, if present, further heat sources.

A critical simulation issue is the implementation of the coupling between the two problems. The transients of the **electrothermal system** are governed by the electrical and thermal time constants, i.e. the charge relaxation time, is defined by

$$\tau_{el} = \frac{\varepsilon(|\mathbf{E}|, T)}{\sigma(|\mathbf{E}|, T)} \approx 1 \text{ (impulse)} \sim 100 \text{ (continuous)}, \quad \tau_{th} = \frac{\rho^2 c_v(T)}{\lambda(T)} \quad (5.336)$$

electrical parameters	$\epsilon$ in As/Vm $6.2 \cdot 10^{-9}$	$\hat{\sigma}$ in S/m $4.0 \cdot 10^{-3}$	$\tau_{el}$ in s $1.6 \cdot 10^{-6}$
thermal parameters	$\lambda$ in W/Km 23	$c_v$ in J/Km <sup>3</sup> $3 \cdot 10^6$	Radius $\varrho$ in m $4 \cdot 10^{-2}$
			$\tau_{th}$ in s 160



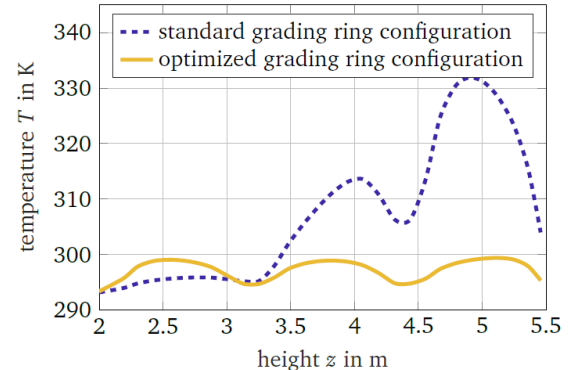
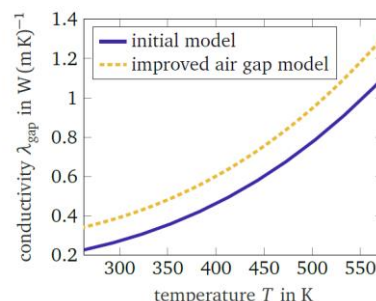
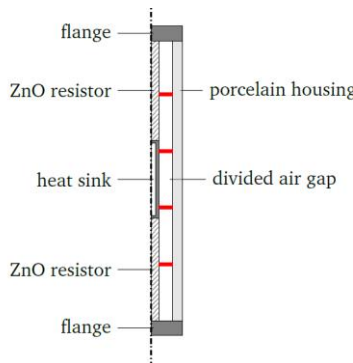
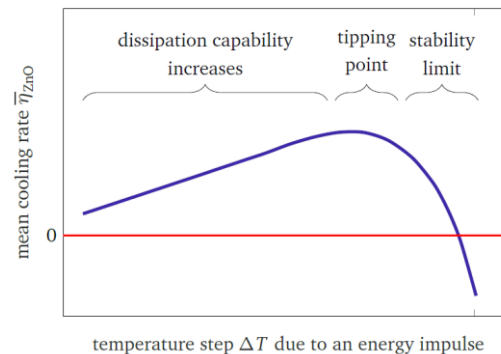


Question:

How to avoid thermal instability  
(i.e. thermal runaway problem)?

Thermal - divided air gap,  
black coating

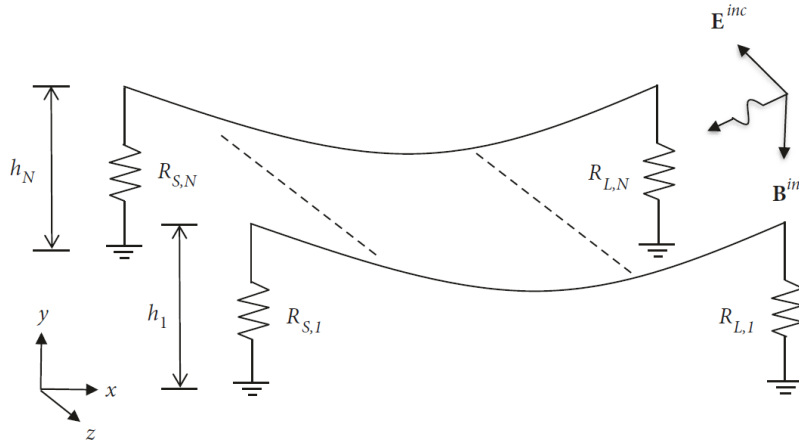
Electrical -  $\alpha$  (nonlinearity of ZnO)  
affect current density



## 5.7 Electromagnetic Transient Analysis of Overhead Lines

In most studies of electromagnetic transients, voltages and currents at interior points of transmission lines in general has no practical importance and is not required to determine the operation state of the electrical network. However, there are some cases where it is necessary to analyze the electromagnetic behavior of the transmission line (TL) over its complete length, such as in the case of lines with distance dependent electrical parameters (nonuniform transmission lines), lines with distributed sources, lines with nonlinear electrical parameters, and lines with time dependent electrical parameters. In particular in this work the phenomena of distance dependent electrical parameters and distributed sources due to incident electromagnetic fields are considered.

**Method of Characteristics** allows transforming the time domain transmission line partial differential equations (PDEs) to ordinary differential equations (ODEs). It has been used in the analysis of single-phase transmission lines with **nonlinear capacitance due to corona effect**, **uniform MTLs with external electromagnetic field excitation**, and **nonuniform MTLs**. The method is simple to apply when dealing with two-conductor uniform lines, but it is a bit more complicated if multiconductor lines are analysed because in this case modal analysis is required. The complexity increases if nonuniformities are considered because modal wave velocities become **distance dependent**; in a consequence the characteristics are curve lines. Moreover, modal transformation matrices are also distance dependent and therefore their derivatives w.r.t. distance are required.



The EM behaviour of a non-uniform MTL with frequency and distance dependent electrical parameters excited by an incident EM field, can be described in the Laplace Domain with the following equations.

$$\begin{cases} \frac{d}{dx} \mathbf{V}(x, s) + s \mathbf{L}_0(x) \mathbf{I}(x, s) + \mathbf{Z}_p(x, s) \mathbf{I}(x, s) = \mathbf{V}_f(x, s) \\ \frac{d}{dx} \mathbf{I}(x, s) + s \mathbf{C}_0(x) \mathbf{V}(x, s) + \mathbf{G}_0(x, s) \mathbf{V}(x, s) = \mathbf{I}_f(x, s) \end{cases} \quad (5.337)$$

For a transmission line with  $N+1$  conductors, including the return path, matrices are of order  $N \times N$  and vectors of  $N \times 1$ . The geometric inductance, capacitance, and conductance matrices are defined as

$$\mathbf{L}_0(x) = \frac{\mu_0}{2\pi} \mathbf{P}(x), \quad \mathbf{C}_0(x) = 2\pi\varepsilon(x)\mathbf{P}^{-1}(x), \quad \mathbf{G}_0 = \frac{\sigma(x)}{\varepsilon(x)} = \mathbf{C}_0(x) \quad (5.338)$$

where  $\mathbf{P}(x)$  is Maxwell's potential coefficients matrix;  $\mu(x)$ ,  $\varepsilon(x)$  and  $\sigma(x)$  are respectively, the permeability, permittivity and conductivity of the dielectric that surrounds the TL.

When the separation between conductors is large and therefore proximity effects can be neglected, the elements of  $\mathbf{P}(x)$  are given by

$$P_{ii}(x) = \ln\left(\frac{2h_i(x)}{r_i(x)}\right), \quad P_{ik}(x) = \ln\left(\frac{D_{ik}(x)}{d_{ik}(x)}\right) \quad (5.339)$$

where  $r_i(x)$  and  $h_i(x)$  are the radius and the height of the i-th conductor, respectively;  $d_{ik}(x)$  is the distance between the i-th and k-th conductors and  $D_{ik}(x)$  is the distance between the i-th conductor and the mirror image of the k-th conductor. In power lines with several conductors per phase  $r_i(x)$  is substituted by the Geometric Mean Radius and all distances are taken from the centers of the bundles.

$$\mathbf{V}_f(x, s) = s \begin{bmatrix} \int_0^{h_1} B_{z,1}^{inc}(x, s) dy \\ \dots \\ \int_0^{h_N} B_{z,N}^{inc}(x, s) dy \end{bmatrix}, \quad \mathbf{I}_f(x, s) = -s \mathbf{C}_0(x) \begin{bmatrix} \int_0^{h_1} E_{y,1}^{inc}(x, s) dy \\ \dots \\ \int_0^{h_N} E_{y,N}^{inc}(x, s) dy \end{bmatrix} \quad (5.340)$$

where  $B_{z,i}^{inc}(x, s)$  and  $E_{y,i}^{inc}(x, s)$  are the incident magnetic flux density in z-direction and incident E-field intensity in y-direction corresponding to i-th conductor.

The penetration impedance takes into account the penetration of the EM field into the non-ideal conductors of the transmission lines and is given by

$$\mathbf{Z}_p(x, s) = \mathbf{Z}_c(x, s) + \mathbf{Z}_E(x, s) \quad (5.341)$$

where  $\mathbf{Z}_c(x, s)$  is the conductor impedance matrix and  $\mathbf{Z}_E(x, s)$  the return path impedance matrix.  $\mathbf{Z}_c(x, s)$  is calculated with formulas for cylindrical conductors in terms of modified Bessel functions and  $\mathbf{Z}_E(x, s)$  using complex penetration depth method.

In order to facilitate the transformation to the time domain of the transmission line equations a rational approximation of  $\mathbf{Z}_p(x, s)$  can be performed using Vector Fitting (VF), thus (5.341) can be expressed as

$$\mathbf{Z}_p(x, s) = \sum_{j=1}^M \left( \frac{1}{s - p_j(x)} \mathbf{K}_j(x) \right) + \mathbf{K}_\infty(x) \rightarrow \mathbf{R}_{DC}(x) = \sum_{j=1}^M \left( \frac{1}{-p_j(x)} \mathbf{K}_j(x) \right) + \mathbf{K}_\infty(x) \quad (5.342)$$

where M is the order of rational approximation,  $p_j$  is the j-th pole,  $\mathbf{K}_j(x)$  is the corresponding residues matrix;  $\mathbf{K}_\infty(x)$  is a real constant matrix.

$$\frac{d}{dx} \mathbf{V}(x, s) + s \mathbf{L}_0(x) \mathbf{I}(x, s) + \left( \sum_{j=1}^M \left( \frac{1}{-p_j(x)} \mathbf{K}_j(x) \right) + \mathbf{K}_\infty(x) \right) \mathbf{I}(x, s) = \mathbf{V}_f(x, s) \quad (5.343)$$

Transforming back to time domain,

$$\frac{\partial}{\partial x} \mathbf{v}(x, t) + \mathbf{L}_0(x) \frac{\partial}{\partial t} \mathbf{i}(x, t) + \mathbf{K}_\infty(x) \mathbf{i}(x, t) + \boldsymbol{\varphi}(x, t) = \mathbf{v}_f(x, t) \quad (5.344)$$

where

$$\mathbf{v}_f(x, t) = \frac{\partial}{\partial t} \begin{bmatrix} \int_0^{h_1} B_{z,1}^{inc}(x, t) dy \\ \dots \\ \int_0^{h_N} B_{z,N}^{inc}(x, t) dy \end{bmatrix}, \quad \boldsymbol{\varphi}(x, t) = L_p^{-1} \left\{ \left( \frac{1}{s - p_j(x)} \mathbf{K}_j(x) \right) \mathbf{I}(x, s) \right\} \quad (5.345)$$

Substituting,

$$\frac{\partial}{\partial x} \mathbf{v}(x, t) + \mathbf{L}_0(x) \frac{\partial}{\partial t} \mathbf{i}(x, t) + \mathbf{R}(x) \mathbf{i}(x, t) + \mathbf{h}(x, t) = \mathbf{v}_f(x, t) \quad (5.346)$$

Where

$$\begin{aligned} \mathbf{h}(x, t) &= \sum_{j=1}^M \frac{1}{1 - p_j \Delta t} \boldsymbol{\varphi}(x, t - \Delta t), & \mathbf{R}(x) &= \mathbf{K}_\infty(x) + \sum_{j=1}^M \frac{1}{1 - p_j \Delta t} \mathbf{K}_j(x), \\ \boldsymbol{\varphi}(x, t - \Delta t) &= \frac{1}{1 - p_j \Delta t} \boldsymbol{\varphi}(x - 2\Delta t) + \frac{\Delta t}{1 - p_j \Delta t} \mathbf{K}_j(x) \mathbf{i}(x, t - \Delta t) \end{aligned} \quad (5.347)$$

The shunt conductance  $\mathbf{G}_0(x)$  is negligible in aerial transmission lines; for this case, transforming (5.447) to time domain gives

$$\frac{\partial}{\partial x} \mathbf{i}(x, t) + \mathbf{C}_0(x) \frac{\partial}{\partial t} \mathbf{v}(x, t) = \mathbf{i}_f(x, t) \quad (5.348)$$

where

$$\mathbf{i}_f(x, t) = -\mathbf{C}_0(x) \frac{\partial}{\partial t} \begin{bmatrix} \int_0^{h_1} E_{y,1}^{inc}(x, t) dy \\ \dots \\ \int_0^{h_N} E_{y,N}^{inc}(x, t) dy \end{bmatrix} \quad (5.349)$$

Method of characteristics – A nonmodal approach:

Grouping (5.344) and (5.349) into the form of

$$\frac{\partial}{\partial t} \mathbf{W} + \mathbf{A} \frac{\partial}{\partial x} \mathbf{W} + \mathbf{B} \mathbf{W} + \mathbf{H} = \mathbf{F} \quad (5.350)$$

Where

$$\begin{aligned}\mathbf{W} &= \begin{bmatrix} \mathbf{v}(x, t) \\ \mathbf{i}(x, t) \end{bmatrix}, & \mathbf{A} &= \begin{bmatrix} \mathbf{0} & \mathbf{C}_0^{-1}(x) \\ \mathbf{L}_0^{-1}(x) & \mathbf{0} \end{bmatrix}, & \mathbf{B} &= \begin{bmatrix} \mathbf{0} & \mathbf{0} \\ \mathbf{0} & \mathbf{L}_0^{-1}(x)\mathbf{R}(x) \end{bmatrix}, \\ \mathbf{H} &= \begin{bmatrix} \mathbf{0} \\ \mathbf{L}_0^{-1}(x)\mathbf{h}(x, t) \end{bmatrix}, & \mathbf{F} &= \begin{bmatrix} \mathbf{C}_0^{-1}(x)\mathbf{i}_f(x, t) \\ \mathbf{L}_0^{-1}(x)\mathbf{v}_f(x, t) \end{bmatrix}\end{aligned}\tag{5.351}$$

Matrices A and B are of order  $2N \times 2N$  and vectors W, H and F of  $2N \times 1$ .

System (5.350) is hyperbolic if A is diagonalizable with real eigenvalues; in other words, there is a matrix function E(x) such that

$$\mathbf{E}(x)\mathbf{A}(x)\mathbf{E}^{-1}(x) = \mathbf{E}(x) \begin{bmatrix} \mathbf{0} & \mathbf{C}_0^{-1}(x) \\ \mathbf{L}_0^{-1}(x) & \mathbf{0} \end{bmatrix} \mathbf{E}^{-1}(x) = \Lambda(x) = \begin{bmatrix} \lambda_{11}(x) & 0 & 0 \\ 0 & \dots & 0 \\ 0 & 0 & \lambda_{NN}(x) \end{bmatrix}\tag{5.352}$$

where  $\lambda_{ii}(x)$  are real and the norm of E(x) and  $\mathbf{E}^{-1}(x)$  are bounded in x, for  $x \in R$ .

It can be shown that the matrix of eigenvectors is given by

$$\mathbf{E}(x) = \begin{bmatrix} \mathbf{U} & +\mathbf{R}_0(x) \\ \mathbf{U} & -\mathbf{R}_0(x) \end{bmatrix}\tag{5.353}$$

where U is the  $N \times N$  identity matrix and  $\mathbf{R}_0(x)$  s the characteristics resistance of the line defined as:

$$\mathbf{R}_0(x) = \sqrt{\mathbf{L}_0(x)\mathbf{C}_0^{-1}(x)} = \eta(x)\mathbf{P}(x) = \sqrt{\frac{\mu(x)}{\varepsilon(x)}} \mathbf{P}(x)\tag{5.354}$$

In addition, it can be proven that the eigenvalues of A are given by

$$\Lambda(x) = \begin{bmatrix} +\lambda(x) & \mathbf{0} \\ \mathbf{0} & -\lambda(x) \end{bmatrix}\tag{5.355}$$

where  $+\lambda(x)$  is a diagonal matrix given by

$$+\lambda(x) = \sqrt{\mathbf{L}_0^{-1}(x)\mathbf{C}_0^{-1}(x)} = v_c(x)\mathbf{U}, \quad v_c(x) = \frac{dx}{dt} = \frac{1}{\sqrt{\mu(x)\varepsilon(x)}}\tag{5.356}$$

Having  $\lambda(x) = \pm dx/dt$  and  $v_c(x) = dx/dt$ ,

$$t = \int \frac{1}{v_c(x)} dx + \alpha; \quad t = - \int \frac{1}{v_c(x)} dx + \beta\tag{5.357}$$

If  $\varepsilon, \mu$  are constant along the line,

$$t = +\sqrt{\mu\varepsilon}t + \alpha; \quad t = -\sqrt{\mu\varepsilon}t + \beta\tag{5.358}$$

Multiply (5.350) with eigenvector matrix  $\mathbf{E}(x)$  gives

$$\left( \frac{\partial}{\partial t} + \lambda(x) \frac{\partial}{\partial x} \right) \mathbf{v}(x, t) + \mathbf{R}_0(x) \left( \frac{\partial}{\partial t} + \lambda(x) \frac{\partial}{\partial x} \right) \mathbf{i}(x, t) + \lambda(x) [\mathbf{R}(x) \mathbf{i}(x, t) + \mathbf{h}(x, t)] = \lambda(x) [\mathbf{R}_0(x) \mathbf{i}_f(x) + \mathbf{v}_f(x)] \quad (5.359)$$

$$\left( \frac{\partial}{\partial t} - \lambda(x) \frac{\partial}{\partial x} \right) \mathbf{v}(x, t) - \mathbf{R}_0(x) \left( \frac{\partial}{\partial t} - \lambda(x) \frac{\partial}{\partial x} \right) \mathbf{i}(x, t) - \lambda(x) [\mathbf{R}(x) \mathbf{i}(x, t) + \mathbf{h}(x, t)] = \lambda(x) [\mathbf{R}_0(x) \mathbf{i}_f(x) - \mathbf{v}_f(x)] \quad (5.360)$$

where

$$\lambda(x) = \mathbf{R}_0 \mathbf{L}_0^{-1}; \quad \mathbf{C}_0^{-1} = \lambda(x) \mathbf{R}_0 \quad (5.361)$$

Consider  $\lambda(x) = \pm dx/dt$ , the term in parenthesis in (5.359) – (5.360) becomes total derivatives, i.e.

$$\frac{d}{dt} \mathbf{v}(x, t) + \mathbf{R}_0(x) \frac{d}{dt} \mathbf{i}(x, t) + \frac{dx}{dt} [\mathbf{R}(x) \mathbf{i}(x, t) + \mathbf{h}(x, t)] = \frac{dx}{dt} [\mathbf{R}_0(x) \mathbf{i}_f(x) + \mathbf{v}_f(x)] \quad (5.362)$$

$$\frac{d}{dt} \mathbf{v}(x, t) - \mathbf{R}_0(x) \frac{d}{dt} \mathbf{i}(x, t) + \frac{dx}{dt} [\mathbf{R}(x) \mathbf{i}(x, t) + \mathbf{h}(x, t)] = \frac{dx}{dt} [\mathbf{R}_0(x) \mathbf{i}_f(x) - \mathbf{v}_f(x)] \quad (5.363)$$

(5.362) – (5.363) along with  $\lambda(x) = \pm dx/dt$  are ODEs that are equivalent to the PDEs system (5.350). It can be observed that the Nonmodal approaches  $R(x)$  and  $h(x, t)$ , which take into account the effects of the penetration of the electromagnetic field in nonideal conductors, are out of the differential operations; therefore they do not change the main features of the propagation; in other words, their effects can be seen as a distortion of the wave that travels along a lossless nonuniform transmission line.

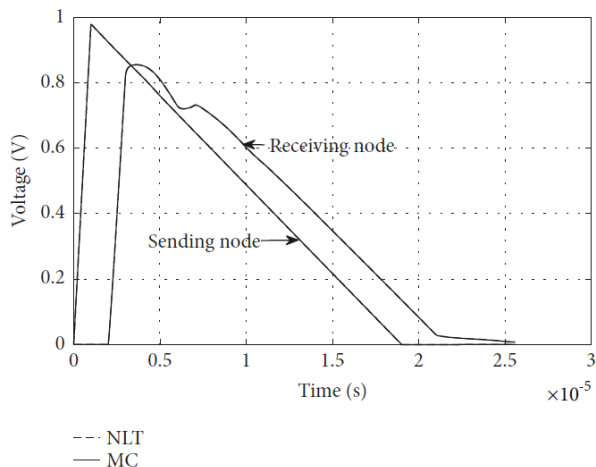


FIGURE 8: Voltages at the sending and receiving ends of the monophasic nonuniform line.

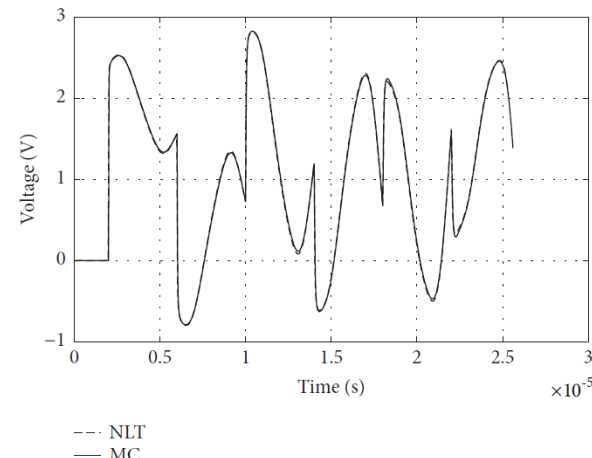


FIGURE 10: Voltages at phase A of the receiving end for the transmission line crossing a river.

## Summary

This set of notes provides studies on advanced topics in overhead line, including insulator designs with different surface conditions, theory of corona on the dynamic response with q-u curve and hence design of corona rings, considerations on HVDC OHL applications such as optimal placement of HVDC substation, polarity reversal on mixed cable – OHL applications, lightning protection on current differential blocking, interference on HVAC to HVDC and ion-flow field simulation. At last, short briefing is provided for grounding and tower modelling for ground potential rise, dynamic rating formulation with real time economic dispatch supported by state estimation and meteorological factors affecting output of RE and thermal rating of OHL, electrothermal analysis for surge arrester (ZnO) and EM transient modelling for power system analysis.

It is noted that the major outcome for this set of note is the understanding of different modelling and solving techniques, including protection threshold setting with **travelling wave**, **finite element** and **finite difference** with Maxwell equations which is based on physical quantities, **neural network** and **support vector machines** for dynamic arc models which can predict or classify based on given input, **time-domain** and **frequency-domain response** for grounding and transient EM fields, and **optimization skills** with Lagrange Multiplier or even evolutionary approach.

Although overhead line has been applied for many years and the construction and O&M skills does not have much development, the actual difficult faced in design and replacement, especially after unplanned environmental change in surrounding and demand in cost reduction with more transmission capacity with safer and stabler approach leads to continuous studies on OHL application. Unlike cable, which is often challenged by dense EM field, OHL seems to have more challenges on environment, hence, basic understanding to meteorology and heat transfer is needed. Also, the application of mixed lines, until the day when wireless power transfer with antennas or distributed powers dominates the market, will be increased and the challenge lies on the mis-understanding or ignorance in OHL theory. It is hoped that this set of note will be updated frequently so that students become more updated to line technology.

## Reference

### Section 1: Theory of Insulator and its Design

- [1] A. A. Salem (2021), Pollution flashover under different contamination profiles on high voltage insulator: Numerical and Experiment Investigation
- [2] D. Doufene (2019), Optimised performance of Cap and pin insulator under wet pollution conditions using a mono-objective genetic algorithm
- [3] F. HADJIRIOUA (2018), Analytical modelling of arc re-ignition conditions on polluted insulating surfaces
- [4] Hussain (2019), Mechanism of saline deposition and surface flashover on high-voltage insulators near Shoreline: Mathematical Models and experimental validations
- [5] J. He (2019), Modeling of dry band formation and arcing processes on the polluted composite insulator surface
- [6] M. Slama (2010), Analytical computation of discharge characteristic constants and critical parameters of flashover of polluted insulators
- [7] M. T. Gencoglu (2009), Prediction of flashover voltage of insulators using least squares support vector machines
- [8] M. T. Gençoğlu (2009), Investigation of Pollution Flashover on high voltage insulators using artificial neural network

### Section 2: Theory of Corona and its Effect

- [1] A. J. Otto (2009), Direct current conductor Corona Modelling and metrology
- [2] B. M'hamdi (2016), Optimal design of Corona Ring on HV composite insulator using PSO approach with dynamic population size
- [3] E. Stracqualursi (2021), The Corona phenomenon in overhead lines: Critical overview of most common and reliable available models
- [4] M. Ignjatovic (2021), Drift-diffusion model of corona discharge in coaxial geometry due to negative lightning impulse voltage
- [5] V. Cooray (2000), Charge and voltage characteristics of Corona discharges in a coaxial geometry
- [6] X. Zhang (2021), Lightning surge analysis for overhead lines considering Corona effect

### Section 3: Overhead Line Application in HVDC

- [1] Shakeel (2021), A study of fast front transients of an HVDC mixed transmission line exposed to bipolar lightning strokes
- [2] D. Wang (2019), Calculation of ion-flow field near the crossing of HVDC transmission lines using equivalent Corona conductors
- [3] F. Xiao (2021), Transient overvoltage on HVDC overhead transmission lines with background DC space charges and Impulse Corona
- [4] F. Xie (2021), A RFTR based Lightning Disturbance Identification Scheme for VSC-HVDC line protection
- [5] J. Tang (2007), Analysis of electromagnetic interference on DC Line from parallel AC line in close proximity
- [6] M. Asif (2019), Assessment of overvoltage and insulation coordination in mixed HVDC transmission lines exposed to lightning strikes
- [7] M. Moradi-Sepahvand (2021), Hybrid AC/DC transmission expansion planning considering HVAC to HVDC conversion under renewable penetration
- [8] O. Alizadeh-Mousavi (2015), Optimal location and sizing of HVDC converters for same-tower AC-DC overhead lines

### Section 4: Ground Potential Rise (GPR)

- [1] R. Shariatinasab (2017), The effect of grounding system modeling on lightning-related studies of transmission lines
- [2] X. Guo (2019), A Non-Uniform Transmission Line Model of the 1100 kV UHV Tower

### Section 5: Dynamic Line Rating (DLR)

- [1] B. Xu (2016), Impact of Dynamic Line Rating on Dispatch Decisions and Integration of Variable RES Energy
- [2] Y. Du (2012), On-line estimation of transmission line parameters, temperature and sag using PMU measurements
- [3] A. David (2016), Dynamic Line Rating - Technologies and Challenges of PMU on Overhead Lines
- [4] J. Hu (2018), Transient Temperature Calculation and Multi-Parameter Thermal Protection of Overhead Transmission Lines Based on an Equivalent Thermal Network

### Section 6: Surge Arrester – Electrothermal Modelling

- [1] YT K Späck-Leigsnering (2020), Electrothermal Modeling, Simulation and Optimization of Surge Arresters

### Section 7: Electromagnetic Transient Analysis of Overhead Lines

- [1] Avila-Sánchez-Alegr-a (2019), Time Domain Electromagnetic Transient Analysis of Aerial Nonuniform Transmission Lines Excited by an Incident Electromagnetic Field

#### Important Formula

Arc Propagation Criterion:

$$\frac{d|Z_{eq}|}{dx} < 0 \rightarrow S\rho_p - S_p k\rho_a > 0 \quad (5.16)$$

Critical Arc Length:

$$\frac{x_1}{L} = 1 + \frac{S_p k\rho_a}{\alpha} (S\rho_p - S_p k\rho_a) \quad (5.30)$$

Dry Band Development:

$$\frac{J_s^2}{\sigma} = -L_e \rho_s \frac{d \ln L}{dt} + \rho_s C_h \frac{dT}{dt} + k\rho \frac{H_e}{L} (T_m - T_p) \quad (5.40)$$

Finite Element Method:  
(Energy Function)

$$F^*(v) = \frac{1}{2} \iint (\sigma + j\omega\varepsilon) |\nabla^* v|^2 ds \rightarrow \frac{\partial F(v_i)}{\partial v_i} = 0, i = 1, 2, 3, \dots, k \quad (5.65)$$

SVM Dynamic Model:

$$A \begin{bmatrix} \alpha \\ b \end{bmatrix} = \begin{bmatrix} K + 1/\gamma & 1_N \\ 1_N^T & 0 \end{bmatrix} \begin{bmatrix} \alpha \\ b \end{bmatrix} = \begin{bmatrix} y \\ 0 \end{bmatrix} \rightarrow \begin{bmatrix} \alpha \\ b \end{bmatrix} = A^{-1} \begin{bmatrix} y \\ 0 \end{bmatrix} \quad (5.78)$$

Corona Inception:

$$E_c = mE_0 \delta \left( 1 + \frac{K}{\sqrt{\delta r_c}} \right), \quad \delta = \frac{273 + t_0}{273 + t} \frac{p}{p_0} \quad (5.104)$$

Fourier Transform – Corona Equation:

$$F(\omega) = \int_{-\infty}^{+\infty} i_p K [(e^{-\alpha t} - e^{-\beta t}) e^{-j\omega t} dt \rightarrow |F(\omega)| = i_p K \frac{\beta - \alpha}{\sqrt{(\alpha^2 + \omega^2)(\beta^2 + \omega^2)}} \quad (5.114)$$

Isothermal Plasma:

$$\vec{v} = \mu \vec{E} - D \frac{\nabla n}{n} \quad (5.123)$$

Drift Equation:

$$\frac{dp_i}{dt} + \mu_p \frac{r_i e_i p_\alpha - r_{i-1} e_{i-1} p_\beta}{s_i \bar{r}_i} + R p_i n_i = 0, \quad \frac{dn_i}{dt} + \mu_n \frac{r_i e_i n_\alpha - r_{i-1} e_{i-1} n_\beta}{s_i \bar{r}_i} + R p_i n_i = 0 \quad (5.164)$$

Townsend Criterion:

$$I = \frac{I_0 e^{\alpha d}}{1 - \nu(e^{\alpha d} - 1)} \quad (5.183)$$

Dynamic Capacitance due to Corona:

$$C_d = C' + i_{corona} \frac{\partial t}{\partial u} = C' + Gu \frac{\partial t}{\partial u} \quad (5.205)$$

Transmission Line Equation with Space Charge Effect:

$$\begin{cases} \frac{\partial u(t, z)}{\partial z} + L \frac{\partial i(t, z)}{\partial t} + R_0 i(t, z) = 0 \\ \frac{\partial i(t, z)}{\partial z} + C'(t) \frac{\partial u(t, z)}{\partial t} + (G_0(t) + G(t)) u(z, t) = 0 \end{cases} \quad (5.207)$$

Maximum Shielding Failure Current:

$$I_{MSF} = \left[ \frac{\gamma(h_c + h_g)}{X(1 - \gamma \sin \alpha)} \right]^{\frac{1}{Y}}, \quad \gamma = \frac{1}{0.36 + 0.17 \ln(43 - h_c)} \quad (5.220)$$

Insulation Ratio between HVAC and HVDC:

$$i_R = k \frac{k_1 E_a}{k_2 V_a} \quad (5.221)$$

Rise-Fall Time Ratio (RFTR):

$$Ratio = \frac{\sum_{k=1}^N T_{rise}(k)}{\sum_{k=1}^N T_{fall}(k)}, \quad Ratio \begin{cases} < 1, & \text{disturbance} \\ > 1, & \text{fault} \end{cases} \quad (5.247)$$

State Estimation for Dynamic Line Rating:

$$H = \frac{\partial F(X_k)}{\partial X_k} \rightarrow X_{k+1} = X_k - (H^T H)^{-1} [H^T F(X_k)] \quad (5.288)$$

Electro-Quasistatic (EQS) Equation:

$$\nabla \cdot \left( \frac{\partial}{\partial t} \epsilon \nabla \varphi \right) + \nabla \cdot (\sigma \nabla \varphi) = 0 \quad (5.300)$$